UNIVERSITÀ DEGLI STUDI FIRENZE

DOCTORAL PROGRAMME

TUSCAN PhD IN NEUROSCIENCES

Cycle XXX

Stefano Doccini

Functional omics approaches towards affected molecular pathways underlying various forms of Neuronal Ceroid Lipofuscinoses

Scientific Disciplinary Sector MED/39

IRCCS FONDAZIONE STELLA MARIS

Unione europea
Fondo sociale europeo

REGIONE TOSCANA

POR FSE VERSO IL 2020
Fondo Sociale Europeo

UNIVERSITÀ
DEGLI STUDI
FIRENZE

DOCTORAL PROGRAMME

TUSCAN PhD IN NEUROSCIENCES

Cycle XXX

COORDINATOR Prof. Renato Corradetti

Functional omics approaches towards affected molecular pathways underlying various forms of Neuronal Ceroid Lipofuscinoses

Scientific Disciplinary Sector MED/39

PhD Student

Dr. Stefano Doccini

Scientific Tutor

Prof. Filippo Maria Santorelli

Tutor

Prof. Giovanni Cioni

Coordinator

Prof. Renato Corradetti

Years 2014-2017

Supervised by

Prof. Filippo Maria Santorelli, MD, PhD
Molecular Medicine,
IRCCS Fondazione Stella Maris, Pisa - Italy.

Prof. Giovanni Cioni, MD
Department of Developmental Neuroscience,
IRCCS Fondazione Stella Maris, Pisa - Italy.
Department of Clinical and Experimental Medicine,
University of Pisa, Pisa - Italy.

Reviewed by

Dr. Pasquale Striano, MD, PhD
Pediatric Neurology and Muscular Diseases Unit, Department of Neurosciences, Rehabilitation, Ophthalmology, Genetics, Maternal and Child Health,
University of Genoa, "G. Gaslini" Institute, Genova - Italy.

Dr. Maciej Lalowski, PhD
Medicum, Biochemistry/Developmental Biology, Meilahti Clinical Proteomics Core Facility,
University of Helsinki, Helsinki - Finland.

Dr. Katja Kanninen, PhD
A.I. Virtanen Institute for Molecular Sciences
University of Eastern Finland, Kuopio - Finland.

ABSTRACT

Neuronal ceroid lipofuscinoses (NCLs) are the most common inherited progressive encephalopathies of childhood. NCL disease genes were first identified in 1995 and since then, nearly 400 mutations (mostly autosomal recessively inherited) in thirteen known genes (*CLN1*-8, *CLN10-14*; http://www.ucl.ac.uk/ncl) have been described. Despite progress in the NCL field, the primary function and physiological roles of most NCL proteins remain unresolved. Evidence suggest that the different proteins work in an intricate molecular network and studying common molecular signatures and the parts that differ is critical to identify biomarkers and modifying factors involved in the disease.

In this thesis we employed systematic approaches, including: functional proteomics, bioinformatics and cellular and murine disease models, in an effort to clarify disease pathways associated with congenital, infantile and late-infantile NCL. We focused on three disease genes with different ages of onset: CLN10 (congenital), CLN1 (infantile classic, late infantile, juvenile, adult), and CLN5 (late infantile variant, juvenile, adult). First, we performed transcriptomic profiling in SH-SY5Y neuroblastoma cells overexpressing wild type CLN1 (SH-p.wtCLN1) and three selected CLN1 patients' mutations and revealed 802 differentially expressed genes (DEGs) in SH-p.wtCLN1 (as compared to empty-vector transfected cells), whereas the number of DEGs detected in the two mutants (p.L222P and p.M57Nfs*45) was significantly lower. Bioinformatic scrutiny linked DEGs with neurite formation and neuronal transmission. Palmitoylation survey identified 113 palmitoylated protein-encoding genes in SH-p.wtCLN1, including 25 assigned to axonal growth and synaptic compartments. Results obtained in this experimental setting outlined a potential role of PPT1 in modulating the function of membrane proteins related with neuronal excitability and, possibly, epileptogenesis which can be associated with an altered gene dosage of wtCLN1.

Second, we investigated the novel c.205G>A/p.Glu69Lys mutation in *CTSD* in patient' skin fibroblasts since transcriptomic data had revealed an up-regulation of *CTSD* mRNA in SH-wtCLN1 cells and suggested a cross-talk between CLN1 and CLN10 forms of NCLs and share some clinical features including epileptic manifestations and both present the same, suggesting a sort of overlap among these two forms: lysosomal CTSD deficiency could represent a common pathogenic link between infantile NCL due by inactivating mutations in the *CLN1* gene and congenital NCL underlie CLN10.

Analyzing CTSD fibroblasts we observed ultrastructural granular osmiophilic deposits (GRODs) abnormalities similar to those seen in CLN1 disease. Conversely, we did not detect alterations in *PPT1* mRNA expression levels suggesting lack of correlation with the observed ultrastructural GRODs abnormalities.

Finally, we investigated *in vitro* the role of human CLN5 by developing cell models of *CLN5* depletion adopting the CRISPR/Cas9 technology.

Upon different functional proteomic approaches, we observed mitochondrial dysfunction and impairment of cellular bioenergetics capacity and a possible role of CLN5 in mitophagy. We also corroborated impairment of mitochondrial functions in brain from 3month-old pre-symptomatic mice and primary cells from CLN5 patients. Also, proteomic profiling of lysosomal fractions from KO cell models identified a possible role of CLN5 in lipid homeostasis and ganglioside signaling pathway and suggested possible connections between mitochondrial and sphingolipid metabolisms.

To sum up, in this study we pinpointed the involvement of specific cellular processes in the pathophysiology of three NCL proteins using innovative experimental approaches. Our results indicate potential biomarker of disease status and remark a common biological process leading to an NCL-disease. Nonetheless, the possibility that individualized or specific mechanisms emerge among others in specific subtypes could offer more personalized approach (-es) to therapy.

List of original publications

The PhD thesis work has been composed on the basis of the following original papers and unpublished material:

- Pezzini F, Bianchi M, Benfatto S, Griggio F, Doccini S, Carrozzo R, Dapkunas A, Delledonne M, Santorelli FM, Lalowski MM, Simonati A. The Networks of Genes Encoding Palmitoylated Proteins in Axonal and Synaptic Compartments Are Affected in PPT1 Overexpressing Neuronal-Like Cells. Front Mol Neurosci. 2017 Aug 22;10:266. doi: 10.3389/fnmol.2017.00266. eCollection 2017

- Doccini S, Sartori S, Maeser S, Pezzini F, Rossato S, Moro F, Toldo I, Przybylski M, Santorelli FM, Simonati A. Early infantile neuronal ceroid lipofuscinosis (CLN10 disease) associated with a novel mutation in CTSD. J Neurol. 2016 May;263(5):1029-1032. doi: 10.1007/s00415-016-8111-6. Epub 2016 Apr 12.

- Doccini S, Pezzini F, Morani F, Calza G, Soliymani R, Huuskonen M, Baumann M, Simonati A., Kanninen KM, Lalowski M, Santorelli FM. Proteomic and bioinformatic characterization of affected mitochondrial and lysosomal pathways in CLN5 deficiency, in preparation.

Abbreviations

ATP13A2, ATPase 13A2 (human)
BCA, bicinchoninic acid assay
BDNF
B-H, Benjamini and Hochberg
Cas9, CRISPR associated protein 9
CHO, Chinese hamster ovary cells
CLN1-14, ceroid-lipofuscinosis, neuronal 1-14
CLN3, battenin (human)
Cln5, CLN5 intracellular trafficking protein (animal model)
CLN5, CLN5 intracellular trafficking protein (human)
Cln5-/-, Cln5-deficient animal model
CLN6, CLN6 transmembrane ER protein (human)
CLN8, CLN8 transmembrane ER and ERGIC protein (human)
CLP curvilinear profiles
CNS, central nervous system
COS-1, African green monkey kidney fibroblast-like cell line transformed by an origin-defective mutant of SV-40
CRISPR RNA crRNA
CRISPR/Cas9, clustered regularly interspaced short palindromic repeats-associated endonuclease 9
crRNA, CRISPR RNA
Ctsd, cathepsin D (animal model)
CTSD, cathepsin D (human)
CTSDm, active-CTSD/mature form
CTSDpro, precursor of mature-CTSD
CTSF, cathepsin F (human)
DAPI, 4,6-diamidino-2-phenylindole dihydrochloride
dbAMP, dibutyril-cyclic adenosine monophosphate
DBS, dried blood spot
DEGs
DNAJC5, DnaJ heat shock protein family (Hsp40) member C5 (human)
ER, endoplasmic reticulum
ERT, enzyme replacement therapy
FBS, fetal bovine serum
FC fold change
FCCP, carbonyl cyanide 4-(trifluoromethoxy)phenylhydrazone
FDR, false discovery rate

FPKM, fragments per kilobase per million mapped reads
FPP fingerprint profiles
GO, gene ontology
GRN, granulin precursor (human)
GRODs granular osmiophilic deposits
HDMS, high definition mass spectrometry
HDR, homology directed repair
HEK293T, human embryonic kidneys transformed with large T antigen.
IDs, identifiers
IF, immunofluorescence
IL 1β, interleukin 1 beta
IMPI, integrated mitochondrial protein index
INCL, infantile neuronal ceroid lipofuscinosis
Indels, insertions and deletions
IPA, ingenuity pathways analysis
KCTD7, potassium channel tetramerization domain containing 7 (human)
KO, knock-out
LC, Liquid chromatography
LSD, lysosomal storage disorders
M6P, mannose 6-phosphate
MFSD8, major facilitator superfamily domain containing 8 (human)
MS, mass spectrometry
NBM neurobasal medium enriched recombinant human BDNF, dbcAMP, B27 Neuromix, KCl, L-glutamine.
NCLs, neuronal ceroid lipofuscinoses
NHEJ, non-homologous end joining
NPCs, neural stem/progenitor cells
OCR, Oxygen consumption rate
ORF, open reading frame
PAM, protospacer adjacent motif
Ppt1, palmitoyl-protein thioesterase 1 (animal model)
PPT1, palmitoyl-protein thioesterase 1 (human)
Ppt1-/-, palmitoyl-protein thioesterase 1-deficient animal model
RA, Retinoic Acid
RLC rectilinear complex
sgRNA, single-guide RNA
SH-p.L222P, mutated PPT1 overexpressing cell line
SH-p.M57Nfs*45, truncated PPT1 overexpressing cell line
SH-p.wtCLN1, wild type PPT1 overexpressing cell line

SH-SY5Y, human neuroblastoma cell line

SMACS subunit c of mitochondrial ATP synthase

TALENs, transcription activator-like effector nucleases

TGN, trans-Golgi network

TIDE, tracking of indels by decomposition

TPP1, tripeptidyl peptidase 1 (human)

tracrRNA, trans-activating crRNA

UB, urea buffer

WB, Western blotting

ZFNs, zinc-finger nucleases

CONTENTS

1. INTRODUCTION

1.1 The Neuronal Ceroid-Lipofuscinoses

The neuronal ceroid lipofuscinoses (NCLs), also grouped under the eponym of Batten disease, are a heterogeneous group of progressive neurodegenerative disorders affecting children and adults, characterized by retinopathy leading to blindness, ataxia and gait abnormalities, drug-resistant progressive myoclonic epilepsy, mental deterioration, and early death.

NCLs have a worldwide distribution and are usually transmitted according to an autosomal-recessive pattern of inheritance, although a rare, autosomal dominant adult-onset form has been identified (Mole SE, Williams RE, 2012).

Recent molecular studies suggest a global incidence ranging from 1 to 4/100,000 (Williams, 2011) with about 6-700 new cases being diagnosed each year.

Molecular epidemiology in Italy on NCLs indicates a lower incidence compared to other European countries and predicts about 5 new cases a year (Santorelli et al., 2013).

Based on consensus clinical, pathological and molecular criteria, NCL diseases were classified according to the age at disease onset (congenital, infantile, late infantile, juvenile, adult) or the designation of the mutated gene (*CLN*). Fourteen different forms have been described to date (Table 1) with over 500 mutations identified (NCL Mutation Database: www.ucl.ac.uk/ncl/mutation;(Cotman et al., 2013; Simonati et al., 2014). However more NCL genes remain to be identified as a small set (less than 10%) patients remain undefined and mutations cannot be demonstrated in any of the known NCL genes although typical NCL features.

NCLs are considered lysosomal storage disorders (LSD), even though only a handful are associated with a primary defect of a lysosomal hydrolase. Their characteristic storage accumulation of autofluorescent ceroid lipopigments and not degraded endo-lysosomal material in the cytoplasm of neuronal cells (as well as other peripheral tissues) is associated with progressive dysfunction and death of neuronal populations, which accounts for the progressive atrophy of the central nervous system (CNS) (Radke et al., 2015). In electron microscopy picture, the accumulated material is visible variable forms, i.e. granular osmiophilic deposits (GRODs), curvilinear profiles (CLP), fingerprint pro-files (FPP), as well as rectilinear complex (RLC) or so called 'condensed forms'. However, unlike classic LSD, "stored" NCL material is not disease-specific and depends on the tissue examined.

At the subcellular level, mutated NCL proteins are classified into three broad categories including four lysosomal hydrolases (encoded by *PPT1, TPP1*, *CTSD* and *CTSF* genes*)* and a non-enzymatic protein encoded by the *CLN5* gene with partly identified function. Membrane

proteins include five genes (*CLN3, CLN6, MFSD8, CLN8, ATP13A2*), related products and secretory or cytosolic proteins (encoded by *DNAJC5, GRN, KCTD7* genes) which are located either in cytosolic compartment or in secretory granules and/or vesicles of different cell populations (Simonati et al., 2014).

Disease mechanisms in NCL involve various pathological alterations concerning the suffering of the mitochondrial compartment, the pathways leading to apoptosis, the cellular events related to autophagy, the endoplasmic reticulum (ER) stress response, all leading to neurodegeneration. However, pathogenetic mechanisms underlying neuronal cell death and brain atrophy in NCLs are not fully known and the function of most affected proteins remains largely elusive.

Similarities between cell pathology and clinical features associated with mutations in genes encoding lysosomal hydrolases or trans-membrane proteins of different cell compartments suggest that the different NCL proteins work in an intricate molecular network interacting at multiple points along common cellular pathways (Faller et al., 2015; Palmer et al., 2013).

Although intensive research has put on the frontline therapeutic approaches, treatment of CNS manifestations in most LSD still remains a considerable challenge. No curative treatments, are still available for NCLs, even to slow down the progressive courses. Indeed, over the last two decades medical treatment of clinical manifestations (epilepsy, movement disorders, behavioral) have been largely palliative in NCL patients.

Animal models are available for different NCL forms, many of which share several common pathological similarities with clinical features, including selective loss of GABAergic interneuron subpopulations, cortical and thalamic atrophy and pronounced early gliosis.

Complementation therapy, either as gene therapy or enzyme replacement therapy (ERT), has been the most used approach in animal models of several forms to relieve disease severity (Bosch et al., 2016; Lu et al., 2010, 2015; Whiting et al., 2016). Other experimental therapeutic strategies have been considered to remove the endolysosomal storage material, either through a direct targeting of the storage material (already tested with unsatisfactory results in CLN1 patients - Levin et al., 2014), or through enhanced exocytosis of pathological intralysosomal content (Sardiello et al., 2009; Song et al., 2013). Eventually, the use of anti-inflammatory drugs was addressed in several animal models of different NCLs (Bosch and Kielian, 2015; Macauley et al., 2014; Seehafer et al., 2011).

Although animal models have been extensively used for the study of the disease in terms of progression and therapeutic approach, they offer relatively limited information on the fine molecular mechanisms of neuronal injury, protein function, and cell localization for most NCL forms (Table 2). This limitations stipulated the development of new *in vitro* models for basic research, to identify affected disease-related pathways and putative biomarkers.

Among cellular models, neuroblastoma cells have been acknowledged as a useful system to investigate the effects of NCL genes expression on neuronal functions and protein interactions.

Overexpression of PPT1 protects LAN-5 neuroblastoma cells from ceramide-induced apoptosis (Cho and Dawson, 2000), whereas antisense treatment (leading to a reduced expression of PPT1) increased the susceptibility to undergo cell death (Cho et al., 2000).

Recently, SH-SY5Y neuroblastoma cells overexpressing either PPT1, CLN3 or CLN5 have been also used to recognize putative interacting proteins by a proteomic approach (Scifo et al., 2013, 2015).

Furthermore, new methods of reprogrammed patient derived primary cells to generate induced pluripotent stem cells (iPSCs) for differentiation into neuronal lineage cells as well as new systems for genome editing adopted to generate stable mutated cell lines by the clustered regularly interspaced short palindromic repeats-associated endonuclease 9 (CRISPR/Cas9) technique represent the new frontier(s) of a NCL research. These new *in vitro* models will allow to overcome the limitations found in animal models related to an incomplete replication of the full spectrum of phenomena associated with human disease and compensate for the restricted availability of human, NCL-affected cell types.

Table 1 *Human Neuronal Ceroid Lipofuscinoses variants*

Disease	Eponym	Affected Gene	Clinical phenotype	Gene Product	Biochemical phenotype
****CLN1**	Haltia–Santavuori	*PPT1* (5538)	Classic infantile, late infantile, juvenile, adult*	PPT1 (soluble protein)	lysosomal enzyme (palmitoyl-thioesterase)
CLN2	Janský–Bielschowsky	*TPP1 (1200)*	Classic late infantile, juvenile*	TPP1 (soluble protein)	lysosomal enzyme (serine protease)
CLN3	Spielmeyer–Sjögren	*CLN3 (1201)*	Juvenile*	CLN3/battenin	membrane protein (6 TMD)
CLN4	Parry	*DNAJC5* (*80331)*	Adult autosomal dominant*	DNAJC5 (soluble protein)	co-chaperone involved in exo-endocytosis cytosol
****CLN5**	Finnish variant late infantile, variant juvenile (previously CLN9)	*CLN5 (1203)*	Late infantile variant, juvenile, adult*	CLN5 (soluble protein)	unknown
CLN6	Early juvenile (Lake Cavanaugh), late infantile Costa Rican-Indian variant, adult Kuf type A	*CLN6 (54982)*	Late infantile variant, adult* (Kuf, type A)*	CLN6	membrane protein (7 TMD)
CLN7	Turkish variant late infantile	*MFSD8 (256471)*	Late infantile variant*, juvenile*, adult*	MFSD8	membrane protein (12 TMD); transporter?
CLN8	Northern epilepsy, progressive EPMR	*CLN8 (2055)*	Late infantile variant EPMR*	CLN8	membrane protein (5 TMD)
CLN9		*CLN9 (497231)*	Juvenile		
****CLN10**	Congenital	*CTSD* (1509)	Congenital classic*, late infantile*, adult*	Cathepsin D	lysosomal enzyme aspartyl-endopeptidase
CLN11	Adult variant	*GRN (2896)*	Adult*	Progranulin	granular protein
CLN12	Juvenile variant	*ATP13A2 (23400)*	Juvenile, Kufor–Rakeb syndrome*	P-type ATPase	membrane protein (10 TMD)

CLN13	Adult Kuf type B	*CTSF (8722)*	Adult Kuf type*	Cathepsin F	lysosomal enzyme cysteine protease
CLN14	Infantile	*KCTD7 (154881)*	Infantile, progressive myoclonus epilepsy 3*	Potassium channel tetramerization domain- containing protein 7 (soluble protein)	unknown

Abbreviation: EPMR, epilepsy with mental retardation; TMD trans-membrane domains.
The human gene unique identifier, ID (from NCBI) is given in brackets.
*** Diseases with neurological involvement.**
****Disorders for which the cellular/mouse models were developed and studied in this Thesis.**

Table 2 *Main features of Ppt1, Cln5 and Ctsd mouse models*

Affected Gene	Mouse Model	Genetic Modification	Molecular Defect	Onset of neurological signs
Ppt1 (19063)	$Ppt1^{-}$ knockout	Ex. 9 neo cassette insertion	No enzyme activity	< 2 month
	$Ppt1^{\Delta ex.4}$	Ex. 4 deletion	No enzyme activity	< 4 month
Cln5 (211286)	$Cln5^{-/-}$ knockout	Ex. 3 neo cassette insertion	Deleted mRNA	13 weeks
Ctsd (13033)	$Ctsd^{-}$ knockout	Ex. 4 neo cassette insertion	No enzyme activity	3 weeks

Mus musculus **(house mouse) gene unique identifier, ID (from NCBI) is given in the brackets.**

1.2 CLN1 disease

Infantile neuronal ceroid lipofuscinosis (INCL, infantile Batten disease, or infantile CLN1 disease) (OMIM #256730) is an early form of NCL caused by defects in palmitoyl protein thioesterase-1 *(PPT1)* gene (Vesa et al., 1995). Mutations in *PPT1* also occur in childhood-, juvenile, and adult-onset forms (Van Diggelen et al., 2001). Mutations in *PPT1* are associated with GRODs and many of the CLN1 mutations are private but two mutations appear with greater frequency: c.364A>T/p.R122W is frequently found in patients of Finnish ancestry, and c.451C>T/R151* identified in a more global population of less defined ancestry. These two mutations represent about 20% each of the total abnormal CLN1 alleles. Recently, a structural basis for the effect of CLN1 mutants was presented showing that mutations associated with a total loss of enzymatic activity affect the core region of the enzyme, whereas less severe mutations are localized at the surface of PPT1 (Ohno et al., 2010).

The majority of patients harboring mutations in *PPT1* are diagnosed as infantile-onset NCL, with manifestations in the second half of the first year of life in the form of seizures, mental decay, loss of vision and brain atrophy. In patients with this NCL form, early development appears normal until 6–18 months of age. At onset, there is typically decreased tone and decreased social interaction followed by rapidly progressive psychomotor regression,

myoclonus, seizures, and visual failure. By 2 years of age, there is blindness with optic atrophy and macular and retinal changes but no pigment aggregation. Progressive brain atrophy is accompanied by a flat electroencephalogram. There is also early extinction on the electroretinogram. Seizures in INCL may not be as prominent as in later-onset forms. Ultimately, spasticity develops and patients become vegetative. Fewer cases are seen with onset of symptoms in later childhood (Simonati et al., 2009), adolescence (Pérez-Poyato et al., 2011) and even in adulthood (Ramadan et al., 2007). Regardless of the age at onset and clinical features, the presence of low-absent PPT1 activity and the ultrastructural evidence of GRODs are hallmarks of proteolipidic storage in all phenotype. The mechanism by which decreased PPT1 activity leads to the formation of GRODs remains to be clarified.

Soluble lysosomal enzyme PPT1 is responsible for cleaving long-chain fatty acid residues from cysteine residues on a multitude of protein targets. The *PPT1* transcript is ubiquitously expressed; the nascent PPT1 polypeptide contains 306 amino acids, including a 25-amino acid signal sequence which is co-translationally cleaved (Camp et al., 1994). Mature PPT1 migrates as a ~37/35 kDa doublet, and it is N-glycosylated at N197, N212, N232 in a manner essential for the activity, stability, and trafficking of the protein (Bellizzi et al., 2000; Camp et al., 1994; Das et al., 2001; Lyly et al., 2007).

The exact physiological function of PPT1 remains elusive, though lines of evidences indicate that in nerve terminals PPT1 is involved in regulation of endo/exocytosis synaptic vesicles recycling, and eventually neurotransmission (Kim et al., 2006). Palmitoylation, the lipidic post-translational modification in which PPT1 is involved, regulates intracellular trafficking and shuttling of proteins among different membrane organelles, particularly in neuronal cells (Fukata and Fukata, 2010).

Lack of PPT1 activity can be used for diagnosis, in this case non-degraded substrates accumulate in both CNS and systemic tissues. PPT1 is preferentially localized in cell soma and presynaptic terminals.

Two mouse models of infantile Cln1 disease (*Ppt1* NCBI Gene ID: 19063) were initially developed and are completely deficient in the enzyme activity (Gupta et al., 2001; Jalanko et al., 2005). More recently, a novel $Ppt1^{R151*}$ knock-in model has been produced (Miller et al., 2015). These models recapitulate many features of the human disease including progressive neurodegeneration, cortical thinning, brain atrophy, autofluorescent accumulation, retinal dysfunction, spontaneous seizures, motor deficits, and shortened lifespan. In addition, immunohistochemical staining for GFAP and CD68 showed reactive changes in astrocytes and microglia cell populations, respectively. Astrocytosis has been reported in almost all forms of human NCL (Haltia et al., 1973). This process mediates how neurons respond to injury, and may also influence neuronal function through direct effects upon the synaptic environment. There is growing evidence that the activation of astrocytes within the thalamus precedes neuronal cell loss (Bible et al., 2004). However, it is still unclear whether astrocytosis directly

affects neuronal cell loss in the cortex, or if it is a downstream consequence of the disease process.

Recent studies have outlined the spatial relationship between lysosomal engulfment and damaged mitochondrial reticulum in CLN1 fibroblasts, and have demonstrated that the mitochondrial compartment is affected in these cells *in vitro*. Abnormalities in the number, intracellular localization pattern and morphology of mitochondria, as well as defects in the mitochondrial enzyme activities and adaptive energy metabolism have been observed in patient fibroblasts. These results are in agreement with previous studies in palmitoyl-protein thioesterase 1-deficient (*Ppt1*$^{-/-}$) sheep, mice, and *Caenorhabditis elegans* (Das et al., 1999; Pezzini et al., 2011; Wei et al., 2011). Furthermore, a relationship between PPT1 interactome network and mitochondrial ATP synthesis-related proteins has been revealed in PPT1 expressing SH-SY5Y stable cells by proteome analysis (Scifo et al., 2015)

Proteome alterations in the brains of a *Ppt1*$^{-/-}$ mouse model and its wild-type age-matched counterpart were studied at different stages (pre-symptomatic, symptomatic and advanced): pre-symptomatic stage thalamus revealed alterations mostly in metabolic processes and inhibition of various neuronal functions, (i.e., neuritogenesis) while changes detected at the symptomatic stage included: mitochondrial functions, synaptic vesicle transport, myelin proteome and signaling cascades, such as RhoA signaling. Considerable dysregulation of processes related to mitochondrial cell death, RhoA/Huntington's disease signaling and myelin sheath breakdown were observed at the advanced stage of the disease.(Tikka et al., 2016).

Additional investigations on alterations of the mitochondrial compartment in neuronal cells could reveal new insights into the cell pathology of the severe CLN1 encephalopathy of childhood.

The expression of PPT1 in mouse brain preparations and cultured neurons parallels with the abundance of presynaptic marker protein and indicates a role for PPT1 in synaptogenesis implicated in the recycling of synaptic vesicles (Pezzini et al., 2017b). The difference in processing and trafficking of PPT1 between non-neuronal and neuronal cell types further highlights putative distinct functions of PPT1 in neurons (Lyly et al., 2007). Several studies found that changes in the levels of PPT1 expression correlated with the activation of caspase-mediated apoptotic pathways in neuroblastoma cells and lymphoblasts (Cho et al., 2000; Cho and Dawson, 2000), which appear to be caused by ER and oxidative stress (Kim et al., 2006; Zhang et al., 2006) PPT1 has been repeatedly associated with lipid metabolism. Post-mortem brain samples of CLN1 patients revealed changes in phospholipid content. Ceramide levels of lipid rafts have been reported to be decreased in Chinese hamster ovary (CHO) cells overexpressing PPT1 most likely due to the fact that PPT1 is involved in the processing of saposin D, a storage component in CLN1 disease, and involved in ceramide catabolism (Ahtiainen et al., 2006). Moreover, early infiltration of CD8(+) T-lymphocytes and an activation of microglia/macrophage-like cells associated with progressive degeneration and loss of retinal ganglion cells was seen in the *Ppt1*$^{-/-}$ mice model (Groh et al., 2013).

Proteomic evidence suggests a novel link between PPT1 deficiency, palmitoylated proteins and cilia organization. The analysis revealed a difference in the distribution and levels of some Rab family of proteins in the retina of mutant mice versus the wildtype, which may be important in the early neurodegenerative phenotype Palmitoylation of these proteins regulates ciliogenesis and is required for their cellular localization. Indeed, an unbiased proteomics analysis on isolated cilia revealed 660 proteins, which differed in their abundance levels between wild type and knock out Ppt1 (Segal-Salto et al., 2016).

Several therapeutic strategies including enzyme replacement, gene therapy, stem cell-mediated therapy, and small molecule drugs have resulted in minimal to modest improvements in the murine model of Ppt1-deficiency. However, more recent studies using various combinations of these approaches have shown more promising results; in some instances, more than doubling the lifespan of Ppt1-deficient mice. These combination therapies that target different pathogenic mechanisms may offer the hope of treating this profoundly neurodegenerative disorder (Hawkins-Salsbury et al., 2013).

1.3 CLN5 disease

In Italy, CLN5 patients represent about 6% of all molecularly diagnosed patients (Santorelli et al., 2013), not taking into account adult presentation (Mancini et al., 2015). In childhood, the disease exhibits a relatively slowly progressive course, behavioral and cognitive domains being affected at onset. Survival studies suggest death usually occurs during the second-fourth decades.

Diagnosis is supported by ultrastructural analysis and confirmed by mutation testing (Anderson et al., 2013; Radke et al., 2015).

The "non-enzymatic" CLN5 disease (MIM 256731) represents a rare form of NCL originally identified as causing a so-called Finnish variant of late infantile NCL. The. *CLN5* gene encodes a soluble, as yet uncharacterized, lysosomal glycoprotein which seems to be involved in endocellular trafficking at ER, Golgi and Endosome levels and it is involved in controlling the itinerary of the lysosomal sorting receptors by regulating retromer recruitment at the endosome likely because of the possible interactions with other NCL proteins *in vitro.*

Human CLN5 is built up from 407 amino acids and has a molecular mass of about 59-60 kDa, with an N-terminal signal sequence that is cleaved after entering the ER. CLN5 is a soluble protein that localizes to the lysosomal compartment. Its localization has been confirmed by several co-localization studies using anti-lysosome associated membrane protein 1 (LAMP1) antibodies in cells overexpressing CLN5. The major post-translational modification in CLN5 is an N-glycosylation. It has been shown that there are eight putative N-glycosylation sites in CLN5 that are utilized *in vivo*, and that mutations in these sites could affect folding, trafficking or lysosomal function(s) (Moharir et al., 2013). CLN5 has been suggested to interact with

other NCL proteins in COS-1 cells overexpressing PPT1, CLN3, CLN6 and CLN8 and in the same cells with endogenously expressed TPP1 (Lyly et al. 2009; Vesa J, et al. 2002).

CLN5/Cln5 mRNA has been detected mostly in human and mouse brain but also in peripheral organs (Holmberg et al., 2004). *Cln5* mRNA expression is particularly high in the cerebral cortex, cerebellum, and in the ganglionic eminence of the embryonic mouse brain. In the postnatal mouse brain, expression of the *Cln5* is prominent in cerebellar Purkinje cells, cortical neurons, hippocampal pyramidal neurons, and hypothalamic neurons.

Although the CLN5 cellular function remains unknown, its interaction with other NCL proteins has been suggested. Recent studies identified interactor partners of CLN5 including mitochondrial carriers and interactors implicated in protein folding/sorting proteins and some of those are shared with other NCL proteins. Thirty-one interactors of CLN5 were identified including 18 proteins shared with CLN3 (Scifo et al., 2013).Thus, there are evidences that NCL proteins are essential components of a common pathway and that they may interact at multiple locations (Scifo et al., 2013). Little is known about energy production in CLN5 disease; low energy metabolism has been recently hypothesized (Staropoli et al., 2012). A component of the storage is the subunit c of mitochondrial ATP synthase (SMACS), a characteristic shared with most NCLs unrelated to an enzymatic deficit.

Murine Cln5 has a prominent homology to human CLN5; *Cln5* KO mouse develops typical symptoms of an NCL disease (Holmberg et al., 2004; Kopra, 2004). Loss of *Cln5* in mice leads to defective myelination *in vitro* and in the developing brain; this is accompanied by a defective sphingolipid transport (Schmiedt et al., 2012). In double KO mice (*Cln1/5* double-KO) comparative gene expression profiling in brain has suggested common defective pathways linked to neuronal growth cone stabilization (Blom et al., 2013). It has also been observed a pronounced accumulation of autofluorescent storage material, and an alteration in lipid metabolism (specific increase in plasma phospholipid transfer protein activity) with prominent downregulation of α-synuclein in mouse brains. Similar to mouse brain, CLN5-deficient skin fibroblast cells manifest increased apoptosis with very low ceramide levels.

The high relative expression level of CLN5 in CNS neurons and microglial cells (Holmberg et al., 2004; Schmiedt et al., 2012) as well as the defective myelination in the brain of $Cln5^{-/-}$ mice and late infantile CLN5 disease patients indicate the particular importance of CLN5 function in the brain. Loss of CLN5 function can lead to selective neurodegeneration in multiple ways: it may directly affect neuronal viability, it could cause abnormal microglial activation leading to neurotoxicity, and finally it definitely causes dysfunction of oligodendrocytes resulting in hypo-myelination that can disrupt axonal signal propagation leading to synapse loss and eventually axonal and neuronal degeneration.

Recent study demonstrated an increased hippocampal neurogenesis in Cln5-deficient mice, related to the increased proliferation of cells but not to changes in hippocampal. Increased neurogenesis is associated with high levels of pro-inflammatory cytokine interleukin 1 beta (IL-

1β) in the diseased brains, and alterations to IL-1β signaling in neural stem/progenitor cells (NPCs) *in vitro* (Savchenko et al., 2017)

Neither animal models nor cell lines investigations have provided convincing support for targeted therapies in CLN5.

As in other variant forms, therapies are lagging behind because of limited knowledge on protein function and a full understanding of pathological mechanisms underlying NCL proteins is critical for designing effective therapeutic approaches for this devastating neurodegenerative disorder.

1.4 CLN10 disease

CLN10 disease is an autosomal recessive congenital disorder due to mutations in the *Cathepsin D (CTSD) gene* encoding the lysosomal enzyme Cathepsin D (CTSD).

CTSD is ubiquitously expressed in most mammalian tissues whereas in the retina it is mostly expressed in the pigment epithelium, ganglion cells, and Müller cells (Whitaker and Rhodes, 1983). This lysosomal enzyme belongs to the pepsin family of proteases and is one of the major lysosomal aspartic protease which thought to be important for neuronal stability (Siintola, 2006; Steinfeld et al., 2006). It is also known that mature cathepsin D is involved in autophagy and plays a crucial role in the control of cell and tissue homeostasis.

The synthesis of CTSD occurs in the ER as a pre-pro-peptide with a molecular mass of ~50 KDa. The cleavage of the leader peptide in the ER generates the 48 kDa form, precursor of mature-CTSD (CTSDpro). In the Golgi complex, attachment of mannose 6-phosphate (M6P) moieties to CTSDpro facilitates its binding to endosomal/lysosomal sorting receptors. The receptor-ligand complexes then exit the trans-Golgi network (TGN) in clathrin-coated intermediates and fuses with the endosomal system. The low pH of the late endosomal lumen facilitates dissociation of the receptor-ligand complexes and allows the ligand (i.e. pro-CTSD) to be delivered to lysosome. The CTSDpro then undergoes further proteolytic cleavage by cathepsin B and cathepsin L, which generates the 31 kDa and 14 kDa fragments, respectively, and their non-covalent dimerization constitutes the mature, catalytically active-CTSD (CTSDm).

The mature form of human CTSD is composed of two polypeptides interlinked by disulphide bridges. Aspartic acid residues contained on both polypeptides are essential for the enzymatic activity of the protein (Metcalf and Fusek, 1993; Rawlings and Barrett, 1995). The consequences of CTSD mutation on the expression, proteolytic activity or cell processing of the enzyme in the development of CLN10 disease have been largely discussed (Cárcel-Trullols et al., 2015).

CLN10 disease is mainly characterized as congenital NCL and affected infants do not survive the first week of life. Seldom there are presentation in childhood whereas early infantile onset

associated with mutations in *CTSD* has been reported once (Doccini et al., 2016). Clinical expression of CLN10 disease is characterized (in the congenital form) by primary microcephaly, neonatal (possibly already intrauterine) epilepsy, respiratory insufficiency, and rigidity. The pathological correlate was GRODs (Steinfeld et al., 2006).
Diagnosis is based on clinical presentation and enzymatic testing in fibroblasts or blood. Genetic testing for mutations in *CLN10* is also available
Lysosomal CTSD activity catalyzes degradation and clearance of exogenous as well as endogenous macromolecules and damaged organelles delivered to the lysosomes. Intracellular accumulation of undigested long-lived proteins and other macromolecules underlies the pathogenesis of several neurodegenerative disorders.
CTSD has been tightly related to apoptosis and autophagy also mediating cytochrome c release and caspase activation during staurosporine-induced apoptosis in human fibroblasts (Johansson et al., 2003). CTSD is a major component of lysosomes and functions as a highly active endopeptidase with an optimum pH between 3.0 and 5.0, playing an obvious role in the degradation and turnover of cellular components. Several studies have reported dysfunctions in macroautophagy in CTSD deficiency, showing accumulation of autophagosomes (Koike et al., 2000) or accumulation of autofluorescent storage material and increased levels of LC3-II (Shacka et al., 2007) in neurons of Ctsd-deficient mice.
These two major functions of CTSD in apoptosis and macroautophagy are closely related and CTSD has been suggested to promote apoptosis upon its translocation to the cytosol.
Cross-talk among CTSD and other NCL proteins has been identified by Chandra et al. (Chandra et al., 2015). *Ppt1* disruption in mice suggests that lysosomal CTSD deficiency is a common pathogenic link between INCL, due to inactivating mutations in *PPT1* and congenital NCL (CNCL), due to mutations in *CTSD*.
Ctsd overexpression is mediated by upregulation of TFEB and predominantly occurs in astrocytes and microglia of $Ppt1^{-/-}$ mice. Similar to the effects of inactivating mutations in *CTSD*, which cause CNCL, lack of *Ppt1* impaired lysosomal degradative function and subsequent Ctsd lysosomal maturation leads to deficiency of catalytically active Ctsd.

1.5 CRISPR-Cas9 system.

CRISPR/Cas9 system, represents the alternative to the current protein-based targeting methods like Zinc-finger nucleases (ZFNs) and transcription activator-like effector nucleases (TALENs) specifically used to target a gene or other DNA sequence.
In prokaryotes CRISPR/Cas system confers resistance to foreign genetic elements such as plasmids and phages.

While there are many bacterial and archaeal CRISPR-Cas systems that have been identified, the mechanism and key components of the *Streptococcus pyogenes* Type II CRISPR/Cas9 system have been well characterized.

In the acquisition phase, foreign DNA is incorporated into bacterial genome as a short sequences (~20bp) separated by a short palindromic repeat and kept like a record against future encounters (a sort of acquired immunity).

CRISPR-Cas systems are composed of a set of Cas genes involved in acquisition of the foreign genetic information, crRNA expression and processing and interference

During interference, the endonuclease Cas9 cleaves the DNA guided by two required small RNA sequences: the CRISPR RNA (crRNA), which binds the target DNA and guides cleavage, and the trans-activating crRNA (tracrRNA), which facilitates the processing of the crRNA array (Ran et al., 2013)

This system has been subsequently modified and adapted for genome engineering in mammalian cells for example fusing together crRNA and tracrRNA to create a chimeric, single-guide RNA (sgRNA).

Unlike ZFN and TALEN techniques which are based-on protein-DNA interactions for targeting, CRISPR/Cas9 system use simple, base-pairing rules between an engineered RNA and the target DNA site. It is easily customizable and has a higher targeting efficiency and ability to facilitate multiplex genome editing.

Although, modifications to the Cas9 enzyme have extended the application of CRISPR to a wide range of different approaches (e.g. gene activation, genome-wide screening), the main use concerns the generation of stable knock-out (KO) cell lines.

In general, the generation of KO *in vitro* models by CRISPR/Cas9 system, required the identification of a genomic target of ~20 nucleotide DNA sequence, which must be unique compared to the rest of the genome and immediately upstream of a Protospacer Adjacent Motif (PAM) which is a very short sequence (about 3 nucleotide), different for each CRISPR system used.

Once expressed, the Cas9 protein and the gRNA form a riboprotein complex which bind any genomic sequence with a PAM, but only when the gRNA spacer matches the target DNA the cut by Cas9 can occur.

In a Non-Homologous End Joining (NHEJ) pathway, the resulting double-stranded breaks (DSBs) is rapidly repaired but frequently results in random insertion/deletion or frameshift mutation leading to premature stop codons of the targeted gene with consequent loss-of-function and generation of knock-out

On the other hand, Homology Directed Repair (HDR) can be used to generate specific nucleotide changes and can be used to generate knock-in models even if it is less efficient.

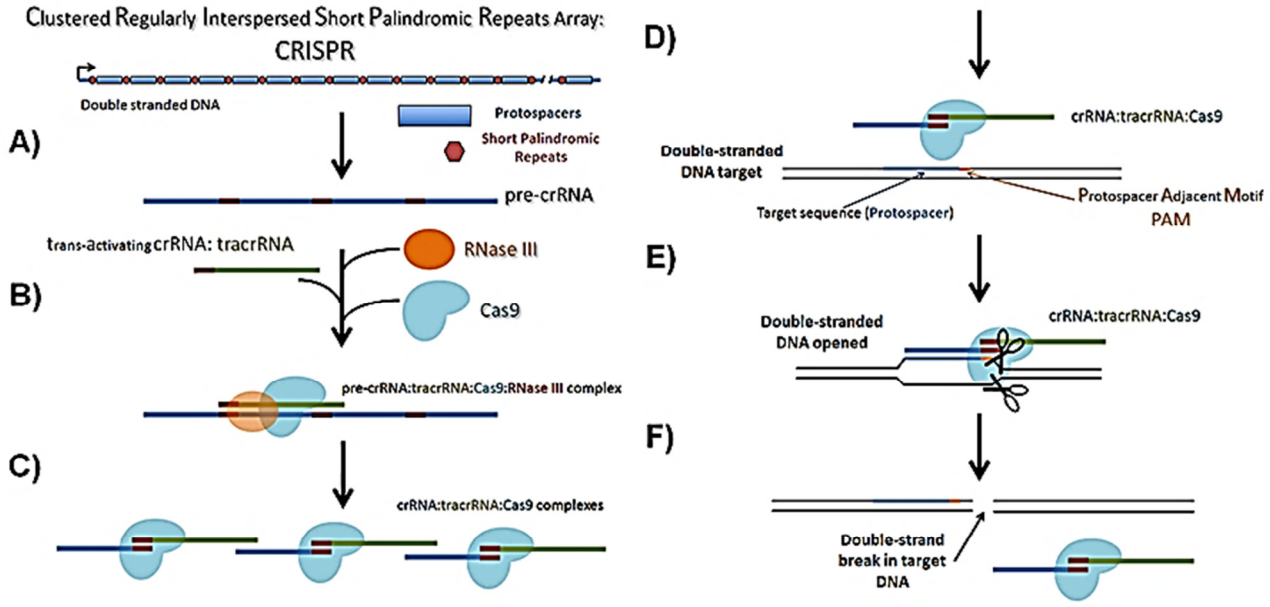

Figure 1 *Overview of the endogenous Type II bacterial CRISPR/Cas system. Within the bacterial genome, a CRISPR array contains many unique protospacer sequences that have homology to various foreign DNA (e.g. viral genome). Protospacers are separated by a short palindromic repeat sequence. (A) The CRISPR array is transcribed to make the pre-CRISPR RNA (pre-crRNA). (B)The pre-crRNA is processed into individual crRNAs by a special trans-activating crRNA (tracrRNA) with homology to the short palindromic repeat. The tracrRNA helps recruit the RNAse III and Cas9 enzymes, which together separate the individual crRNAs. (C) The tracrRNA and Cas9 nuclease form a complex with each individual, unique crRNA. (D) Each crRNA:tracrRNA:Cas9 complex seeks out the DNA sequence complimentary to the crRNA. In the Type II CRISPR system a potential target sequence is only valid if it contains a special Protospacer Adjacent Motif (PAM) directly after where the crRNA would bind. (E) After the complex binds, the Cas9 separates the double stranded DNA target and cleaves both strands after the PAM. (F) The crRNA:tracrRNA:Cas9 complex unbinds after the double strand break.* http://www.addgene.org

The generation of KO cell lines by CRISPR/Cas9 occurred through the following basic steps which will be analyzed and discussed in the following sections:

- target selection for sgRNA,
- plasmid design,
- transient transfection of plasmids into model cells,
- proper selection of clones that have successfully been modified by CRISPR nucleases,
- verification of the genomic modification in transfected cells by sequencing methods,
- verification of a gene knockout by Western blotting (WB) analysis using a specific antibody.

2. AIMS

The overall aim of this research project was to investigate the cellular and molecular mechanisms underlying three different forms of NCLs. In this work, we proposed new experimental approaches for the identification of potential modifier factors and biomarkers with possible clinical and therapeutic implications.

Different disease-models were developed and used in order to improve NCL genotype/phenotype characterizations, by monitoring bioenergetic processes, autophagy and lysosomal dysregulation in the pathogenesis of the disease.

The reasons to investigate CLN1, CLN5, and CLN10 disorders are three-fold. First, both CLN1 and CLN5 are relatively frequent among the Italian NCL cohort and the molecular pathogenesis is less clear than other forms such as CLN3 and CLN6. Second, the Center where this work was largely undertaken (Molecular Medicine - IRCS Fondazione Stella Maris – Pisa) is part of the CLNet, a nationwide network of child neurology units and has specific expertise in the clinical, pathological, and molecular definition of affected children. Third, the exciting identification of an early infantile onset of CLN10 disease associated with a novel mutation in CTSD allowed us to further investigate the biochemical, ultrastructural and molecular features of the disease.

Even if the NCL represent rare pediatric diseases, the new knowledge about the role of autophagy and impaired mitochondrial function gained in this project could have an important impact on pathogenic processes involved in neuronal injury and on the of the "lysosomal" pathogenesis increasingly involved in the most frequent neurodegenerative diseases

Thus, the specific objectives of this PhD work were:

- to recognize molecular signatures and functional modules connected with over-expressed CLN1 in a human neuronal cellular system. We utilized SH-SY5Y neuroblastoma cells (differentiated into a neuronal-like phenotype as in Pezzini et al., 2017) to overexpress wtCLN1 and a selection of disease related mutations previously detected in CLN1-affected children. The differentiated cell lines underwent whole transcriptomic profiling by RNA-seq, to identify differentially expressed genes (DEGs) functionally related to the overexpression of wild-type or mutated PPT1.
- to investigate the role *in vitro* of CLN5p (the product mutated in variant late infantile subtype of NCL, vLINCL-CLN5) at lysosome and mitochondrial level. By an organelle-specific analysis, we studied differential proteome profile in health and disease conditions to outline protein pathways involving CLN5p and its function within the intricate NCL molecular network. For this study, we developed a knock-out CLN5 HEK293T model, by adopting the CRISPR/Cas9 technology. The high replicative capacity of HEK293 genetic background made it possible to obtain sufficient amount of cell material and fractionate lysosomal and mitochondrial

compartments for a more targeted and accurate detection of the different degrees of protein expression.

Using the same methodology developed for HEK293T cell lines, we also generated a tissue specific SH-SY5Y CRISPR CLN5 KO model. Human neuroblastoma cells (SH-SY5Y) represent an excellent *in vitro* system and provide an invaluable experimental tool for investigating the molecular pathophysiology of NCL disorders in neuronal-like cells. In this regard, SH-SY5Y are also valuable because of unlimited proliferation and the ability to differentiate. Furthermore, both cellular systems offer an opportunity to develop *in vitro* pharmacological treatments, to modulate mitochondrial functions.

For a deeper characterization of the cellular features CLN5 disease-related, we also analyzed the organelle-specific proteome in murine brains derived from *Cln5*$^{-/-}$ and wild-type siblings.

A label-free quantitative LC-MS^{E} approach for proteome analysis enabled a highly reproducible detection of the different degrees of protein expression

– to characterize at the cellular level a novel mutation in *CTSD* associated with early infantile onset of NCL. We investigated genetic and biochemical features of a predicted, likely CTSD function damaging mutation and its relation to mechanisms implicated in the disease mechanisms i.e. autophagy, lysosomal alterations and ultrastructural abnormalities. The possibility that defect in CTSD maturation process lead to alterations in *PPT1* mRNA expression levels was also evaluated.

3. MATERIAL AND METHODS

3.1 Cell cultures

- Primary culture of human fibroblasts from:

CLN5 patients carrying different mutations in CLN5:

c.788T>A/p.V263Q

c.335G>A/p.R112H

c.595C>T /p.R99*.

CLN10 patients' derived fibroblasts were obtained from punch biopsies of the affected individuals, described in (Doccini et al., 2016).

Human fibroblasts collected according to standard procedures from diagnostic skin biopsies Primary fibroblast cell lines were grown at 37 °C with 5% CO_2 in Dulbecco's modified Eagle's medium (DMEM), containing 10% fetal bovine serum (FBS), 4.5 g/L glucose and 1% antibiotics/antimycotics.

- Stable *CLN1* transfected clones replicating mutations described in Mediterranean patients affected by classical and variant CLN1 disease. Specifically, we investigated the wtPPT1 overexpressing cell line (SH-p.wtCLN1), three cell lines carrying a missense mutation (c.665T>C/p.L222P, c.541G>A/p.V181M and c.541G>T/p.V181L), a mutation leading to premature protein truncation (c.169dupA/p.M57Nfs*45), a deletion of exon 2 in which an open reading frame (ORF) is maintained (c.125_235del/p.G42_E78del). An empty vector transfected cell line (mock) and parental SH-SY5Y cells were also analyzed as a reference.
  Stable CLN1 cell lines (except for the parental line) were cultured in presence of 600 µg/ml G-418 (Geneticin, Euroclone).
- Neuroblastoma cell line SH-SY5Y (ATCC®) and derived CRISPR KO and control clones were cultured in MEM/F12 1:1 with 10% FBS, 2mM L-glutamine, 1% penicillin/streptomycin.
- HEK293T cell line (ATCC®) and derived CRISPR KO and control clones were cultured in DMEM containing 10% FBS, 4.5 g/L glucose and 1% 1% penicillin/streptomycin, and supplemented with L-glutamine to achieve a final concentration of 6mM.

3.2 Generation of stable *CLN1* transfected clones and neuronal differentiation

Molecular analysis and transfection of neuroblastoma cells were performed in collaboration with the Unit of Molecular Medicine of Children Hospital "Bambino Gesù", Roma.

Transient transfection of wt and mutated cDNAs was performed in SH-SY5Y cells. Wild-type and mutated *PPT1* cDNAs (NM_000310) were inserted into pcDNA3 expression vector (Invitrogen, Life Technologies, LT) by PCR methods. The sequences of PPT1 constructs were confirmed by direct sequencing. SH-SY5Y cells were plated one day before transfection at 80% confluence in 35mm dishes, and then transfected with 250ng of cDNAs per dish using lipofectamine method (Applied Biosystems, LT) following the manufacturer's instructions. At 70-80% of confluence, cells were trypsinized and seeded at lower concentration (about one tenth). Clones which stably overexpressed the different *PPT1* cDNAs were finally isolated through antibiotic selection with 600 µg/ml geneticin (G418, Gibco, LT). Cells overexpressing the empty pcDNA3 vector (hereafter also referred as mock) served as a control.

For neuronal differentiation, we set up a 9 days long paradigm (hereafter referred as RA-NBM treatment) consisting of 2 phases: a 6 days pre-differentiation step in basal medium with 5% FBS and 10 µM all trans Retinoic Acid (RA, Sigma Aldrich) followed by a 3 days differentiation step in neurobasal medium (GIBCO, Life Technologies), enriched with 50ng/ml recombinant human BDNF (rhBDNF, Peprotech), 2 mM dibutyril-cyclic AMP (dbcAMP, Sigma Aldrich), B27 Neuromix (Euroclone), 20mM KCl, 1% L-glutamine (NBM).

Briefly, 5E+03cells/cm^2 were seeded in flasks, or alternatively, on coverslips previously coated with ECMax gel (Sigma Aldrich), allowed to adhere for 24-48 hours and then exposed to basal or conditional media. Media were routinely changed every 2-3 days and the morphological features of the cultures were checked by phase contrast microscopy.

3.3 Generation of CLN5 KO cell lines using CRISPR/Cas9 system

3.3.1 CLN5 CRISPR guide RNA

The CLN5 CRISPR sgRNA sequences were designed in order to efficiently target the *CLN5* gene with minimal risk of off-target Cas9 binding elsewhere in the genome. For complete details on the criteria and process for sgRNA design and selection, please see Sanjana, Shalem, & Zhang, 2014.

Theoretically a sgRNA construct is sufficient to knock-out a gene of interest, however, to increase a chance of success we selected at least three gRNA constructs per gene.

Table 3 *CLN5 target sequencing and guide RNAs*

sgRNA	target sequence	top and bottom strand for cloning	***CLN5*** **exon**
CLN5 CRISPR Guide RNA 1	5′- CATGCGCCGGAACCTGCGCT -3′	5′- CACCCATGCGCCGGAACCTGCGCT -3′ 3′- GTACGCGGCCTTGGACGCGACAAA -5′	1
CLN5 CRISPR Guide RNA 2	5′- GCGCCTTGATTACACCAGAA -3′	5′- CACCTTCTGGTGTAATCAAGGCGC -3′ 3′- AAGACCACATTAGTTCCGCGCAAA -5′	3
CLN5 CRISPR Guide RNA 3	5′- CATCCATTTCAGGTCGGAGA 3′	5′- CACCTCTCCGACCTGAAATGGATG -3′ 3′- AGAGGCTGGACTTTACCTACCAAA -5′	3

3.3.2 Cloning

We created construct carrying plasmid expression vectors, by using the pSpCas9(BB)-2A-Puro V2.0 plasmid (Addgene Plasmid #62988) backbone, developed for CRISPR/Cas9 purposes and subsequent insertion of the sgRNA sequences.

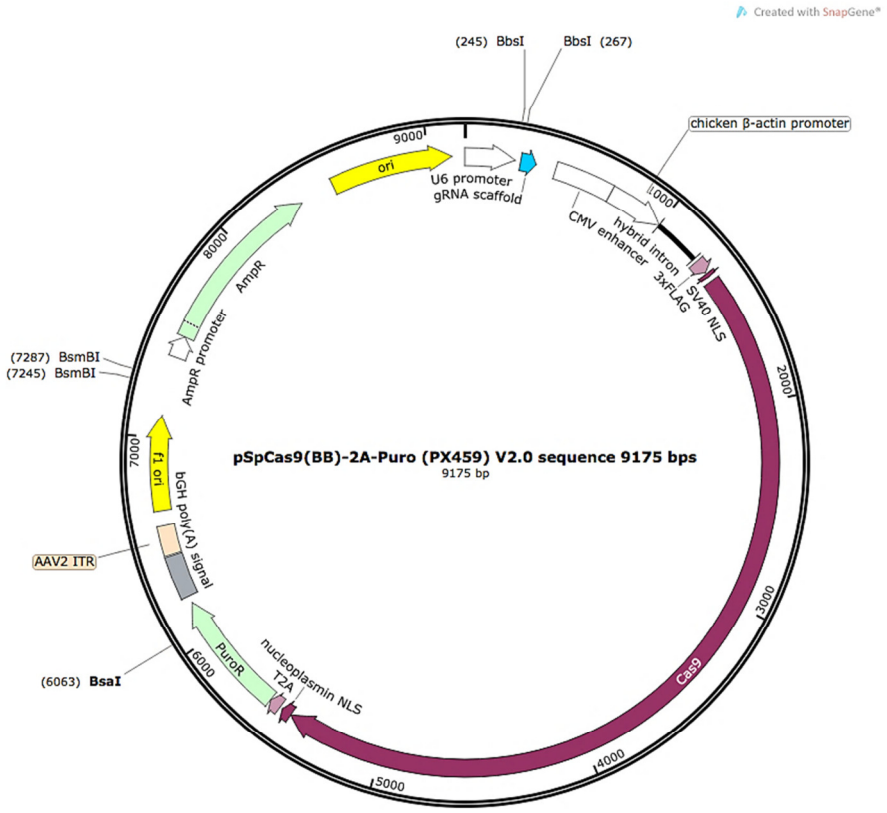

Figure 2 *Addgene pSpCas9(BB)-2A-Puro plasmid map (created with SnapGene http://www.snapgene.com)*

pSpCas9(BB)-2A-Puro V2.0 vector was linearized using restriction endonuclease BbsI (New England Biolabs); and gel purified using Gel Extraction kit (Qiagen).

To insert the sequence inside the plasmid, top and bottom strands of oligos for each sgRNA were phosphorylated by T4 polynucleotide kinase (New England BioLabs) and annealed in a thermocycler.

Ligation reaction by T4 DNA ligase (New England BioLabs) allows the site-specific incorporation.

Plasmid-Safe™ ATP-Dependent DNase (Epicentre- Illumina) selectively removes contaminants from ligation reaction by digesting each linearized DNA fragment. The plasmid was than transformed into a competent *E. coli* strain (One Shot Stbl3 Chemically Competent *E. coli*; Invitrogen). Plasmid replicates in cells expressing ampicillin resistance.

Cells were thenplated on selective LB agar plates; few colonies were subsequently picked up to isolate the plasmid DNA (QIAprep® spin miniprep Kit; Qiagen). To check for the correct insertion of a guide construct (annealed top and bottom strand of sgRNA), U6 plasmid fragment was amplified and sequenced.

Like cells model for transfection has been used the HEK293T cell line that expresses a mutant version of the SV40 large T antigen to facilitate amplification of transfected plasmids and extended temporal expression of desired gene products. This makes them particularly suitable for retroviral production, gene expression and protein production.

We also replicated the method in SH-SY5Y cell line

3.3.3 Transfection

HEK293T and SH-SY5Y cell lines were transfected by Lipofectamine 3000 (Invitrogen) following the standard protocol.

The transfected cells will encode for the Cas9 nuclease and use the sgRNA as a template to drive the DSB on genome DNA.

One-day post transfection, the cells were grown in regular media supplemented with puromycin (2 or 5ug/mL for HEK293T and SH-SY5Y respectively) for 48-72 hours in order to select the cells, which have incorporated the exogenous DNA. A parental cell line was treated in puromycin under the same condition in order to drive the treatment time. When 100% of parental cells is not viable due to puromycin effect the antibiotic selection can be stopped, and cells that survived are those which incorporated the plasmid.

Transient overexpression by standard transfection protocol resulted in the more suitable option since the lack of integration of the plasmid DNA with the genomic one prevents long-term expression of CRISPR components and potential accrual of off-target cleavages in long-term culturing.

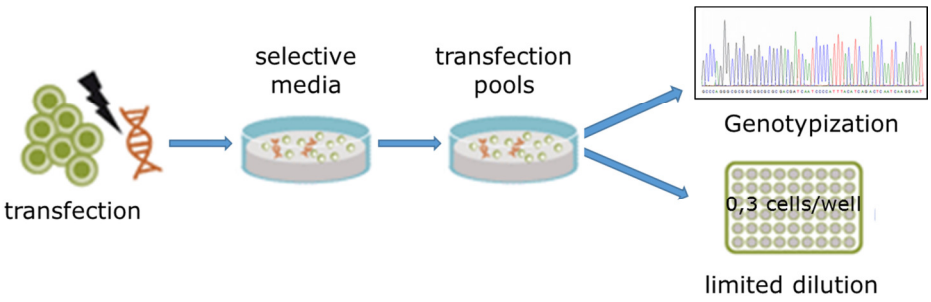

Figure 3 *Genome editing by CRISPR/Cas9 system: post-transfection steps*

Tracking of Indels by Decomposition (TIDE) web tool, an assay to accurately characterize and quantify the induced mutations, was used to assess genome editing events. Using the quantitative sequence trace, and data from two standard capillary sequencing reactions, TIDE software quantified the editing efficacy and identified the predominant types of insertions and deletions (indels) in the DNA of a targeted cell pool (Brinkman et al., 2014). Furthermore, a WB analysis for the target protein was performed, to correlate the genotype modifications with protein expression.

Once evaluated for the overall editing efficiency, the transfection pools was used to isolate single clones by "limiting-dilution technique"; cells suspension was diluted and plated at a density of 0.3cell/well (in a 96 multi-well plate) to allow convenient tracking of wells that contain only one cell.

3.3.4 Verification of the genomic modification of clones

Genotypes and phenotypes of clones grown in wells under regular conditions (grown-time ≅ 3 weeks), were verified by standard sequencing methods and WB analyses respectively. The edited clones with lack of protein expression were expanded for downstream applications.

As a result, generated CRISPR KO cell lines could be considered stable and capable to grow like the parental cells.

3.4 *Cln5*$^{-/-}$ mouse model and tissue collection

All the experiments were approved by the national Animal Experiment Board of Finland and followed the animal protection guidelines of the Council of the European Union.

Animals involved in this study were made available by the Institute for Molecular Sciences, University of Eastern Finland, Kuopio (collaboration with Adj. Professor Katja Kanninen).

A total of 30 male and female homozygous *Cln5*$^{-/-}$ mice and, age matched wild-type littermates were used in this study. We focused our analyses on pre-symptomatic (3 months) and symptomatic stages (9 months) of disease. A complete list of sacrificed mice is reported in the supplementary table S1.

Homozygous mutant *Cln5*$^{-/-}$ mice were generated on a mixed C57BL/6Jx129SvEv strain background as described previously in Jalanko et al., 2005; Kopra, 2004, and subsequently backcrossed for three generations with C57Bl/6 controls to produce the mice used in this study.

Mice were not pre-treated by transcardial perfusion. Before sacrifice, they were anesthetized with tribromoethanol (Avertin, Sigma-Aldrich, St. Louis, MO, USA), and the brains were dissected under a stereotactic microscope. For each set of mice cerebral cortex area was isolated, weighed and maintained on ice until mitochondrial and lysosomal fraction separation.

3.5 Oxygen consumption rate measurements

Oxygen consumption rate (OCR) was measured in HEK293T and SH-SY5Y CRISPR CLN5 KO cell lines (together with their respective empty-vector transfected cell lines used as control lines), using an XFe24 Extracellular Flux Analyzer (Seahorse Bioscience, Agilent, CA, USA). Each control and mutant cell line was plated in XF 24-well cell culture microplates at a density 6E+05 cells/well in 250µL of normal culture media, and incubated for 24h at 37 °C in 5% CO_2 atmosphere. After replacing the growth medium with 500µL of XF media (non-buffered DMEM medium, containing 10mM glucose, 2mM pyruvate, 2mM glutamine; pH 7.4), pre-warmed at 37°C cells were preincubated for 30 min. before starting the assay procedure. After baseline measurements, OCR was measured after sequentially adding to each well oligomycin and carbonyl cyanide 4-(trifluoromethoxy)phenylhydrazone (FCCP) to reach a working concentration of 1µg/ml and 1.5µM. We evaluated the fraction of non-mitochondrial oxygen consumption, by measuring OCR after complete inhibition of the mitochondrial respiratory chain by a mix of antimycin A and rotenone, both at a concentration 0.5µM (all chemical from Sigma Aldrich, MO, USA) (Invernizzi et al., 2012).

Plates were normalized post-assay by CyQUANT Cell Proliferation Assays (Thermo Fisher Scientific, MA, USA) based on DNA content and analyzed using Seahorse Bioscience Report Generators.

The mean+SEM values of at least three independent experiments are presented. Statistical comparison of the data sets was performed using Student's t-test. The measured differences are presented with the corresponding statistical significance.

Table 4*Cell Mito Stress protocol optimized for HEK293T and SH-SY5Y cell models*

Seahorse XFe24 Analyzer	**XF Cell Mito Stress**
Injection Strategy	Port A: Oligomycin Port B: FCCP Port C: Rotenone + antimycin A Port D: N/A
Assay Media	XF Base Medium Supplement with: 10 mM glucose 2 mM sodium pyruvate 2 mM glutamine, pH 7.4
Initial Assay Volume	500 µL
Cell Seeding Density	60000 cells/well
Instrument Protocol	Include 2 min Wait time Calibrate Equilibrate Basal: 4 cycles - 3 minute Mix, 2 minute Wait, 3 minute Measure Inject Port A (followed by 3 cycles) - 3 minute Mix, 2 minute Wait, 3 minute Measure Inject Port B (followed by 3 cycles) - 3 minute Mix, 2 minute Wait, 3 minute Measure Inject Port C (followed by 3 cycles) - 3 minute Mix, 2 minute Wait, 3 minute Measure

3.6 Functional mitochondrial assay

ATP levels were measured using the Luminescence ATP Detection Assay System (ATPlite one step, PerkinElmer Life Sciences). Cultured fibroblasts were seeded in a 96-well plate (1 x 104 cells/well density) and incubated in 10% FBS/DMEM medium for 48h. After discarding the medium, cells were washed with ATP record buffer (156mM NaCl, 3mM KCl, 2 mM MgSO4, 1.25mM KH_2PO4, 2mM $CaCl_2$, 20mM HEPES, pH 7.35) and incubated for 2h in buffer supplemented with 10 mM glucose for an estimate of total ATP production, or 5 mM 2-deoxy-D-glucose plus 5 mM pyruvate to block glycolytic ATP production and evaluation of the mitochondrial ATP content (McKenzie et al., 2007).

The cells were then incubated with the luciferin/luciferase reagent, and samples ATP content was measured using an Orion L Microplate Luminometer (Berthold Detection Systems GmbH).

Data were normalized by CyQUANT Cell Proliferation Assays (Thermo Fisher Scientific, MA, USA) based on DNA content.

The statistical representation of the data was performed as described in **3.5.**,

3.7 Proteome analyses

3.7.1 Cellular fractionation methods

Fractionation methods for the isolation of single cellular compartments, allow targeted and organelle-specific proteome analysis reducing the complexity of samples and represent a powerful strategy for the discovery of modifying factors involved in specific disease.

Mitochondrial fraction preparation

Isolation of mitochondrial fractions from HEK293T cell lysate and mice cerebral cortex, were performed using Qproteome Mitochondria Isolation Kit (Qiagen) according to manufacturer instructions.

A pellet from about 1E+07 HEK293T cells (collected without using trypsin) or 40 mg of fresh cerebral cortex homogenized tissue were suspended in provided lysis buffer, which selectively disrupts the plasma membrane without solubilizing it, resulting in the isolation of cytosolic proteins.

Plasma membranes and compartmentalized organelles, such as nuclei, mitochondria, and the ER, remain intact and were pelleted by centrifugation. The resulting pellet was suspended in provided disruption buffer, repeatedly passed through a narrow-gauge needle (to ensure complete cell disruption), and centrifuged to pellet nuclei, cell debris, and unbroken cells.

The supernatant containing mitochondria and the microsomal fraction was centrifuged to yield mitochondria.

For high-purity preparations, the mitochondrial pellet was suspended in Mitochondria Purification Buffer and carefully pipetted on top of layers of Purification Buffer and Disruption Buffer. During a subsequent separation, mitochondria migrated through the liquid to form a band towards the bottom of the tube. The band was removed and the high-purity mitochondrial fraction was further pelleted and snap-frozen in liquid nitrogen.

Mitochondrial protein solubilization was carried out by suspending the pellet in a proper volume of lysis buffer (7M urea, 2M thiourea, 4% CHAPS and protease inhibitors).

The protein concentration was determined using bicinchoninic acid (BCA) assay.

Lysosomal Protein Preparation

Isolation of lysosomal fraction from HEK293T cell lysate and mice cerebral cortex, was performed by Lysosome Enrichment Kit for Tissue and Cultured Cells (Thermo Scientific) according to manufacturer instructions.

A HEK293T cells pellet obtained (harvested without using trypsin) from about 4 confluent F75 flasks or 150mg of fresh cerebral cortex homogenized tissue were lysed. Plasma membranes and nuclei were pelleted by centrifugation and discarded. The resulting supernatant was loaded on a discontinuous density gradient and ultra-centrifuged at 145.000 × g for 2 hours at 4°C.

After centrifugation, the bands containing lysosomes band were collected.

The isolated lysosome fraction was mixed with 2-3 volumes of PBS to decrease the concentration of gradient media and transferred into a micro-centrifuge tube and centrifuged at 18.000 × g for 30 minutes at 4°C.

Supernatant was removed and the lysosome pellet was maintained on ice until protein solubilization in a proper volume of 7M urea, 2M thiourea, 4% CHAPS and protease inhibitors buffer.

The protein concentration was determined by BCA assay.

3.7.2 Sample preparation and proteolytic digestion

Ten micrograms of protein from mitochondrial or lysosomal fraction obtained from HEK293T cell lysate and mice cerebral cortex was digested using a modified FASP protocol (Scifo et al., 2015). In brief, lysate buffer was exchanged by washing it several times with 8 M urea and 0.1 M Tris, pH 8 (urea buffer; UB). The proteins were reduced by addition of 10mM DTT in UB, washed, alkylated with 50mM iodoacetamide in UB, and 1:50 w/w of lysine-C endopeptidase (Wako, Richmond, VA, USA) was added in ~ 4 M urea with 0.1M Tris, pH 8, followed by incubation overnight at room temperature. The peptide digest was collected by centrifugation, and trypsin solution was added in a ratio of 1:50 w/w in 50mM ammonium bicarbonate. The peptide digests were cleaned using C18 reverse phase ZipTipTM (Millipore), suspended in 1% trifluoroacetic acid and sonicated for 1 min in a water bath.

3.7.3 Nano-Liquid chromatography (LC)–high definition mass spectrometry ($HDMS^E$)

Three-hundred nanograms of digested proteins (three technical replicates per sample) were used for LC-$HDMS^E$ analysis. The peptides were separated with the nanoAcquity UPLC system (Waters) equipped with a 5-µm Symmetry C18 trapping column, 180µm x 20mm, reverse-phase (Waters), followed by an analytical 1.7µm, 75µm x 250mm BEH-130 C18 reversed-phase column (Waters), in a single-pump trapping mode. The injected sample was trapped at a flow rate of 15µL/min in 99.5% of solution A (0.1% formic acid), and the peptides were separated with a linear gradient of 3–35% of solution B (0.1% each of formic acid and acetonitrile), for 100 min at a flow rate 0.3µL/min and a column temperature of 35 °C. The columns are flushed with an additional 5-min wash with up to 85% of solution B, followed by two empty runs to wash out any remaining peptides. The randomized samples were run in ion mobility-assisted data-independent analysis mode ($HDMS^E$), in a Synapt G2-S mass spectrometer (Waters), by alternating between low collision energy (6V) and a high collision energy ramp (20–45V) in the transfer compartment and using a 1s cycle time. The separated peptides were detected online with a mass spectrometer, operated in positive resolution mode in the range m/z 50–2000amu. Human [Glu1]-fibrinopeptide B (150fmol/lL; Sigma) in 50%

acetonitrile with 0.1% formic acid solution at a flow rate of 0.3μL/min was used for a lock mass correction, applied every 30s.

3.7.4 Quantitation of nano-LC-HDMS^E data

Relative quantification of randomized samples was performed with Progenesis QI™ for Proteomics software (Nonlinear Dynamics/Waters) and ProteinLynx Global Server (PLGS v3.0), using precursor ion intensities. MS^E parameters were set as follows: low energy threshold of 135 counts, elevated energy threshold of 30 counts and intensity threshold of precursor/fragment ion cluster 750 counts. Chromatograms were automatically aligned by the Progenesis QI™ software, and those that had alignment score ≥85% to the reference run, based on their retention and *m/z* values (2D map) were selected for further analysis.
To compare the control(s) to other subjects, we utilized the between-subject design scheme of the software. The ANOVA calculation applied by this scheme assumes that the conditions are independent and applies a statistical test which presumes that means of the conditions are equal. Database searches were carried out against Human (for HEK293T samples) or *Mus musculus* (for mice samples) UniProtKB–SwissProt, reviewed, database with ion accounting algorithm and using the following parameters: peptide and fragment tolerance: automatic, maximum protein mass: 500kDa, minimum fragment ions matches per protein 7, fragment ions matches per peptide 3, peptide matches per protein 1, primary digest reagent: trypsin, missed cleavages allowed: 2, fixed modification: carbamidomethylation C, variable modifications: NQ deamidation, oxidation of methionine (M) and false discovery rate (FDR) below 4%. Protein quantitation was performed entirely on non-conflicting protein identifications, using precursor ion intensity data and standardized expression profiles.

3.7.5 Development of a scoring system for mitochondrial proteins

Additional filters were applied to final data set in order to increase the stringency of accepted protein leads.
Proteins identifiers (IDs) obtained by MS analysis from mitochondrial fractions, were selected generating a ranking for final score of mitochondrial confidence using MitoMiner 4.0 v2017 SEP (http://mitominer.mrc-mbu.cam.ac.uk/release-4.0/begin.do) based on individual scores from various mitochondrial and functional annotation databases.
IMPI- evidence for mitochondrial localization from IMPI (Integrated Mitochondrial Protein Index) database, MitoCarta- evidence for mitochondrial localization from MitoCarta (MitoCarta Inventory of Mammalian Mitochondrial Genes) database were scored as 2 and 1 respectively. Mass-Spec- evidence for mitochondrial localization from high-throughput MS experiments ≥2 was scored as 1. Evidence for mitochondrial localization from Gene Ontology (GO) cellular component annotation and Human Protein Atlas database were both scored as 1. GFP and IMPI score for mitochondrial evidence were also reported.

IDs with a total score between 8 and 6 out of 8, were selected as identified mitochondrial proteins with High Confidence (Mito HC) whereas IDs with a total score between 3 and 5 out of 8, were selected as identified mitochondrial proteins with Medium Confidence (Mito MC). IDs with a score below 3 were discarded from the data set

Proteins identifiers (IDs) obtained by MS analysis from lysosomal fractions, were selected by evidence for lysosomal localization from GO cellular component annotation.

All data sets were further filtered by unique peptides used for label-free quantitation ≥ 2, fold change (FC) from averaged, normalized protein intensities ≥ 1.2, for dataset from mice tissue and ≥ 1.5 for HEK293T cell line, in either direction of up- or down-regulation and $P<0.05$ by ANOVA for all comparisons.

The lists of up-/down-regulated served as inputs into Ingenuity pathways (www.ingenuity.com), network and other functional analyses.

3.8 Whole transcriptomic analysis by RNA-seq

The whole transcriptomic analysis was carried out on CLN1 transfected SH-SY5Y cells following RA-NBM treatment.

RNA samples were collected in three independent experiments by TRI Reagent (LT) and checked for purity (by Nanodrop 1000, Agilent Technologies), and integrity (RNA Integrity Number ≥8.0). Indexed cDNA libraries' preparation, sequencing by Illumina HiSeq 1000 sequencer and alignment of reads to reference human genome (hg19) were performed as previously reported (Pezzini et al., 2017). To allow the comparison of gene expression profiles, the normalized expression values for each transcript were calculated as Fragments Per Kilobase per Million mapped reads (FPKM). The expression profile of each CLN1 transfected cell line (SH-p.wtCLN1, SH-p.L222P and SH-p.M57Nfs∗45) was then compared to the profile of mock cells: for each gene the ratio between average FPKM of each cell line, and an average FPKM of mock cells was calculated and reported as log2FC. Transcripts showing a $|\log2(FC)| \geq 1$ and a FDR, q-value ≤0.05 were assigned as differentially expressed.

3.8.1 Bioinformatic analysis and categorization of transcriptomic data

Sets of DEGs (corresponding to identified transcripts) of each CLN1 transfected cell line, were evaluated by QIAGEN's Ingenuity Pathway Analysis (IPA, Winter release 2017, QIAGEN2), to recognize meaningful biological processes and associated molecular pathways. Specifically, we carried out a Core Analysis followed by Downstream Effects Analysis; IPA macro-categories of Molecular and Cellular Functions and Physiological System Development and Function were further scrutinized. P-value, which was ascertained by right-tailed Fisher's exact test following Benjamini and Hochberg (B-H) correction, indicated the robustness of correlation between a

subset of DEGs of the dataset with a given biological function. Moreover, IPA algorithm calculated a ''z-score'' which estimates a predicted activation or inhibition of a given biological function. In particular, to compare the three independent Core Analyses of SH-p.wtCLN1, SH-p.L222P and SH-p.M57Nfs*45, we selected the most meaningful functional annotations (p-value < 0.05) assigned to each CLN1 transfected cell lines. Subsequently, only annotations demonstrating a |z-score| >0.5 in at least one cell line were taken into account for the heat-map representation.

Furthermore, selected subsets of DEGs were also queried through PANTHER database (Protein Analysis THrough Evolutionary Relationships) to elucidate the association with gene ontology (GO) terms/attributes. Cytoscape software (version 3.4.0) with GeneMANIA Cytoscape plugin were utilized to draw networks.

3.8.2 Identification of differentially expressed genes encoding for palmitoylated proteins

Datasets of DEGs from each CLN1 expressing cell line were subsequently queried for genes encoding the palmitoylated proteins. Specifically, we inquired SwissPalm—Protein Palmitoylation database from which both evidence-based and predicted palmitoylated proteins were retrieved. In addition, we used the curated compendium of mammalian palmitoylome reported by Sanders et al., (2015), and containing 1838 candidate proteins identified by screening of 15 palmitoylation-related proteomic publications. Several DEGs encoding palmitoylated proteins, and assigned to relevant IPA biological functions were further investigated by semi-quantitative WB.

3.9 Immunofluorescence

Following fixation in 4% paraformaldehyde or methanol for HEK293T and SH-SY5Y respectively, coverslips previously treated in Poly-D-Lysine (Sigma) were rinsed in PBS and incubated in blocking solution and then probed overnight at 4◦C with primary antibodies diluted in incubation buffer. Goat anti-mouse and anti-rabbit conjugated with AlexaFluor 488 or AlexaFluor 594 dyes (1:800, Cat# A11005 and A11008 respectively, Molecular Probes, LT) were used as secondary antibodies for 1 hour at RT.

Finally, nuclei were counterstained with 5 μg/ml DAPI (4.6-diamidino-2-phenylindole dihydrochloride, Sigma-Aldrich). Images were acquired by an AxioLab microscope equipped with an AxioCam and AxioVision 4.3 software (Zeiss).

A list of primary antibodies used for immunofluorescence (IF) analysis is illustrated in appendix.

3.10 Western Blotting

For WB analysis, cultured skin fibroblasts, HEK293T and SH-SY5Y stable clones or transfected cells, were collected at confluence, washed twice with PBS and then homogenized in RIPA buffer (150mM NaCl, 50mM Tris–HCl, 6mM EDTA, 1% NP-40, 0.1% SDS, 0.5% deoxycolic acid, pH 8.0) containing inhibitors of proteases (Roche Diagnostics GmbH, Mannheim, Germany). The cells were disrupted by plastic pestle on ice and centrifuged for 10 min at 16,000×g at 4°C. Supernatant (soluble fraction) was collected and either used immediately or stored at −20 °C for later use. The pellets (insoluble fraction) were solubilized in 50µl of 1% (v/v) SDS in PBS for 10 min at room temperature; then, following addition of 50µl RIPA buffer, they were sonicated for 10 s. An 8-16% gradient denaturing gel was loaded with 30-50 µg proteins. Proteins were then electron-transferred to a PVDF membranes (Bio-Rad Laboratories, Hercules, CA); the membranes were blocked with TBS/0.1% Tween20 (TTBS) containing 10% non-fat dry milk and then subjected to immunoblotting analysis. Primary antibodies were incubated overnight at 4°C in TTBS with 2.5% non-fat dry milk, and those not bound specifically were removed by washing in TTBS. Peroxidase-conjugated anti-mouse and anti-rabbit were used as secondary antibody (Jackson ImmunoResearch, laboratories Inc.) were added for 1 hour at room temperature in the same buffer as used for the primary antibodies (5% non-fat dry milk in TTBS). Reactive bands were detected using Immobilon Western Chemiluminescent HRP Substrate (Millipore Corporation, Billerica, MA), according to the manufacturer's instructions.
For densitometry analysis, the optical density (OD) of each band was assessed by ImageJ software (http://rsbweb.nih.gov/ij/) and normalized to OD of a loading control (GAPDH)
A list of primary antibodies used for WB analysis is illustrated in appendix.

3.11 Aggresome detection

Cellular aggresomes were detected using the ProteoStat® Aggresome Detection kit according to the manufacturer's instructions (Enzo LifeSciences, Lausanne, Switzerland). Cultured cells were grown on coverslips and incubated for 12 h with MG-132, a cell-permeable proteasome inhibitor (5µM), which was used as a positive control. The cells were then washed with PBS, fixed in 4% paraformaldehyde for 30 min at room temperature, and permeabilized in experimental solution (0.5% Triton X-100, 3 mM EDTA, pH 8.0 in 1× assay buffer) with gentle shaking on ice for 30 min. After this step, the cells were washed again in PBS and stained using the ProteoStat® Aggresome Detection Reagent and Hoechst 33342 nuclear stain for 30 min at room temperature protected from the light. The aggresomes were visualized using a

Zeiss AX10 inverted fluorescence microscope equipped with an AxioCam MRc5 camera. The images were processed using AxioVision rel 4.8 acquisition software (Zeiss).

3.12 Transmission electron microscopy

Specimens from skin biopsies were fixed in 2.5% glutaraldehyde in 100 mM phosphate buffer for 3 hours at 4°C. After washing in buffer, samples were the post-fixed in 1% osmium tetraoxide for 2 hours at 4 °C, dehydrated by increasing concentrations of acetone and subsequently embedded in Spurr resin. Ultra-thin slices were cut by microtome, stained in uranyl acetate and lead citrate and finally observed under the EM 109 electron microscope (Carl Zeiss, Munich Germany).

3.13 Enzymatic activities of NCL-related lysosomal hydrolases

Multiplex enzyme assay was developed to analyze in a single test on dried blood spots (DBS) the activities of palmitoyl-protein thioesterase 1 (PPT1), tripeptidyl peptidase (TPP1), and cathepsin D (CTSD) (Maeser S. et al, in preparation). In brief, DBS from patient, healthy carriers and age/sex-matched control individuals was mixed with 60 µL buffer (20 mM ammonium acetate, pH 4.5, 0.02% NaN3) under agitation for 45 minutes at 25°C. 50 µL was taken and introduced into a 96 well black plate. On top of the blood extract, 50 µL substrate solution and 500 µM in water was added. The plate was then sealed, covered with aluminum folia and incubated with agitation at 37°C for 17h. The reaction was stopped by using 10 µL of formic acid.

The fluorometric determinations were performed with a Victor2 plate reader using a standard umbelliferone filter before incubation (used as reference and the value was extracted from the final measurement), and after stopping the reaction.

The mass spectrometric assay for CTSD took advantage of a specific Arg-Arg- dipeptidyl umbelliferyl-substrate analog that is specifically monitored by tandem-MS fragmentation and an internal standard solution (15µM H-Tyr-7-amino-4-metylcoumarin).The concentration of the product can be translated into enzymatic activity in µM/L blood/h.

CTSD enzyme activity assay was performed in collaboration with Prof. Michael Przybylski (Biomedical Mass Spectrometry Unit, University of Konstanz, Germany).

4. RESULTS

4.1 Transcriptomic analysis of whole CLN1 transfected SH-SY5Y cells

4.1.1 Characterization of CLN1 transfected SH-SY5Y cells

A complete characterization of *CLN1* transfected SH-SY5Y cells was performed in collaboration with the department of Neuroscience, Biomedicine and Movement, University of Verona (Pezzini et al., 2017b).

In brief, mRNA expression in transfected *CLN1* cells resulted overexpressed from 5 to 15- FC as compared to basic expression in parental SH-SY5Y line and an empty vector (pcDNA3) transfected cells.

The expression of PPT1 was subsequently characterized by IF, WB analysis and enzyme activity.

Double IF assay for PPT1 and the lysosomal marker LAMP2 revealed a strong signal of PPT1 in cells which stably expressed either wtCLN1 or two different missense mutations (p.L222P; p.V181L). A partial localization inside lysosomes was observed for SH-p.wtCLN1, whereas a more diffuse cytoplasmic pattern was detected for SH-p.L222P and SH-p.V181L. Overexpression of PPT1 in both SH-p.wtCLN1 cells and cell lines harboring a missense mutation was confirmed by immunoblotting analysis. A different pattern was associated with the missense mutation-bearing proteoforms of PPT1. In cells transfected with indel mutations, the PPT1 signal was identified following high exposure only, suggestive for a representation of the endogenous PPT1 signal.

Strong increase in PPT1 enzymatic activity was observed in SH-p.wtCLN1 as compared to SH-pcDNA3 empty vector cells whereas parental SH-SY5Y and cell lines carrying different mutations demonstrated some variability in PPT1 enzymatic activity.

The neuronal differentiation paradigm in RA-NBM media was effective in all analyzed cell lines, as reported for the parental SH-SY5Y neuroblastoma cells (Pezzini et al., 2017a). Changes in shape of neuronal cell bodies and a significant elongation of their main processes also occurred.

4.1.2 Comparative analysis and bioinformatic examination reveals differential transcripts in the three *CLN1* transfected cells

We generated a transcriptomic profile of three *CLN1* transfected cells as compared to empty-vector pcDNA3 expressing cells. We chose three cell lines (SH-p.wtCLN1, SH-p.L222P, SH-p.M57Nfs*45), which expressed the highest amount of *CLN1* mRNA upon transfection. The transcriptomic profiles revealed 802 DEGs in SH-p.wtCLN1 cells (of which 286 were up-

regulated and 516 down-regulated, supplementary table S2). The number of differentially expressed transcripts identified in the two mutated clones was significantly lower (50 up- and 162 down-regulated for SH-p.L222P, supplementary table S3, 54 up- and 157 down-regulated for SH-p.M57Nfs*45, supplementary table S4). Moreover, 629 transcripts were specifically dysregulated in cells overexpressing the wild-type form of PPT1.

Categorization through the IPA bioinformatic suite of DEGs identified in SH-p.wtCLN1 demonstrated *Cellular Development*, *Cell-to-Cell Signalling and Interaction* and *Cell Morphology* as the most meaningful *Molecular and Cellular Functions* categories. Moreover, *Nervous System Development and Function* was among the three high-ranked categories related to the *Physiological System Development and Function*, suggesting an alteration of neurobiological processes in these cells (Figure 4A). Likewise, the same IPA categories were significantly annotated in the two mutants (Figure 4B and C). SH-p.wtCLN1 cells displayed a higher number of DEGs which were assigned to each IPA category. Further scrutiny of the four main categories in SH-p.wtCLN1 profile pinpointed functional annotations related to changes of neuronal cell shape and formation of neurites (*neuritogenesis; growth, branching and morphogenesis of neurites; axonogenesis*) as well as neuronal differentiation (*differentiation of neurons, development of neurons*; Figure 3D). Taking into account the z-scores, most of these annotations were severely affected in SH-p.wtCLN1 and predicted to be inhibited; a similar trend was seen for SH-p.L222P (even though the number of annotated functions was lower than wt*CLN1* clone), whereas bioinformatics predictions for SH-p.M57Nfs*45 were less pronounced. Functions related to neuronal transmission (such as *long-term potentiation, secretion of neurotransmitter* and *neurotransmission*) were also annotated. Additional IPA attributes referred to sprouting of neuronal processes (*dendritic growth/branching, shape change of neurites*, *shape change/branching of neurons*, *guidance of axons*) as well as synaptic transmission (*developmental process of synapse*, *long-term potentiation of synapse, plasticity of synapse, release of neurotransmitter* and *action potential of cells*) were selectively assigned to SH-p.wtCLN1 cells (lower part of the Figure 4D). Notably, both the relative high number of annotations and associated z-scores indicated that these functions were remarkably affected in SH-p.wtCLN1 as compared to other analyzed cell lines.

Table 5 *The compendium of selected PPT1 overexpressing SH-SY5Y neuroblastoma cell lines used in the study.*

Cell line	Transfected *PPT1* cDNA	Effect on PPT1 protein
SH-SY5Y	-	-
SH pcDNA3	pcDNA3 (empty vector)	-
SH p.wtCLN1	wt*CLN1*	-
SH p.L222P	c.665T>C	p.L222P
SH p.M57Nfs*45	c.169dupA	p.M57Nfs*45

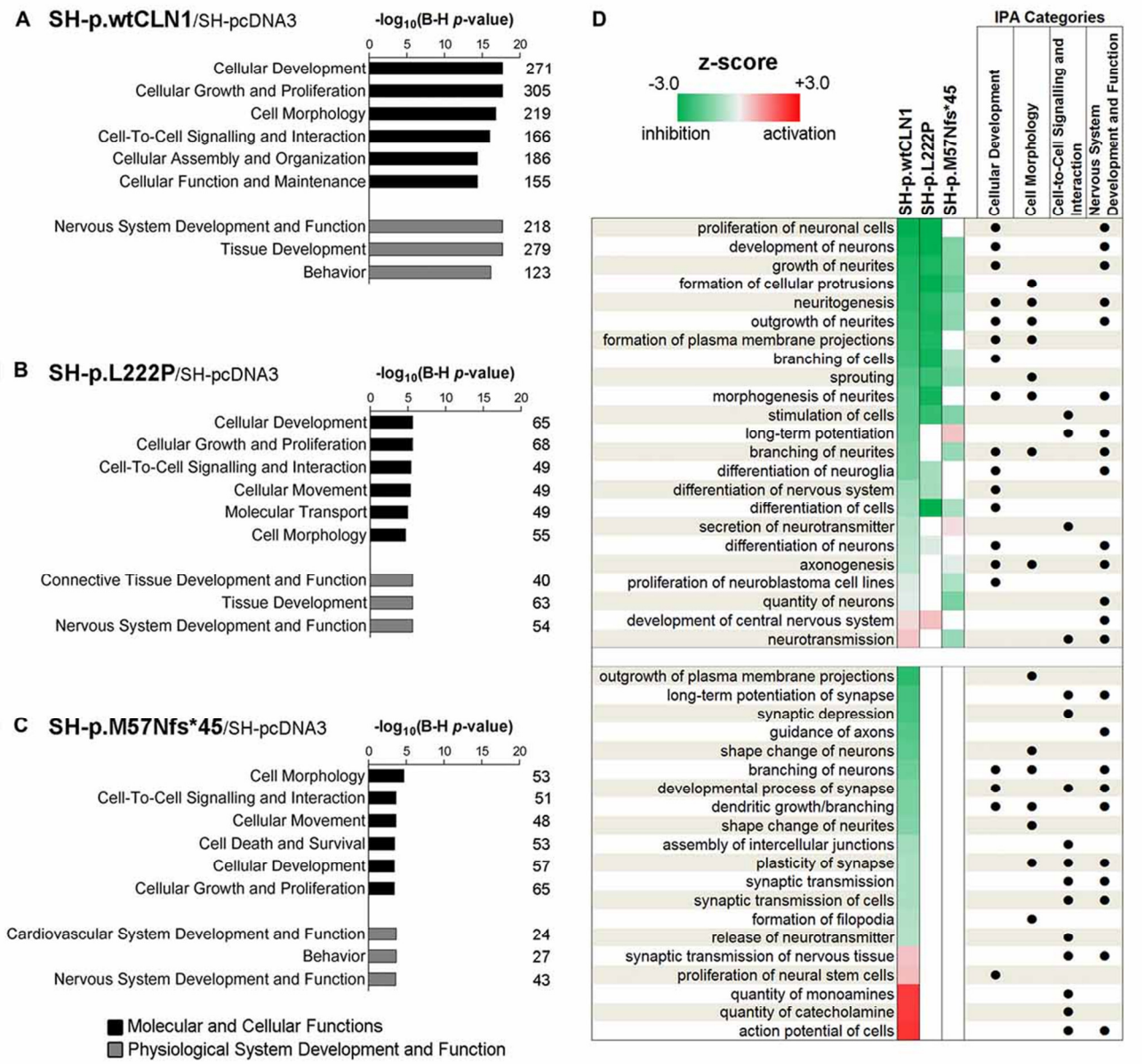

Figure 4 *Bioinformatic survey of identified DEGs in wild-type and mutated CLN1 cell lines. (A–C) Categorization by IPA of DEGs in differentiated SH-SY5Y cells. The number of genes assigned to each category is reported. Statistical significance is reported as –log10 of B-H corrected p-value. (D) Heat-map representation depicting statistically meaningful IPA functional annotations. Functional annotations, shared among the IPA classes are marked by dots. Colored squares represent either a predicted activation (red) or a predicted inhibition (green) according to z-score calculated by IPA algorithm; higher color intensity correlates with more significant bioinformatic prediction.*

4.1.3 Transcriptomic data suggest a defective palmitoylation process and synaptic compartment

Taking into account the process of palmitoylation in which CLN1/PPT1 is involved, we further scrutinized DEGs identified in the three CLN1 transfected cell lines to seek for genes which are known to encode palmitoylated proteins. Survey of the mammalian palmitoylome derived from Blanc et al., 2015; Sanders et al., 2015 in SH-p.wtCLN1, revealed 113 palmitoylated protein-

encoding genes, corresponding to ~14% of the full DEGs dataset in this cell line (Supplementary table S5). Conversely, a lower amount of DEGs coding for palmitoylated proteins was identified in the two mutants (n = 38 for SH-p.L222P, 18% of DEGs; n = 36 in SH-p.M57Nfs*45, 17% of DEGs; Supplementary tables S6, S7). Eighty-five genes coding for palmitoylated proteins were specifically found in p.wtCLN1, whereas only a small portion was selectively expressed in the two mutants, (n = 9 in p.L222P and n = 15 in p.M57Nfs*45). Eight genes were common to all mutated cell lines.

Bioinformatic categorization of 113 palmitoylated protein-encoding genes seen in SH-p.wtCLN1 using PANTHER revealed twenty five genes, connected to Nervous System Development and Function as well as to annotations related to neurites formations and cell Component GO terms (Figure 5B). For an exhaustive compendium of identified genes encoding the palmitoylated proteins and assigned IPA functions and GO terms see supplementary table S7.

Notably, CTSD, associated with CLN10 disease was found to be up-regulated in wild-type PPT1-overexpressing cells, further supporting a genetic interaction between these two NCL genes.

Furthermore, transcriptomic profiling and bioinformatic inquiry of DEGs identified in SH-p.wtCLN1 put forward several functional annotations related to synaptic compartment and synapse function (Figure 4D). Therefore, we focused on four IPA annotations related to neurotransmission (81 DEGs), namely developmental process of synapse, long-term potentiation of synapse, synaptic transmission and neurotransmission (see Venn diagram in Figure 6A). Further inquiry through GeneMANIA revealed close associations between DEGs as far as genetic and physical interactions were concerned (Figure 6B). Moreover, fold enrichment analysis through PANTHER disclosed important functional relations of those DEGs with synaptic and axonal compartments (Cell Component GO terms of pre/post-synaptic membrane, axon terminus and synaptic vesicle, Figure 6C) as well as with regulatory activities of membrane channels (Molecular Functions GO terms, Figure 6C). Specifically, various genes were assigned to glutamate receptor activity (*GRM1, GRM2, GRM7, GRIN1*), calcium channel regulator activity (*GRM2, NPY, GRM7, NRXN1*) and voltage-gated cation channel activity (*KCNB1, OPRM1, KCNQ3, CACNA2D2, KCNK3, GRM7*). Among queried DEGs, 23 genes encoded palmitoylated proteins (red nodes in Figure 6B).

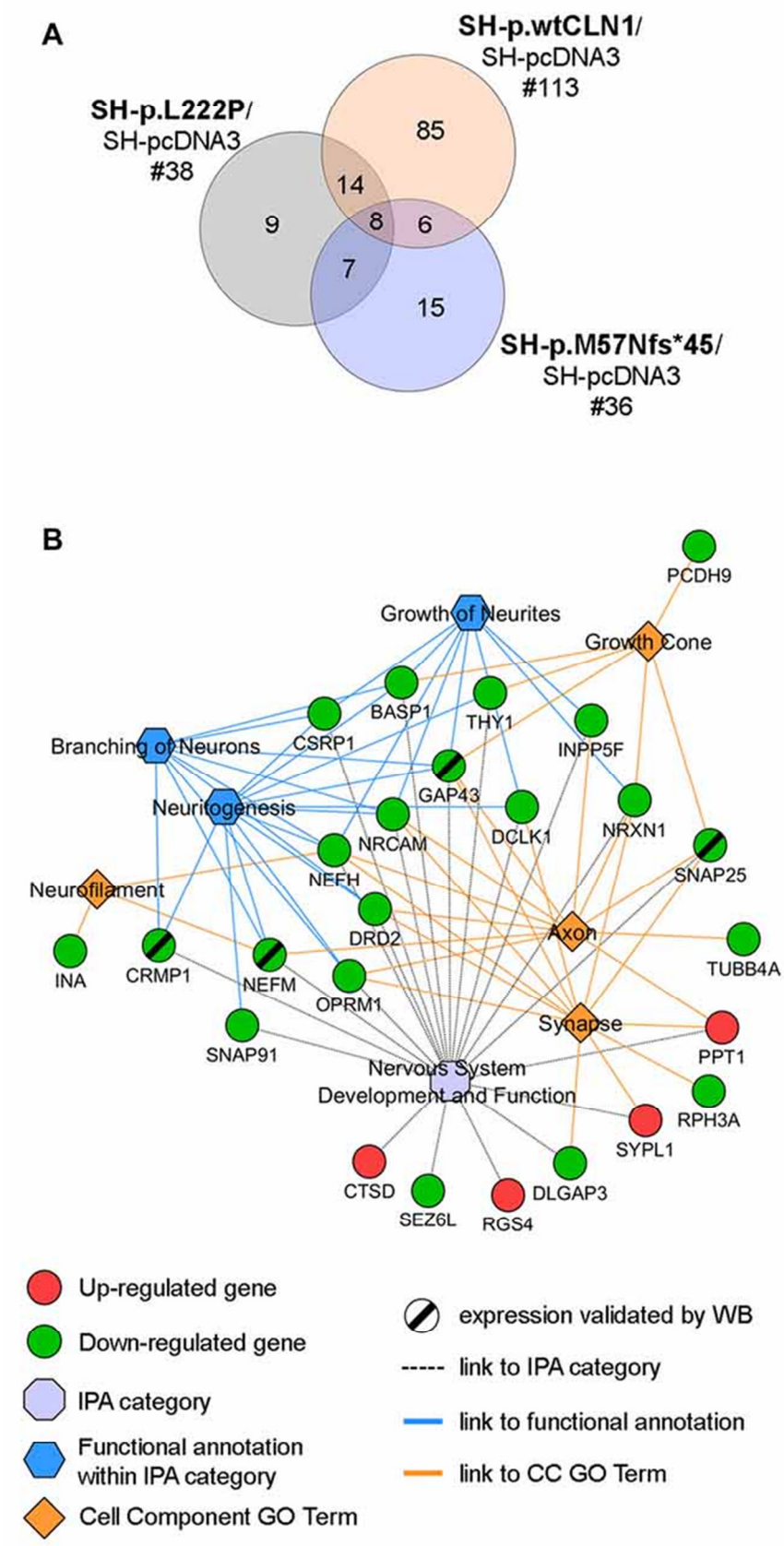

Figure 5 *(A) Venn diagram of identified palmitoylated gene products (palmitoylated proteins) among DEGs in the transcriptomic profiles of SH-p.wtCLN1, SH-p.L222P and SH-p.M57Nfs*45, compared to an empty-vector (SH-pcDNA3) expressing cells. The amount of identified DEGs is stated below the cell line name, whereas the numbers of genes shared among the three comparisons are reported in the intersections of the Venn diagram. (B) Network of the twenty five genes, specifically expressed in SH-p.wtCLN1 cells.*

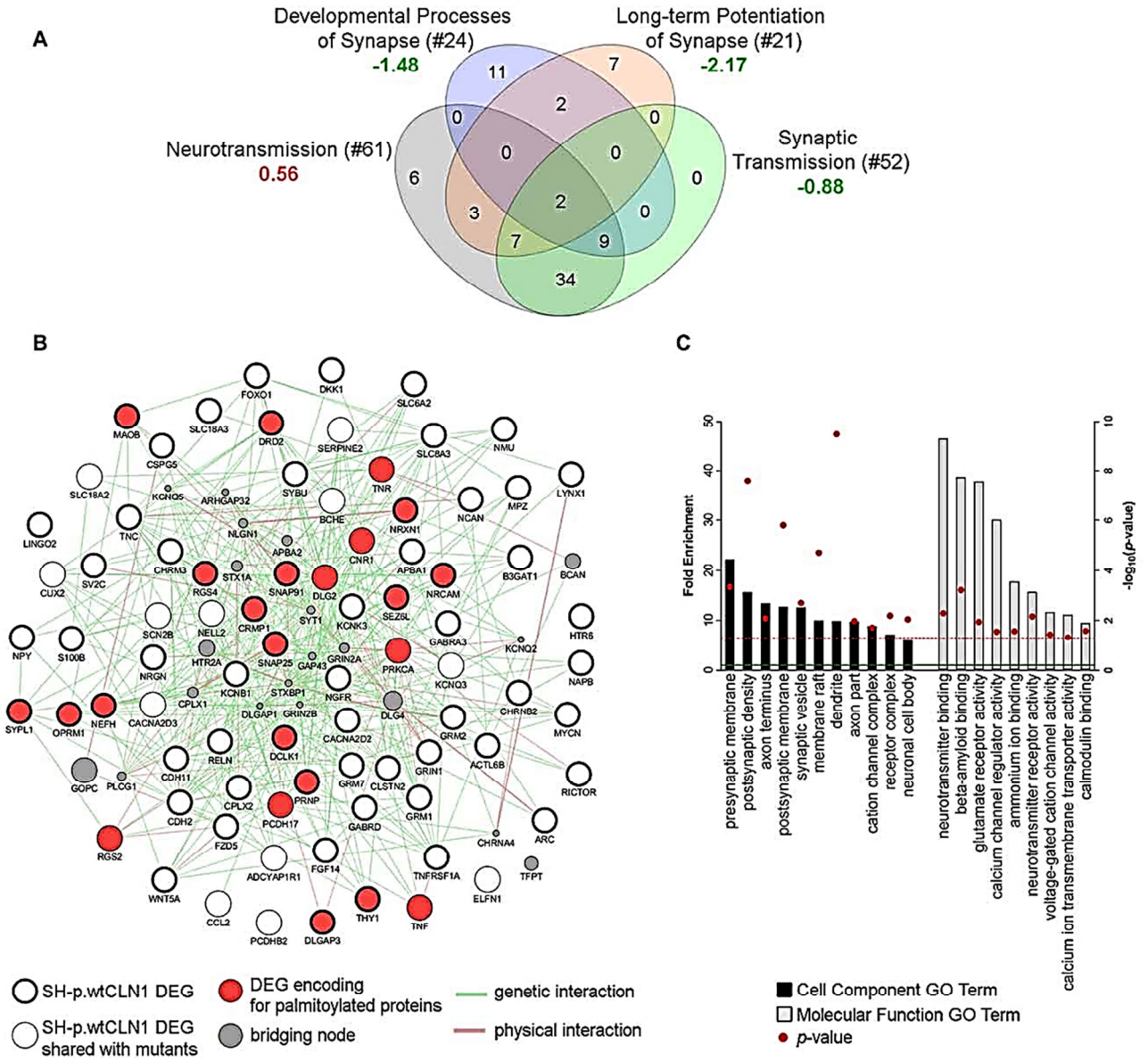

Figure 6 *Bioinformatic survey of DEGs assigned to the synaptic compartment. (A) Four IPA functional annotations of SH-p.wtCLN1 transcriptomic profile, and related to neuronal transmission were investigated. The number of DEGs assigned to each category is reported between brackets whereas the associated z-score is reported below (green = predicted inhibition; red = predicted activation). The four IPA attributes enclosed 81 unique DEGs, which served as input for further bioinformatic queries. (B) A functional network encompassing 81 DEGs drawn using GeneMANIA plugin in Cytoscape software. Both genetic and physical interactions were used to denote the bridging nodes. Thick borders pinpoint DEGs which were specifically expressed in SH-p.wtCLN1, and not shared with the other two mutants. Genes encoding for palmitoylated proteins are marked in red. (C) Statistical overrepresentation profile of 81 DEGs derived through PANTHER classification system. Fold Enrichment (FE) score represents a portion of genes enclosed in a specific term. Enrichment above a score of 1 (marked by green line) indicates an overrepresentation. GO terms were grouped for related ontological classes and sorted hierarchically according to a decreasing FE score, starting from the most specific subclass towards less specific ones. Only the most specific categories for each class associated with a FE score above the set threshold are shown. P-value was adjusted using Bonferroni correction for multiple testing and reported as* $-\log_{10}$*(p-value); red line represents a p-value equal to 0.05.*

4.2 Validation of transcriptomic data in *CLN1* transfected SH-SY5Y model

Among DEGs coding for palmitoylated proteins detected in SH-p.wtCLN1 cells, we selected genes relevant to elongation of neuronal structures (*GAP43, CRMP1* and *NEFM*) and assessed their protein expression by WB. Immunoblotting showed a decreased expression of the corresponding proteins in cellular lysates of SH-p.wtCLN1, whereas no significant changes in the other *CLN1*-mutated cell lines were observed (Figure 7A). The quantification analysis in SH-p.wtCLN1 and other cell lines (Figures 7B–E) confirmed a significant down-regulation of these markers in SH-p.wtCLN1, and to a lesser extent in SH-p.L222P cells. A reduced expression of these proteins was already evident under basal conditions, suggesting that down-regulation of these proteins (and transcripts) is not related to the RA-NBM differentiation process.

A slight down-regulation in expression of a short 60 kDa isoform of CRMP1 (isoform 2), NF-M and SNAP25 (another DEG specifically identified in SH-p.wtCLN1) following RA-NBM differentiation was detected in SH-p.L222p lysates whereas no significant change in GAP43 expression was observed in the same cell line.

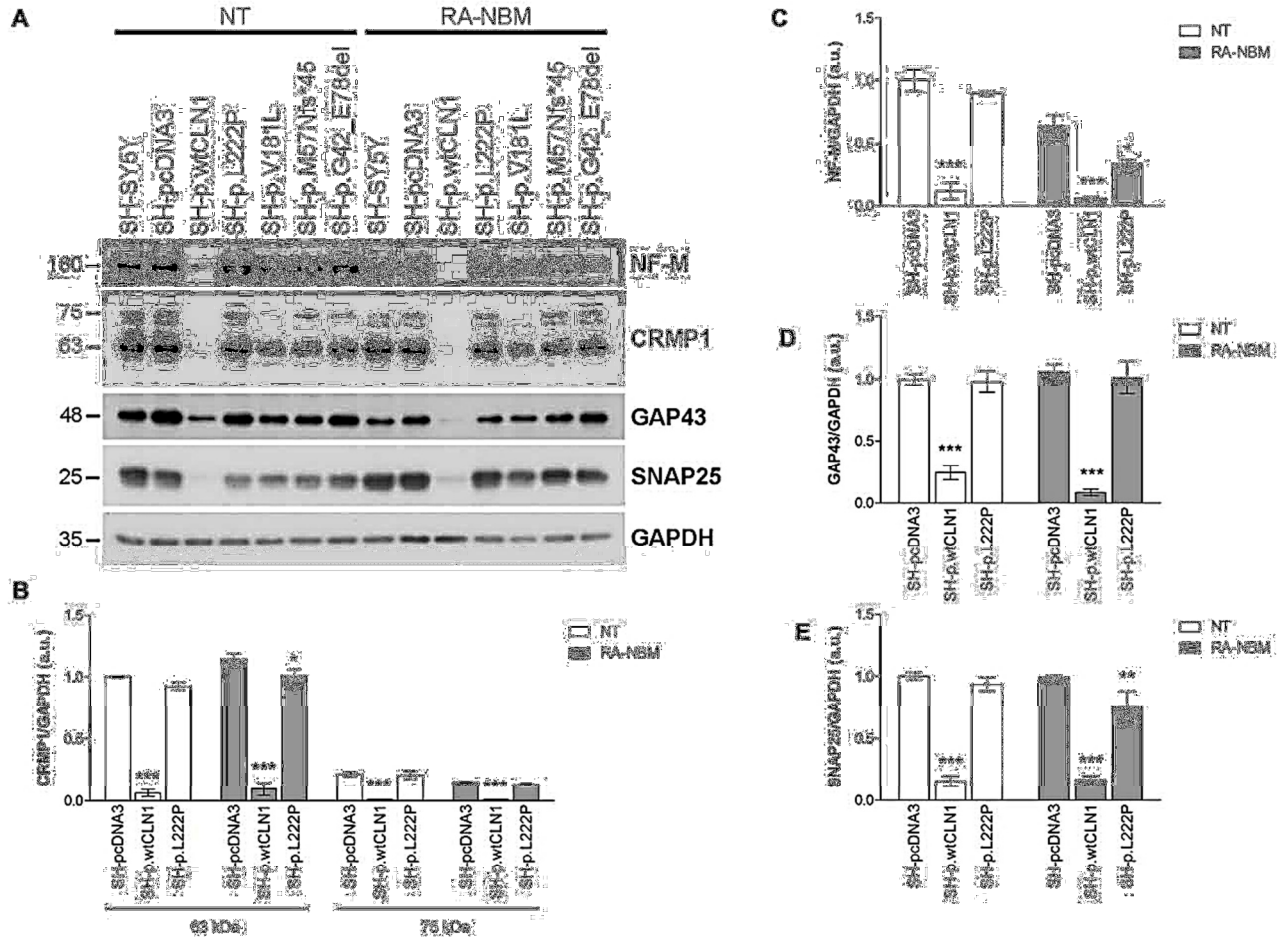

Figure 7 *Immunoblotting analysis of selected DEGs identified in SH p.wtCLN1 cells and encoding for palmitoylated proteins. (A) Representative WB of proteins coded by four down-regulated genes (NF-M, CRMP1, GAP43 and SNAP25) identified in SH p.wtCLN1 transcriptomic profile. (B–E) Semi-quantitative WB analysis of the same markers, both under basal condition and following differentiation in RA-NBM medium. GAPDH served as internal standard; a.u. arbitrary units; mean ± SEM of three independent experiments; Two-way ANOVA followed by Bonferroni's post-test; *p < 0.05, **p < 0.01, ***p < 0.001.*

Transcriptomic analysis and bioinformatic investigations suggested a defective capacity of SH-p.wtCLN1 cells to generate elongated cellular processes. We thus evaluated the morphological changes undergoing in *CLN1* transfected cells during the differentiation process in RA-NBM medium. Under basal conditions, all analyzed cells showed similar morphological features and growth characteristics, except those overexpressing wtCLN1, which exhibited a slow rate of proliferation and a more flattened shape. Differentiation in RA-NBM medium significantly stimulated the outgrowth of neuronal processes in all cell lines. However, SH-p.wtCLN1 cells showed less arborized, stunted neurites in comparison to mock-transfected cells and other CLN1 transfected cell lines.

Considering the predicted defect of neuritogenesis, we subsequently tested the expression of β-III tubulin, a cytoskeletal marker of neurites. β-III tubulin immunolabelled processes pinpointed a significant paucity of neurites longer than 30μm in SH-p.wtCLN1 cells, in accordance with the bioinformatics findings. Likewise, a similar, even though not significant,

trend was seen for SH-p.L222P clone. Higher variability was detected in SH-p.M57Nfs*45 (Figures 8A, B).

Accordingly, immunoblotting analysis of β-III tubulin demonstrated a reduced expression of this cytoskeletal marker in SH-p.wtCLN1 following differentiation in RA-NBM medium (Figures 8C, D).

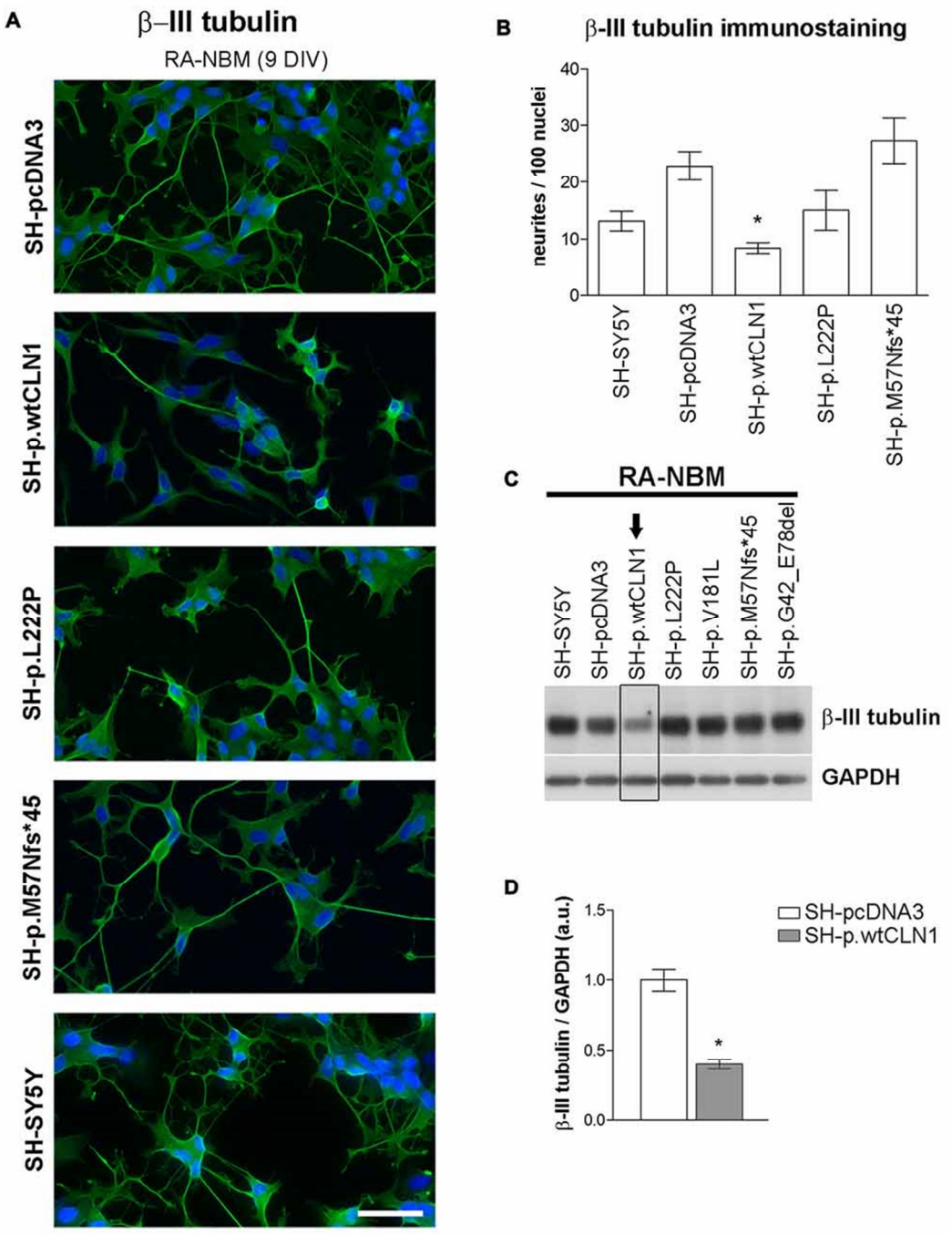

Figure 8 *Neurite growth features of CLN1 transfected cell lines following neuronal differentiation in RA-NBM medium. (A) Outgrowth of neurites in CLN1 transfected cells lines evaluated by β-III tubulin immunostaining during neuronal differentiation. Scale bars equal to 50 μm. (B,C) Morphometric analysis of β-III tubulin. Mean ± SEM of three independent experiments; One-way ANOVA followed by Bonferroni's post-test; *p < 0.05. (C) Immunoblotting analysis of β-III tubulin cytoskeletal marker in differentiated CLN1 transfected cell lines. Arrow pinpoints to a decreased expression of β-III tubulin in SH-p.wtCN1 cells. (D) Semi-quantitative WB analysis. GAPDH served as internal standard; a.u. arbitrary units; mean ± SEM of three independent experiments; unpaired t-test; *p < 0.05.*

4.3 Bioenergetics involvement in CLN1 disease

In order to verify a bioenergetics implication in CLN1 disease (described in primary cells, see Pezzini et al., 2011 and observed in in the brain of $Cln1^{-/-}$ mice model (Tikka et al., 2016)), we tested changes in mitochondrial energy metabolism in *CLN1* transfected cells.

Compared to SH-pcDNA3 cell line (mock), we detected a more pronounced decrease of basal oxygen consumption as well as the ATP-linked respiration in SH-wtCLN1 and SH-p.V181M. Furthermore, the rate of oligomycin-sensitive oxygen consumption, which reflects proton leakage across the inner mitochondrial membrane was lower in all *CLN1* transfected cell lines. Higher variability was recorded in non-mitochondrial respiration (Figure 9).

Our results show an overall impairment of mitochondrial function in CLN1 models, once again with more significant alterations in the cell line overexpressing the *CLN1* gene.

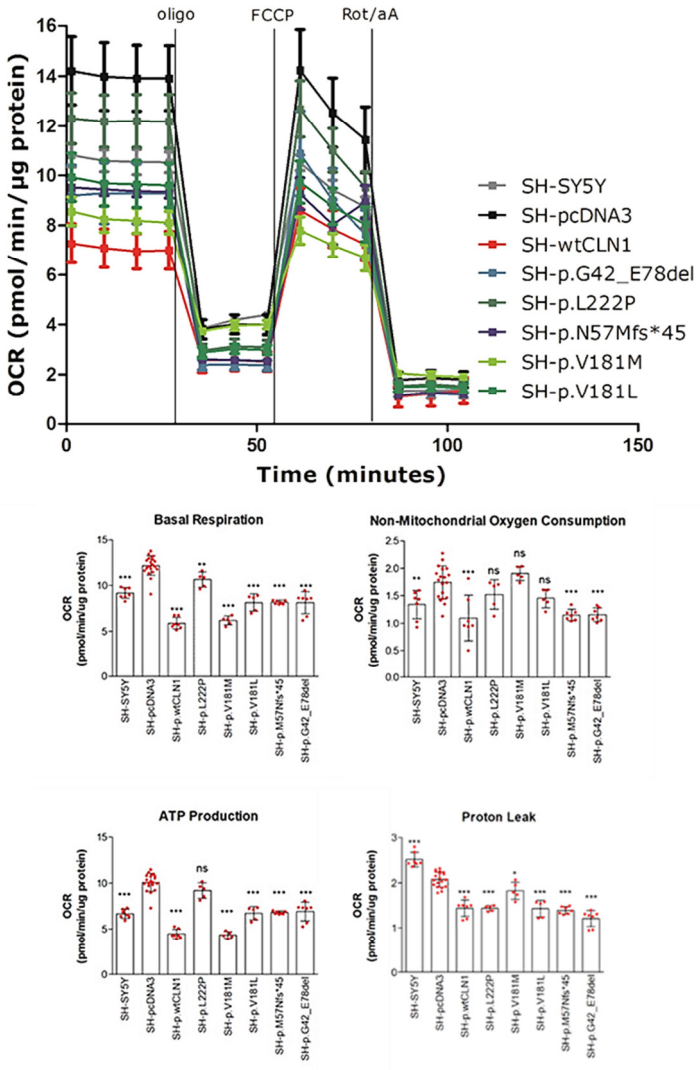

Figure 9 *Oxygen consumption and rate in CLN1 transfected neuroblastoma cells. Kinetic micro-oxygraphy graphs depict means and standard deviations whereas quantitative parameters are reported as histograms. Statistical significance was calculated using one-way ANOVA followed by Bonferroni's post-hoc test; ***p < 0.001.*

4.4 Organelle-specific proteome analysis of CLN5 and Cln5$^{-/-}$ KO models

4.4.1 Generation of CLN5 CRISPR KO HEK293T and SH-SY5Y cell lines

By using a gene specific CRISPR/Cas9 system, we obtained 40 and 12 different HEK293T and SH-SY5Y clonal lines, respectively. Cells were grown and assayed by WB analysis for protein immunoreactivity using a monoclonal anti-CLN5 antibody. In clones which lacked CLN5-immunoreactivity, the achievement of a high editing efficiency (>80%) was confirmed by direct Sanger sequencing.

Out of 7 clones, 3 stable HEK293T and 1 out of 3 stable SH-SY5Y clones, in which *CLN5* was knocked-out were used for cell fractionation. Molecular features of selected clones are reported below (Figure 11).

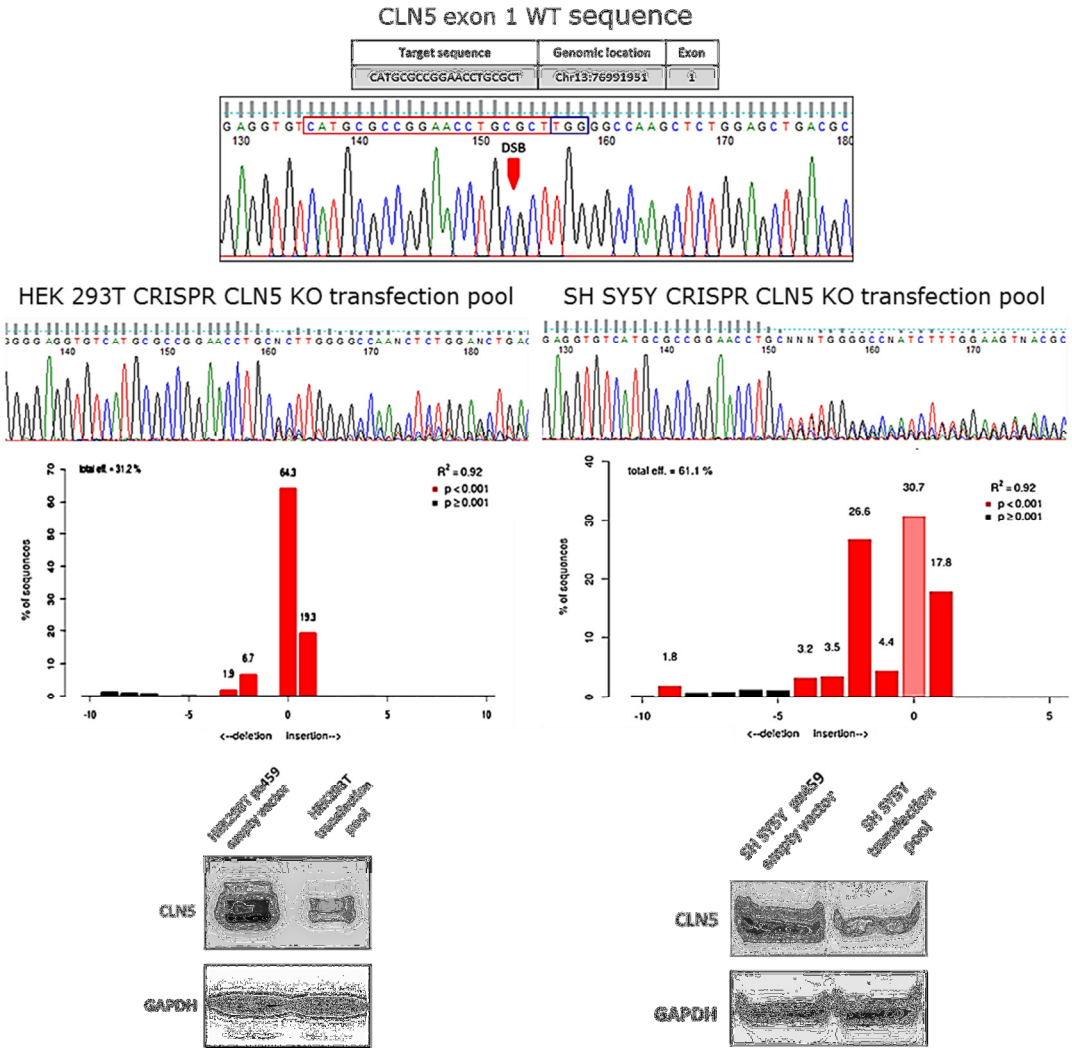

Figure 10 *Genome editing events and pCLN5 expression in HEK293T and SH-SY5Y transfection pool. Quantification of editing efficacy and identification of the predominant types of indels mutation by TIDE software and WB analysis for the target protein to correlate the genotype modifications with protein expression.*

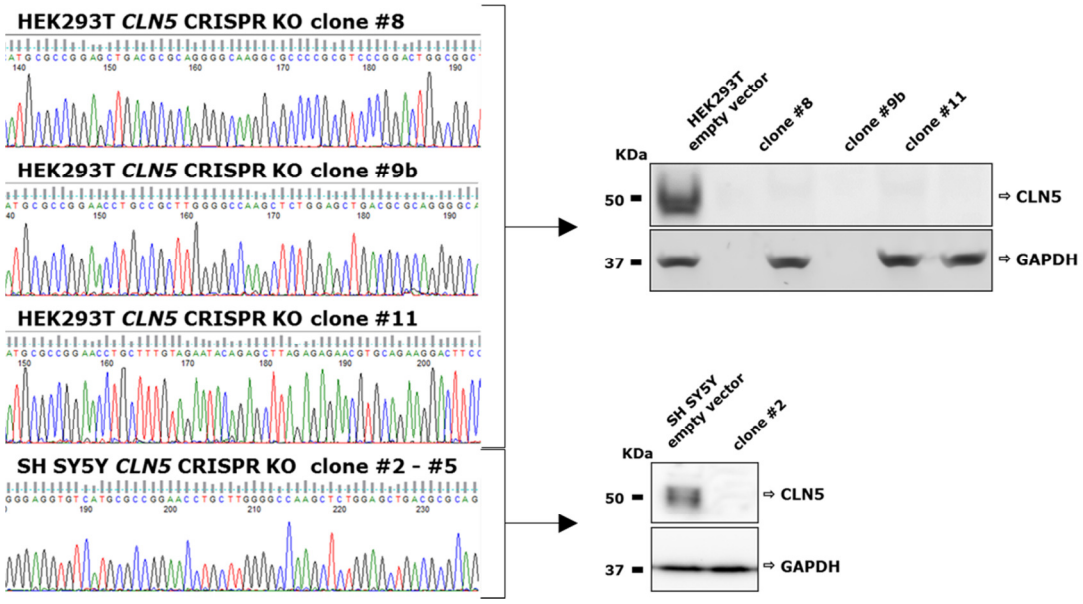

Figure 11 *Stable HEK293T and SH-SY5Y CRISPR CLN5 KO clones and genotype-phenotype correlation*

Table 6 *The compendium of CLN5 KO and WT cell lines used in this study*

Cell line	Genotype		Effect on CLN5 protein
HEK293T empty vector	wt*CLN5*	-	-
HEK293T clone #8	c.11_32del	del 23 bp	p.N4fs*2
HEK293T clone #9b	c.16_17ins	ins 1 bp	p.R6fs*9
HEK293T clone #11	c.16_17ins	ins 389 bp	p.R6fs*24
SH-SY5Y empty vector	wt*CLN5*	-	-
SH-SY5Y clone #2	c.17_18del	del 2 bp	p.R6fs*7

4.4.2 Isolation of mitochondrial and lysosomal compartments for proteomic investigations

Fractionation methods for the isolation of single cellular compartments in cell lines and mouse cortex allowed reducing the complexity of samples and targeted, organelle-specific proteome analysis.

In order to assess the efficacy of the methods, we monitored the degree of enrichment and contamination level in mitochondrial and lysosomal preparations by WB analysis.

Fractionations were performed in control HEK293T cell lines. The fractions were probed with antibodies specific for lysosomes (CTSD and LAMP2 like soluble and membrane lysosomal marker, respectively), mitochondria (SDHA and Core2) and cytosol (GAPDH).

We obtained a high degree of enrichment in both mitochondrial and lysosomal preparations. A low level of contamination with mitochondria was detected in lysosome-enriched fractions.

Cross contamination within the lysosome and mitochondria-enriched extracts is frequent and difficult to avoid, due to overlapping physicochemical properties of both organelles.

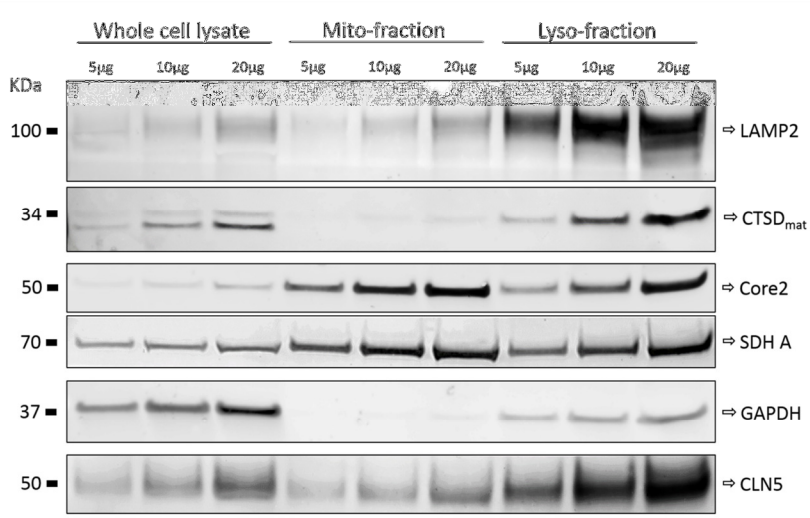

Figure 12 *Cellular fractionation. Different protein amount from each fraction was separated on a 8-16% SDS-PAGE gel. WB were then probed with antibodies specific for cytosolic, mitochondrial and lysosomal compartment to monitor the degree of enrichment and contamination level in mitochondrial and lysosomal preparations*

4.4.3 Bioinformatic analyses of differential proteome profiles in HEK293T CRISPR *CLN5* KO mitochondria

The mitochondrial proteome analysis was carried out in preparations obtained from three HEK293T *CLN5*-KO clones (clones #8, #9b and #11) and compared to empty vector carrying cells (controls). Samples were collected in two independent experiments, and the overall expression profile from *CLN5* KO clones (n=6 mitochondrial preparations) was compared to two control profiles. The samples were run in technical triplicates, for each IDs the average relative protein abundance in *CLN5* KO group was calculated, compared to respective controls, and reported as FC. Following a filtering step for mitochondrial proteins (see paragraph mitochondrial scoring system), IDs showing a FC ≥ 1.5 and p value < 0.05 (FDR < 4%) were assigned as differentially expressed.

Proteome profiling of mitochondrial fractions revealed differentially expressed proteins (DEPs, 62 IDs) in HEK293T *CLN5* KO with assigned high and medium mitochondrial confidence score. Among these, 51 DEPs were down-regulated and 11 up-regulated (see supplementary table S9).

Bioinformatic examination of DEPs showed an impairment of cellular respiration and metabolic processes in *CLN5* KO mitochondria. Categorization of DEPs through IPA demonstrated *Mitochondrial dysfunction* and *Cell death and survival* as the most statistically meaningful top canonical pathway and molecular and cellular function category, respectively. Moreover, *Nervous system development and function* was related to the Physiological System

Development and Function category, suggesting an alteration of neural processes in *CLN5* KO cells. Further scrutiny of selected proteins by GO biological process identified common altered pathways with down-regulation of *Cellular respiration* (GO 0045333) and *Metabolic process* (GO 0008152) in *CLN5* KO HEK293T cells (Figure 13)

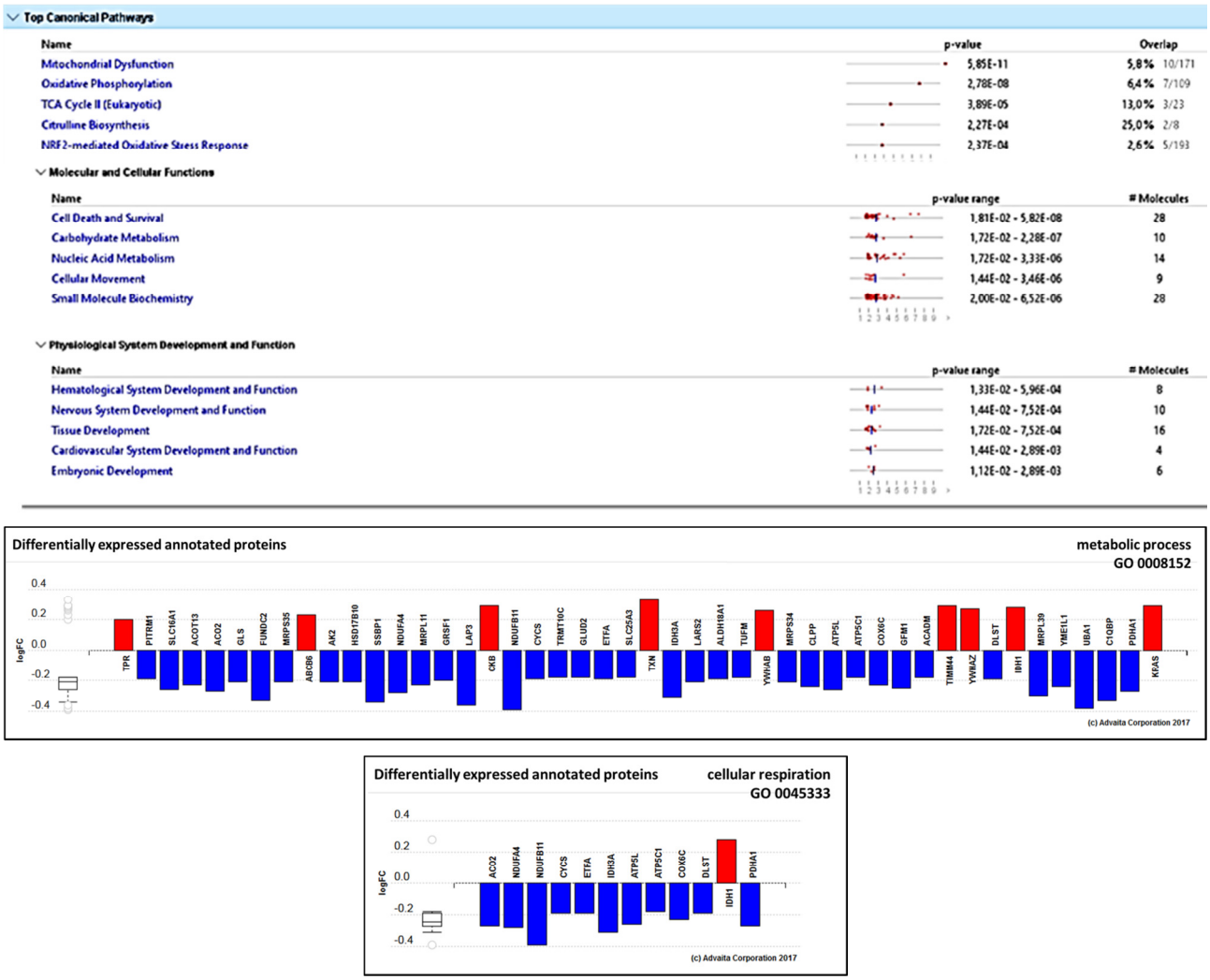

Figure 13 Bioinformatics classification of DEPs in *CLN5* KO mitochondria. In red-up-regulation, in blue-down-regulation.

4.4.4 Bioinformatic analyses of differential proteome profiles in HEK293T CRISPR *CLN5* KO lysosomes

The proteome analysis of lysosomal fractions was carried out in preparations obtained from three *CLN5* KO clones (clones #8, #9b and #11) compared to that from empty vector cells. Samples were collected in two independent experiments and the overall expression profile of the six lysosomal preparations from *CLN5* KO clones was then compared to the profile of the two lysosomal preparations from empty vector clones.

Lysosomal proteins were identified and selected by evidence for lysosomal localization from GO cellular component annotation. DEPs showing a FC ≥ 1.5 and p value < 0.05 were assigned as differentially expressed.

Proteome profiling revealed DEPs (19 IDs) in HEK293T *CLN5* KO lysosomes. Among these, 3 DEP were down-regulated and 16 up-regulated in *CLN5* KO cells (supplementary table S10). CLN5 protein was found only in lysosomes derived from an empty vector control HEK293T cells. Proteomes of lysosomal fractions from *CLN5* KO were devoid of CLN5 protein.

Bioinformatic examination of DEPs by GO biological process identified common altered pathways with an overall up-regulation of *Sphingolipid and glycosphingolipid metabolic process* (GO 0006665; GO 0006687), *Ceramide metabolic process* (GO 0006672), *Lipid metabolic process* (GO 0006629) and *Autophagy* (GO0006914) (Figure 14A). A possible involvement of CLN5 in lipid homeostasis and ganglioside signaling pathways underpins new features in the lysosomal biology of CLN5 disease. IPA algorithms suggested TFEB activation (indicated as *top transcriptional upstream regulator*) in *CLN5* KO lysosomes promoting lysosome biogenesis, indicating a strong activation of autophagy in these cells (Figure 14B).

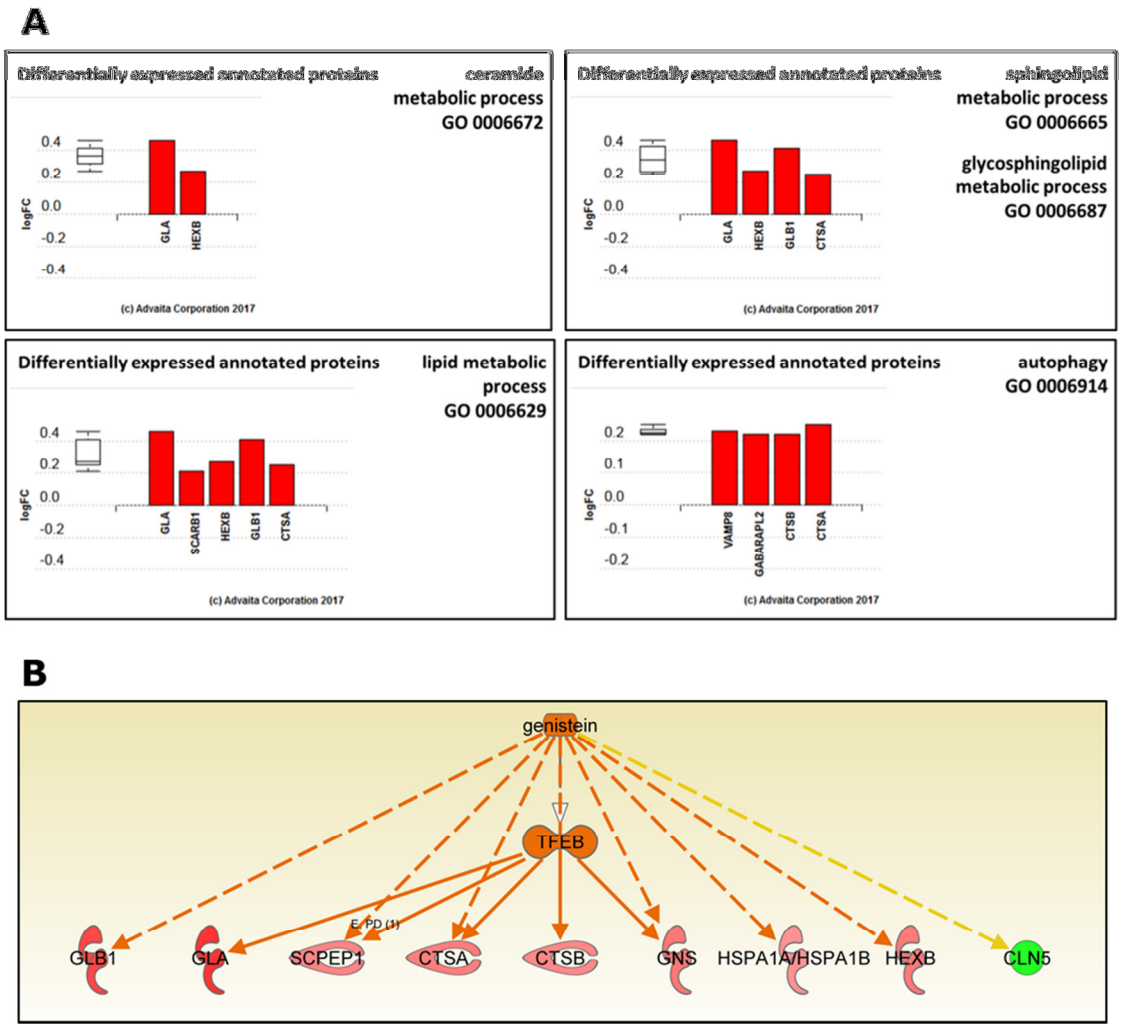

Figure 14 *(A) GO biological process analysis in CLN5 KO lysosomes. The analyses pinpoint to common up-regulation of sphingolipid and glycosphingolipid, lipid, ceramide metabolic process and autophagy. (B) TFEB activation in CLN5 KO lysosomes and pathway modulation by the isoflavonoid Genistein*

4.4.5 Analysis of differential proteome profiles in mitochondria from *Cln5* $^{-/-}$ mice cerebral cortex

The mitochondrial proteome analysis was carried out in preparations obtained from homozygous *Cln5*$^{-/-}$ and wild-type littermates, age matched control male mice. We analyzed pre-symptomatic (3 months) and symptomatic stages (9 months) sacrificing four animals per group at two time points (sixteen animals in total).
Following a selection of mitochondrial proteins (see paragraph mitochondrial scoring system), DEPs showing a FC ≥ 1.2 and p value < 0.05 were assigned as differentially expressed.
Proteome profiling of mitochondrial fractions revealed 19 DEPs differentially expressed in presymptomatic *Cln5*$^{-/-}$ mice with high and medium mitochondrial confidence score. 13 DEPs were found to be down-regulated and 6 up-regulated (supplementary table S11). Profiling experiments at the symptomatic stage revealed 32 DEPs with high and medium mitochondrial confidence, including 12 down-regulated and 20 up-regulated ones (supplementary table S12). Categorization of DEP, at the presymptomatic stage, indicated a *Dysregulated OXPHOS* (GO:0006119) related to *ATP synthase deficiency. Proteomic* categorization in symptomatic mice revealed a *Dysregulation of vesicle transport* (GO 0016192) and an impairment of Cyt c oxidase activity suggesting a role in disease progression related to the reduced bioenergetic capacity and ROS production by respiratory chain complex III.

4.5 Validation of proteomic profiling data

As revealed by proteomic profiling, mitochondrial compartment seems to be significantly involved in the pathogenesis of CLN5 disease.
In order to validate the DEPs, related functions and associated pathways the mitochondrial organization was further studied at the structural and a functional level. Furthermore, selected mitochondrial and lysosomes-related DEP were semi-quantitatively evaluated by WB analysis.

4.5.1 Analysis of mitochondrial compartments and bioenergetics capacity in CLN5 KO cellular model

To investigate how *CLN5* KO impacts on mitochondrial structure, we analyzed the shape of the mitochondrial reticulum by porin (VDAC) immuno-staining. We observed a punctuate profiles in HEK293T *CLN5* KO cells in comparison to the controls, with mitochondria centered around the nuclei (Figure 15), similarly as demonstrated in other forms of NCL (*i.e.* CLN1 disease, Pezzini et al., 2011). In order to investigate how the detected stress-induced mitochondrial fission affected bioenergetics capacity and metabolic condition, we assayed the mitochondrial energy metabolism in HEK293T and SH-SY5Y *CLN5* KO cells.

In comparison to the control cell line, we detected a decrease of basal oxygen consumption as well as a decrease in the ATP-linked respiration in both models. Furthermore, the rate of oligomycin-sensitive oxygen consumption, which reflects proton leakage across the inner mitochondrial membrane was lower in *CLN5* KO cells as compared to the controls. By contrast, no significant differences were observed in non-mitochondrial respiration (Figure 16A-B)

Our results showed a general impairment of mitochondrial function in *CLN5* KO cell models pronouncing the possible mitochondrial involvement in the pathogenesis of the disease.

To link these findings to CLN5 disease, we also tested cellular ATP production *in vitro* using a luminometry assay in cultured skin fibroblasts derived from CLN5 patients. Fibroblasts were cultured with glucose (G) and under conditions that supported only glycolytic (glucose with oligomycin, G+O), or mitochondrial ATP production (2-deoxy-D-glucose with pyruvate, D+P). Under oxidative conditions we observed a significantly reduced ATP production in the patients' fibroblasts as compared to healthy controls (Figure 16C).

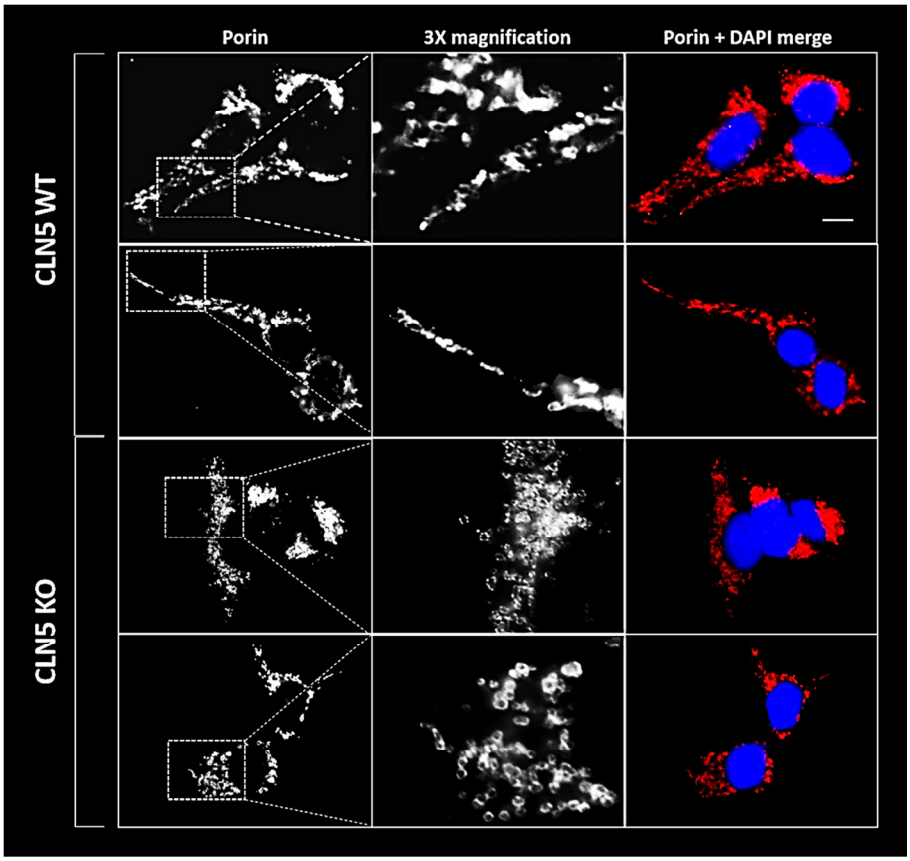

Figure 15 *Mitochondrial network organization in CLN5 KO HE293T cells. Scale bar, 10µm. Increased incidence of mitochondrial fragmentation with a punctuate profiles and perinuclear clustering were observed in cellular model of the CLN5 disease.*

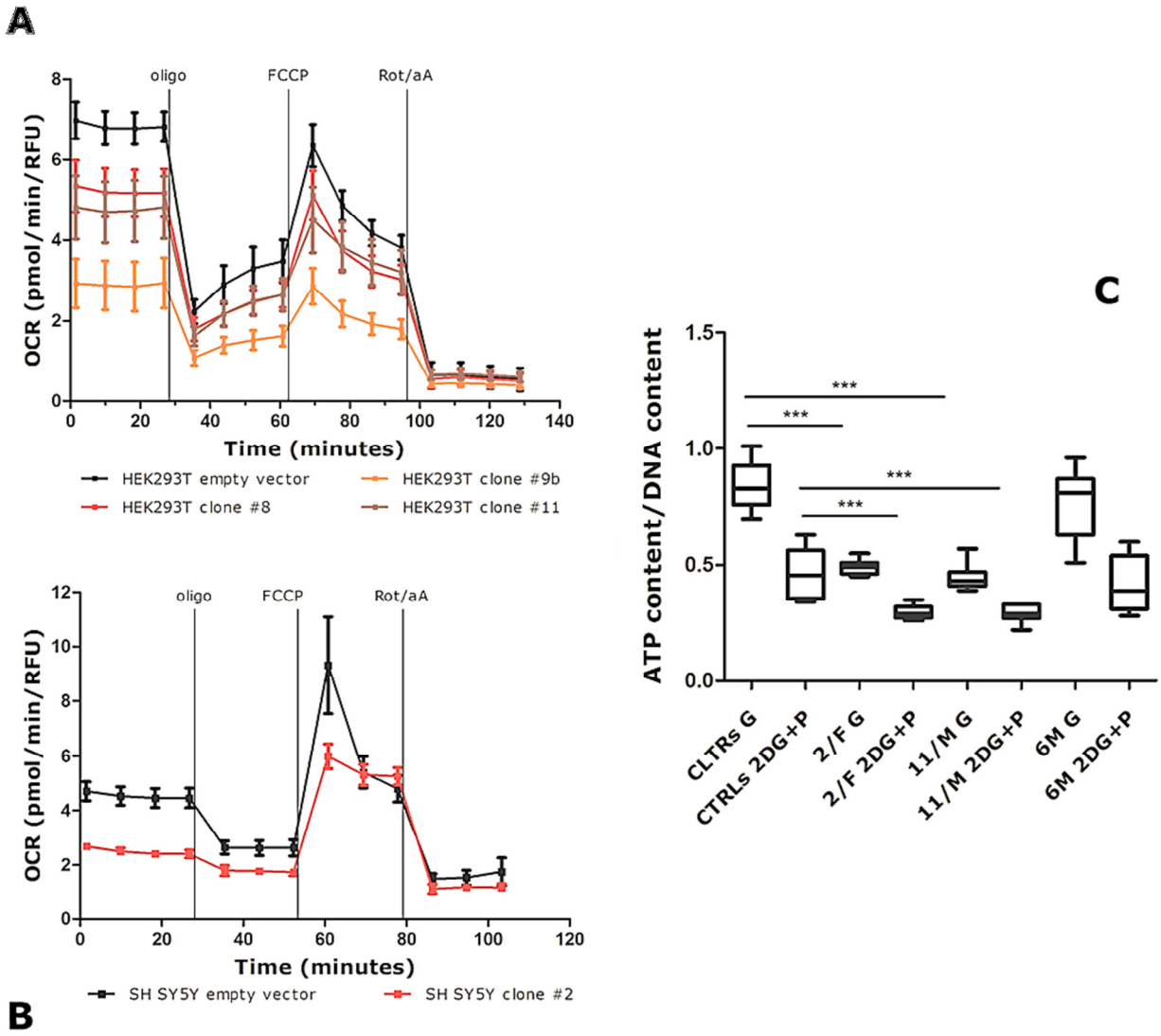

Figure 16 *Oxygen consumption and rate in HEK293T (A), SH-SY5Y (B) models and ATP content in patients' fibroblasts (C). Micro-oxygraphy graphs depict means and standard deviations whereas ATP content graph report a box plot with whiskers indicating min to max range. *** p<0.001.*

Table 7 *CLN5 patients' molecular profiles.*

Patient / Sex	Age of Onset	Gene Mutations	Predicted Protein Changes
2/F	4	c.595C>T/c.595C>T	p.Arg199*/p.Arg199*
6/M	5	c.1137G>A/c.1137G>A	p.Trp379*/p.379*
11/M	5	c.772T>G/c.772T>G	p.Tyr258Asp/p.Tyr258Asp

*= stop codon formation;

4.5.2 Western blotting analysis of selected DEPs validates proteomic data

In order to validate the changes in protein expression of selected DEP, we assessed protein expression level in whole cell lysates from HEK293T, SH-SY5Y and patients' fibroblasts (molecular findings are summarized in Table 5) in which the CLN5 function was defective. Using this strategy we could compare the organelle-specific proteome data in cell lysates and patients' biological material.

To validate the differential down-regulation in mitochondrial proteome, we selected two proteins (ACO2, ATP5L) related to cellular respiration, and one (FUNDC2) related to mitophagy process. To validate the differential changes observed in lysosomal proteome, we analyzed GLA, HEXB enzymes related to ceramide metabolic process (Platt, 2014).

As shown in Figure 17A, ACO2 protein expression level was reduced in HEK293T and SH-SY5Y KO cells. Interestingly, we also observed low ACO2 expression in two of the three CLN5 patients' fibroblasts whereas a normal expression pattern was observed in cells from a single case (Pt 6/M), in which we also observed normal ATP content values (Figure 16C).

Probing with FUNDC2 antibody did not show a significant signal in SH-SY5Y and skin fibroblasts samples. Low protein levels were detected in HEK293T CLN5 KO cells as compared to the control. Finally, ATP5L was reduced in HEK293T and SH-SY5Y KO cells, but a detectable signal in primary skin fibroblasts was observed.

WB analysis of lysosome-related DEPs (Figure 17B) indicated strong signal of HEXB in SH-SY5Y and, to a lesser extent, in HEK293T *CLN5* KO cells, while GLA signal intensity was similarly increased in both KO models.

When tested in patients' fibroblasts we observed higher levels of GLA and HEXB in comparison to the control cells. Protein expression changes in Pt M/6 fibroblasts seemed to be more attenuated. Using LAMP2 antibody, a specific lysosomal marker, we further verified that the overall up-regulation of DEP was not related to an increase in the amount of lysosomes, but to specific changes in their expression.

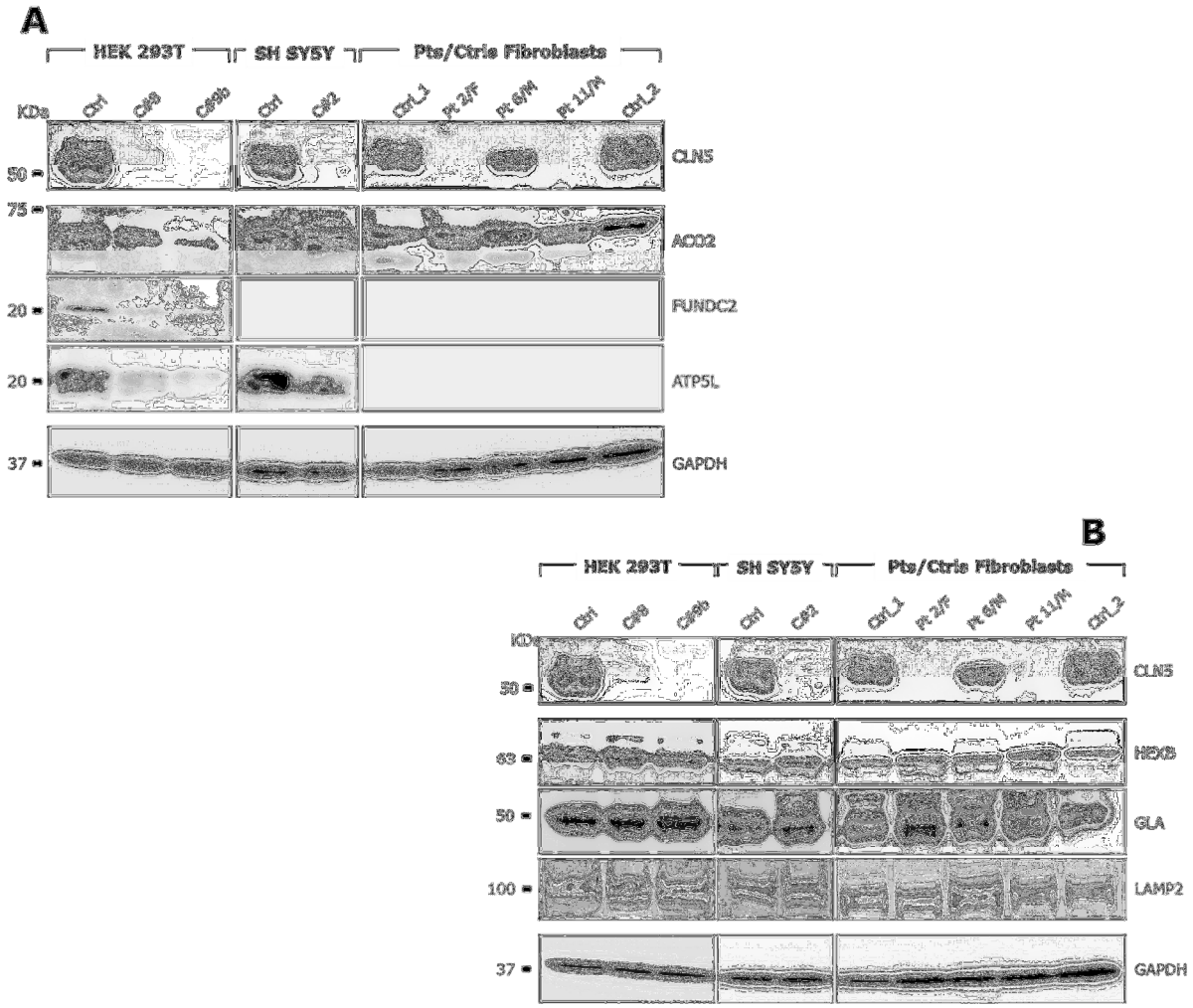

Figure 17 *WB analysis of differentially expressed mitochondrial (A) and lysosomal (B) proteins. 20µg whole cell lysates from HEK293T, SH-SY5Y and primary human skin fibroblasts was separated on a 8-16% SDS-PAGE gel. WB were then probed with antibodies specific for identified DEPs validating the differential changes observed in lysosomal and mitochondrial proteome*

4.6 CLN10 disease

4.6.1 Analysis of the novel homozygous c.205G>A/p.Glu69Lys mutation on CTSD expression and enzyme activity

The conclusive diagnosis of NCL in this patient was confirmed by Sanger sequencing, whichconfirmed the novel homozygous mutation in *CTSD* (c.205G>A/p.Glu69Lys) (Figure 18A), and an MS-based multiplex enzyme test in dried blood spot (DBS). The mutation was homozygous in the patient, heterozygous in healthy parents and absent in large exome polymorphic databases (ExAC, ESP6500). *In silico* predictions (Mutation Taster - www.mutationtaster.org, PolyPhen-2 - genetics.bwh.harvard.edu and by PANTHER - www.pantherdb.org/tools/csnpScoreForm.jsp) suggested a damaging role of a highly conserved amino acid.

WB analysis in patient's cultured skin fibroblasts revealed low levels of mature form of CTSD (CTSDm) whereas the signals related to the pro- and the single chain forms, although less visible, seemed to be normal suggesting an incomplete process of protein maturation, most likely due to the mutation (Figure 18B).

Both WB and enzyme assays clearly showed a reduced activity in the child harboring the novel p.Glu69Lys in *CTSD* while carrier parents showed intermediate values (Figure 18C). The activities of CLN1/PPT1 and CLN2/TPP1 in the same samples were normal, as judged by mass spectrometry (not shown). These results corroborated the pathogenic significance of the novel mutation in *CTSD* and suggested a loss of function mechanism.

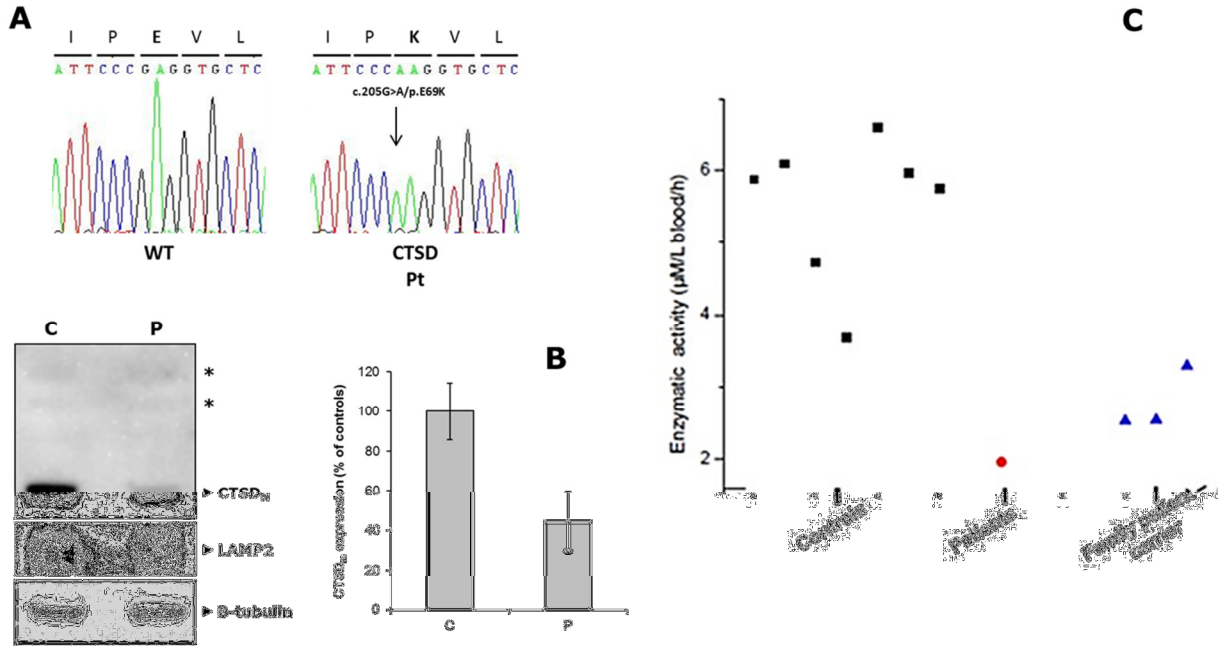

Figure 18 *Molecular and biochemical features in CTSD patient. (A) Molecular analysis of the novel p.Glu69Lys CTSD mutation. (B) Wester blotting analysis shows the band at 34 kDa representing the mature CTSD. The pro (52 kDa) and the single chain (43 kDa) forms of CTSD (indicated by asterisks) are slightly visible in human fibroblasts. LAMP2 protein has been used as lysosomal marker. β-tubulin staining of the samples shown as a loading control. Histogram quantify the reduction levels of mature CTSD. Data refers to three independent experiments. (C) Biochemical analysis of CTSD in DBS obtained from the proposita, her carrier parents and six healthy, age/sex-matched controls. The enzymatic rate clearly showed a reduced activity in the child harboring the novel p.Glu69Lys in CTSD while carrier parents showed values intermediate between controls and the patient.*

4.6.2 Ultrastructural examination reveals the presence of granular osmiophilic deposits

The electron microscopy of patient' skin biopsy showed evidence of granular appearance of stored material (GRODs) (Figure 19A).

To test for the possible effect(s) of a novel *CTSD* mutation on *PPT1* mRNA expression, we analyzed it by qPCR in cultured patient's skin fibroblasts. Alterations in *PPT1* mRNA expression levels were not observed (Figure 19B) suggesting a lack of correlation with the accumulation of

stored material and that the observed ultrastructural GRODs abnormalities are unlikely related to downregulation of PPT1 activity but closely linked to the novel mutation in *CTSD*.

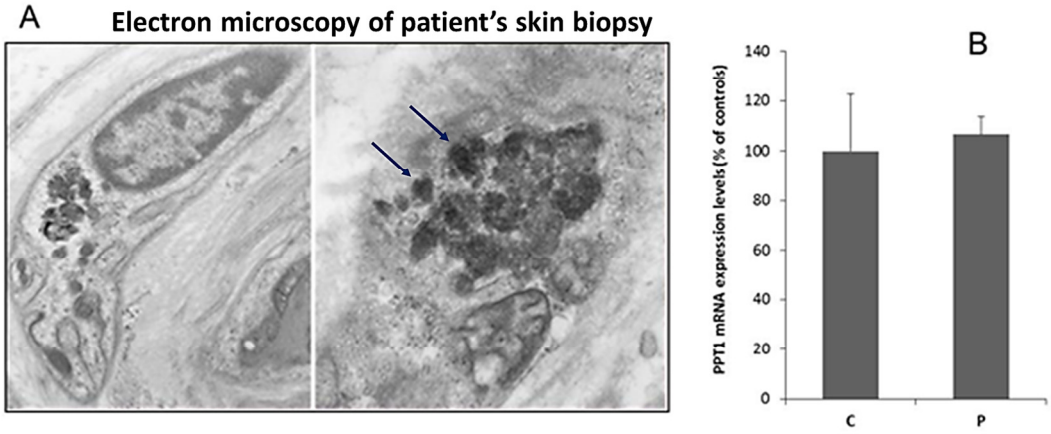

Figure 19 *(A) Electron microscopy of patient's skin biopsy harboring the homozygous c.205G>A/p.Glu69Lys mutation in CTSD. Arrows point out the granular appearance of stored material (GRODs). (B) Analysis of PPT1 mRNA expression levels by qPCR. Unlike the INCL, characterized by a correlation between GRODs abnormalities and downregulation of PPT1 activity, normal PPT1 mRNA expression levels measured in patient's fibroblasts suggested a specific relationship between the observed ultrastructural abnormalities and the novel mutation in CTSD*

4.6.3 Analysis of autophagy process in *CTSD* patient's fibroblasts

We performed a study of the autophagy process in cultured skin fibroblasts of the new CLN10 patient presenting the clinical phenotype of chronic NCL.

Using an aggresome detection dye (red fluorescence), which is essentially non-fluorescent until it binds to the structural features associated with aggregated protein cargos, we did not detect there were no aggresome-like inclusions accumulating in CTSD patient's fibroblasts (Figure 20A).

By WB analysis we also evaluated the expression of LC-III and p62, the major biomarkers of autophagy, in basal condition and after appropriate stimuli with torin1 (an activator of autophagy through the inhibition of mTOR pathway), and cloroquine (an autophagy inhibitor through lysosome neutralization and inactivation of lysosome enzymes) (Figure 20B). The p62/SQSTM1 protein is an ubiquitin-binding scaffold protein that localizes with ubiquitinated protein aggregates in many neurodegenerative diseases. p62/SQSTM1 binds directly to LC-III family proteins via a specific sequence motif. The protein itself is degraded by autophagy and may serve to link ubiquitinated proteins to the autophagy machinery to enable their degradation in the lysosome. Since p62 accumulation occurs when autophagy is inhibited and decreased levels can be observed when autophagy is induced, p62 may be used as a marker to study the accuracy of the autophagy flux.

By fluorescent microscopy we labeled lysosomes in patient's live cells (Figure 19C) evaluating the lysosomal compartment to observe the number and distribution of lysosomal pattern that might be dysregulated if the autophagy pathway is disrupted.

Our results suggest a correlation between the data on aggresome formation and the biomarkers of autophagy indicating a normal flux and autophagy process in CTSD patient's fibroblasts.

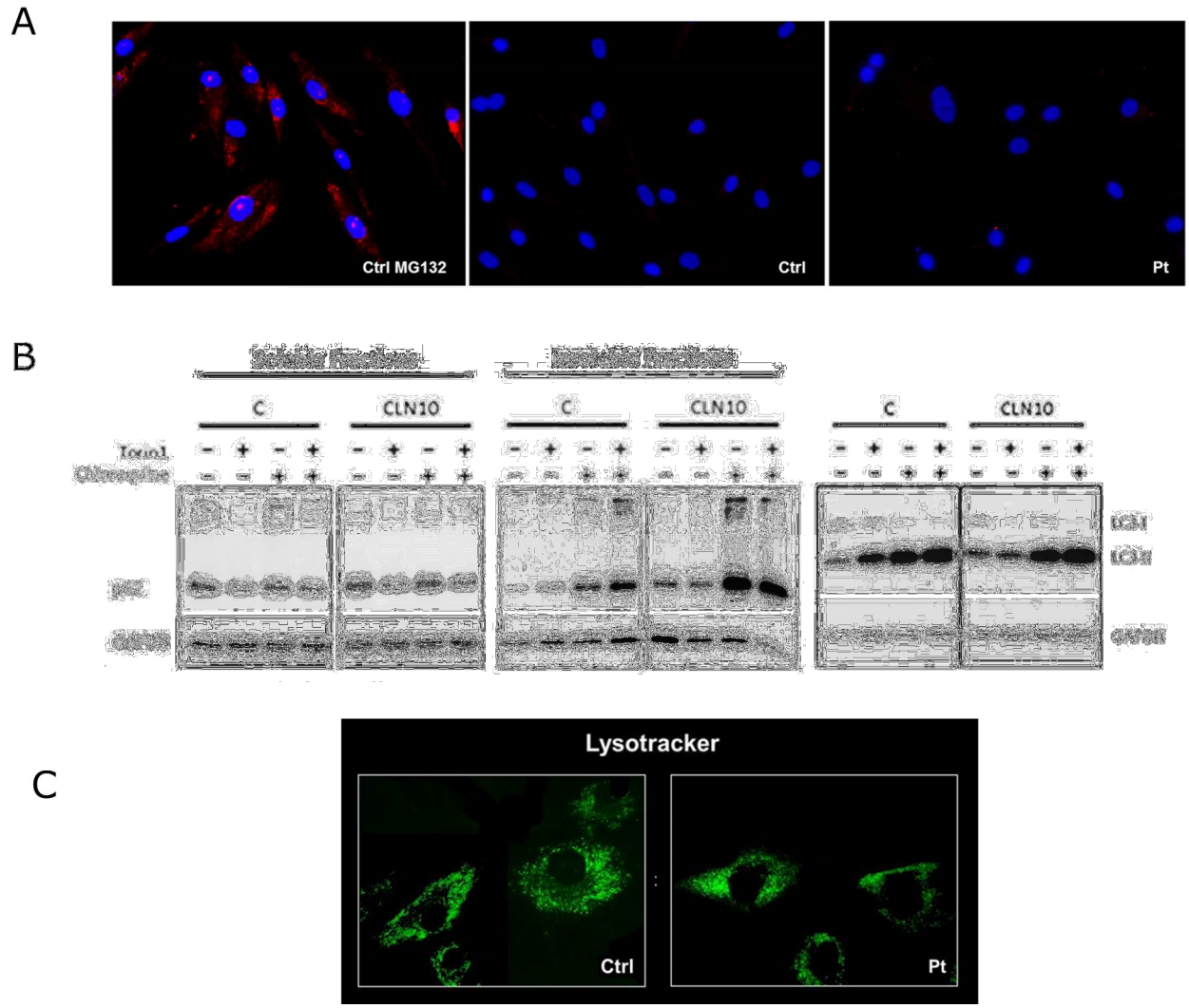

Figure 20 *Analysis of autophagy process. (A). Analysis of aggresome formation.by ProteoStat® aggresome detection dye (red fluorescence). Hoechst 33342 (blue fluorescence) was used as nuclear stain. (B) WB analysis of the major biomarkers of autophagy in basal condition and after appropriate stimuli. (C) Analysis of lysosomal pattern by LysoTracker fluorescent probe*

5. DISCUSSION

The Neuronal Ceroid Lipofuscinoses (NCLs) represent a progressive group of inherited neurodegenerative diseases.

No rational basis for effective treatments is available for most of the enzymatic and non-enzymatic NCL forms. Enzyme replacement therapy (ERT) is currently in use to treat peripheral symptoms in various lysosomal storage disorders but it is ineffective for the neuronal symptoms since the recombinant enzyme cannot penetrate the blood-brain-barrier (Kohan et al., 2011; Lu et al., 2010). Other therapies such as gene therapy are still under development (Kohan et al., 2011). In late April of 2017, FDA approved Brineura (Cerliponase alfa) for the treatment of CLN2. Although the genetic underpinnings of most NCL forms have been identified, the pathway(s) in which neuronal impairment results in the severe degenerative phenotype remain unknown.

In this work we attempted to clarify the cellular and molecular mechanisms underlying three different forms of early-onset NCLs disease using patients' material, cell and animal models analyzed by multiomics techniques, to obtain large-scale data and bring evidence about molecular pathways shared among different NCL proteins. Our focus was on the identification of distinctive pathways that could characterize, at least in part, the diseases associated with different genes: *CLN1* (causing an infantile form of NCL), *CLN5* (determining a variant-late infantile form) and *CLN10-CTSD* (responsible for the congenital form).

Our results offer at least three explanations: 1) dysregulation of synaptic proteins in a model of PPT1 dysregulation; 2) further evidence for a tight cross-talk between PPT1, CLN5, and CTSD proteins; 3) involvement of ceramide metabolism and mitochondrial network impairment as a potential signature of CLN5 disease.

Analyzing the link between increased expression of a wild-type *PPT1* and DEGs encoding palmitoylated neuronal proteins we brought novel evidence about the possible PPT1 target substrates. Our findings on the effects of dysregulated networks of genes coding for palmitoylated proteins suggest that hyper-depalmitoylating activity may perturb the expression of proteins implicated in neurogenesis and synaptic transmission.

It has been recently demonstrated that PPT1 itself is regulated by the palmitoylation at cysteine residue in position 6 of the signal peptide, creating a sort of a positive feedback loop (Segal-Salto et al., 2016).

Our results are supported by a recent study on the role of palmitoylation in axonal dynamics (Holland and Thomas, 2017) and may be consistent with the extra-lysosomal role of PPT1 in the nerve terminals (Kim et al., 2008; Lehtovirta, 2001).

A potential role of PPT1 in modulating the function of membrane proteins related with neuronal excitability and, possibly, epileptogenesis were also identified by dysregulation of calcium and potassium channel activities at the presynaptic level.

Dysregulated expression of synapse-related genes are associated with the pathological effects related to loss-of-function, and are known to be affected in *Ppt1*$^{-/-}$ mice, including pathological changes of a synaptic compartment (Kielar et al., 2009; Tikka et al., 2016; Virmani et al., 2005); moreover, a severe epilepsy associated with typical Electroencephalogram (EEG) pattern occurs in CLN1 patients, who are lacking PPT1 functional activity.

Although an overexpression and a loss-of-function models cannot be compared straightforwardly, the results of this study can be considered as the effect of a likely altered gene dosage of wtCLN1 due to wild type gene overexpression.

Our transcriptomic analyses also revealed an up-regulation of *CTSD* mRNA consistent with CTSD overexpression mediated by TFEB upregulation occurring in astrocytes and microglia of *Ppt1*$^{-/-}$ mice (Chandra et al., 2015). CLN1 and CLN10 are enzymatic forms of NCL and share some clinical features including epileptic manifestations and ultrastructural GRODs abnormalities, suggesting a sort of overlap among these two forms. In this scenario, lysosomal CTSD deficiency could represent a common pathogenic link between infantile NCL due by inactivating mutations in the *CLN1* gene and congenital NCL which underlies CLN10. The link was exemplified by studies in tissues from a patient whose clinical features were highly reminiscent of the CLN1 disease in spite of the presence of genetic and ultrastructural signs of a CLN10 disease. In this study we presented the association of the novel *CTSD* mutation with an early infantile form of CLN10 and by linking biochemical and molecular results we proposed a strategy for planning the early diagnostic screening in enzymatic forms of NCL.

An additional aspect described in this thesis emerges from the proteomic study at the mitochondrial and lysosomal level, by analyzing bioenergetic and lysosomal dysregulation processes in the pathogenesis of CLN5 disease. Our data facilitate a wider view on the protein signatures when the CLN5 protein is depleted and assisted in the identification of possible disease-relevant functions of pCLN5.

Proteomic analysis of mitochondrial compartment indicated an important role of CLN5 in mitochondrial dysfunction. Impairment of cellular bioenergetics capacity was identified at the functional level in HEK293T CLN5 KO cell lines and animal model.

Mitochondrial dysfunction is an important issue in the pathogenesis of neurodegenerative disorders, since neurons are highly dependent on energy supplied by oxidative metabolism (Meyer et al., 2017; Wong-Riley, 1989).

Functional annotations suggested by the bioinformatics analyses and the availability of patients' biological material allowed us to translate organelle-specific proteome analysis into a disease relevant scenario.

Interacting partners of CLN5 include mitochondrial carriers implicated in protein folding/sorting proteins and some of those are shared with other NCL proteins (e.g. CLN1 and CLN3; Scifo et al., 2013). PPT1 and CLN5, along with other NCL proteins, share common interaction partners, the F1 subunit of ATP synthase, the complex V of oxidative phosphorylation, essential for mitochondrial ATP synthesis (Lyly et al., 2009). Recent studies on double knock-out *Ppt1*$^{-/-}$

/*Cln5*$^{-/-}$ murine model showed myelination and immune response defects as well as a downregulation of α-synuclein suggesting that the two proteins are closely connected (Blom et al., 2013).

Cross-talk among NCL proteins in mitochondrial pathways was evaluated in micro-oxygraphy studies showing an impairment of mitochondrial function common to both overexpressing wtCLN1 and CLN5 KO CNS suggesting mitochondria as a final step in neurodegeneration of NCLs.

Similarly as in the human *CLN1* mutated fibroblasts (Pezzini et al., 2011), cellular model CLN5 KO showed alterations in mitochondrial network, characterized by a prevalence of fragmented mitochondria, indicator of an oxidative stress. Fission of mitochondria induced by damage to bioenergetics functions has been described previously (Ni et al., 2015). A similar effect can be achieved by uncoupling agents and respiratory inhibitors, or by mitochondrial overproduction of reactive oxygen species (ROS), which play a crucial role in cell death signaling (Fleury et al.)

Defects of mitochondrial function were also seen in brain from pre-symptomatic *Cln5*$^{-/-}$ mice

In 3-month-old mice we observed OxPhos dysregulation characterized by ATP synthase deficiency whereas in 8-month-old mice (symptomatic stage) we detected a specific impairment in cyt *c* oxidase activity (complex IV), suggesting that mitochondrial pathways are affected early in the disease process and contribute to neurodegeneration. Progressive overproduction of ROS causes OxPhos dysregulation and subsequently triggers cell death and neuronal injury processes (Fleury et al.)

A novel aspect in the pathogenesis of CLN5 disease is brought up by the possible implication in mitophagy, which contributes to mitochondrial quantity and quality regulation, by eliminating the number of mitochondria to fulfilling cellular energy requirements. Down regulation of proteins involved in this pathway could represent a further link to autophagy and more broadly an emerging new role in a lysosomal disorder.

In line with these findings, both mitochondria and lysosomes seem to play relevant roles in the initiation of the apoptotic cascade, which is known to occur in different NCL forms (Patwardhan et al., 2016; Pezzini et al., 2011).

Proteomic profiling of lysosomal fractions from HEK293T CRISPR CLN5 KO implies a putative role in lipid homeostasis and ganglioside signaling pathways. Increased amount of glycosphingolipids has been described in human cultured skin fibroblasts derived from CLN5 patients (Staropoli et al., 2012).

An overload of glycosphingolipid catabolism and ceramide metabolism was noticed by overexpression of enzymes implicated in gangliosides pathway and proteins implicated in sphingolipid transporter has already been identified as a CLN5 interacting partner (Scifo et al., 2013). This feature represents a possible connection with the activation of autophagy or mitophagy pathways, and the ensuing consequences on sphingolipid and phospholipid metabolisms.

These findings provide targets for future design of new lines of drugs.

The observed metabolic dysregulation has been recently linked with the impairment of mitochondrial function (Vilaça et al., 2017) suggesting a synergic action of these two organelle specific altered pathways. Both mitochondria and lysosomes participate in the pathogenesis of CLN5 disease through impairment of mitochondrial function and increased ROS triggering apoptotic processes, which is mitochondria-mediated and on the other hand, by overloading the metabolic processes common to other forms of neurodegeneration from lysosomal storage disorders.

To summarize, in this study we dissected some of the specificities in three different forms of NCL pathology using innovative functional omics approaches pinpointing the involvement of specific cellular processes in the NCL pathophysiology.

The results achieved in this study indicated shared pathways which may crosstalk with each other at multiple cellular locations. Disruption in these shared processes leads to evolvement of NCL pathology. Yet, the possibility that individualized or specific mechanisms are implicated in specific NCL subtypes suggests the more personalized approaches towards cure are feasible.

REFERENCES

Ahtiainen, L., Luiro, K., Kauppi, M., Tyynelä, J., Kopra, O., and Jalanko, A. (2006). Palmitoyl protein thioesterase 1 (PPT1) deficiency causes endocytic defects connected to abnormal saposin processing. *Exp. Cell Res.* 312, 1540–53. doi:10.1016/j.yexcr.2006.01.034.

Anderson, G. W., Goebel, H. H., and Simonati, A. (2013). Human pathology in NCL. *Biochim. Biophys. Acta - Mol. Basis Dis.* 1832, 1807–1826. doi:10.1016/j.bbadis.2012.11.014.

Bellizzi, J. J., Widom, J., Kemp, C., Lu, J. Y., Das, A. K., Hofmann, S. L., et al. (2000). The crystal structure of palmitoyl protein thioesterase 1 and the molecular basis of infantile neuronal ceroid lipofuscinosis. *Proc. Natl. Acad. Sci. U. S. A.* 97, 4573–8. doi:10.1073/pnas.080508097.

Bible, E., Gupta, P., Hofmann, S. L., and Cooper, J. D. (2004). Regional and cellular neuropathology in the palmitoyl protein thioesterase-1 null mutant mouse model of infantile neuronal ceroid lipofuscinosis. *Neurobiol. Dis.* 16, 346–59. doi:10.1016/j.nbd.2004.02.010.

Blanc, M., David, F., Abrami, L., Migliozzi, D., Armand, F., Bürgi, J., et al. (2015). SwissPalm: Protein Palmitoylation database. *F1000Research*. doi:10.12688/f1000research.6464.1.

Blom, T., Schmiedt, M.-L., Wong, A. M., Kyttala, A., Soronen, J., Jauhiainen, M., et al. (2013). Exacerbated neuronal ceroid lipofuscinosis phenotype in Cln1/5 double-knockout mice. *Dis. Model. Mech.* 6, 342–357. doi:10.1242/dmm.010140.

Bosch, M. E., Aldrich, A., Fallet, R., Odvody, J., Burkovetskaya, M., Schuberth, K., et al. (2016). Self-Complementary AAV9 Gene Delivery Partially Corrects Pathology Associated with Juvenile Neuronal Ceroid Lipofuscinosis (CLN3). *J. Neurosci.* 36, 9669–9682. doi:10.1523/JNEUROSCI.1635-16.2016.

Bosch, M. E., and Kielian, T. (2015). Neuroinflammatory paradigms in lysosomal storage diseases. *Front. Neurosci.* 9. doi:10.3389/fnins.2015.00417.

Brinkman, E. K., Chen, T., Amendola, M., and van Steensel, B. (2014). Easy quantitative assessment of genome editing by sequence trace decomposition. *Nucleic Acids Res.* 42, e168–e168. doi:10.1093/nar/gku936.

Camp, L. A., Verkruyse, L. A., Afendis, S. J., Slaughter, C. A., and Hofmann, S. L. (1994). Molecular cloning and expression of palmitoyl-protein thioesterase. *J. Biol. Chem.* 269, 23212–9. Available at: http://www.ncbi.nlm.nih.gov/pubmed/7916016.

Cárcel-Trullols, J., Kovács, A. D., and Pearce, D. A. (2015). Cell biology of the NCL proteins: What they do and don't do. *Biochim. Biophys. Acta - Mol. Basis Dis.* 1852, 2242–2255. doi:10.1016/j.bbadis.2015.04.027.

Chandra, G., Bagh, M. B., Peng, S., Saha, A., Sarkar, C., Moralle, M., et al. (2015). Cln1 gene disruption in mice reveals a common pathogenic link between two of the most lethal childhood neurodegenerative lysosomal storage disorders. *Hum. Mol. Genet.* 24, 5416–5432. doi:10.1093/hmg/ddv266.

Cho, S., and Dawson, G. (2000). Palmitoyl protein thioesterase 1 protects against apoptosis mediated by Ras-Akt-caspase pathway in neuroblastoma cells. *J. Neurochem.* 74, 1478–88. Available at: http://www.ncbi.nlm.nih.gov/pubmed/10737604.

Cho, S., Dawson, P. E., and Dawson, G. (2000). Antisense palmitoyl protein thioesterase 1 (PPT1) treatment inhibits PPT1 activity and increases cell death in LA-N-5 neuroblastoma cells. *J. Neurosci. Res.* 62, 234–40. doi:10.1002/1097-4547(20001015)62:2<234::AID-JNR8>3.0.CO;2-8.

Cotman, S. L., Karaa, A., Staropoli, J. F., and Sims, K. B. (2013). Neuronal ceroid lipofuscinosis: Impact of recent genetic advances and expansion of the clinicopathologic spectrum topical collection on genetics. *Curr. Neurol. Neurosci. Rep.* 13, 1–17. doi:10.1007/s11910-013-0366-z.

Das, A. K., Lu, J. Y., and Hofmann, S. L. (2001). Biochemical analysis of mutations in palmitoyl-protein thioesterase causing infantile and late-onset forms of neuronal ceroid lipofuscinosis. *Hum. Mol. Genet.* 10, 1431–9. Available at: http://www.ncbi.nlm.nih.gov/pubmed/11440996.

Das, A. M., Jolly, R. D., and Kohlschütter, A. (1999). Anomalies of mitochondrial ATP synthase regulation in four different types of neuronal ceroid lipofuscinosis. *Mol. Genet. Metab.* 66, 349–55. doi:10.1006/mgme.1999.2811.

Doccini, S., Sartori, S., Maeser, S., Pezzini, F., Rossato, S., Moro, F., et al. (2016). Early infantile neuronal ceroid lipofuscinosis (CLN10 disease) associated with a novel mutation in CTSD. *J. Neurol.* 263, 1029–1032. doi:10.1007/s00415-016-8111-6.

Faller, K. M. E., Gutierrez-Quintana, R., Mohammed, A., Rahim, A. A., Tuxworth, R. I., Wager, K., et al. (2015). The neuronal ceroid lipofuscinoses: Opportunities from model systems. *Biochim. Biophys. Acta - Mol. Basis Dis.* 1852, 2267–2278. doi:10.1016/j.bbadis.2015.04.022.

Fleury, C., Mignotte, B., and Vayssière, J.-L. Mitochondrial reactive oxygen species in cell death signaling. *Biochimie* 84, 131–41. Available at: http://www.ncbi.nlm.nih.gov/pubmed/12022944.

Groh, J., Kühl, T. G., Ip, C. W., Nelvagal, H. R., Sri, S., Duckett, S., et al. (2013). Immune cells perturb axons and impair neuronal survival in a mouse model of infantile neuronal ceroid lipofuscinosis. *Brain* 136, 1083–101. doi:10.1093/brain/awt020.

Gupta, P., Soyombo, A. A., Atashband, A., Wisniewski, K. E., Shelton, J. M., Richardson, J. A., et al. (2001). Disruption of PPT1 or PPT2 causes neuronal ceroid lipofuscinosis in knockout mice. *Proc. Natl. Acad. Sci. U. S. A.* 98, 13566–71. doi:10.1073/pnas.251485198.

Haltia, M., Rapola, J., and Santavuori, P. (1973). Infantile type of so-called neuronal ceroid-lipofuscinosis. Histological and electron microscopic studies. *Acta Neuropathol.* 26, 157–70. Available at: http://www.ncbi.nlm.nih.gov/pubmed/4763201.

Hawkins-Salsbury, J. A., Cooper, J. D., and Sands, M. S. (2013). Pathogenesis and therapies for infantile neuronal ceroid lipofuscinosis (infantile CLN1 disease). *Biochim. Biophys. Acta*

1832, 1906–9. doi:10.1016/j.bbadis.2013.05.026.

Holland, S. M., and Thomas, G. M. (2017). Roles of palmitoylation in axon growth, degeneration and regeneration. *J. Neurosci. Res.* 95, 1528–1539. doi:10.1002/jnr.24003.

Holmberg, V., Jalanko, A., Isosomppi, J., Fabritius, A. L., Peltonen, L., and Kopra, O. (2004). The mouse ortholog of the neuronal ceroid lipofuscinosis CLN5 gene encodes a soluble lysosomal glycoprotein expressed in the developing brain. *Neurobiol. Dis.* 16, 29–40. doi:10.1016/j.nbd.2003.12.019.

Invernizzi, F., D'Amato, I., Jensen, P. B., Ravaglia, S., Zeviani, M., and Tiranti, V. (2012). Microscale oxygraphy reveals OXPHOS impairment in MRC mutant cells. *Mitochondrion* 12, 328–335. doi:10.1016/j.mito.2012.01.001.

Jalanko, A., Vesa, J., Manninen, T., von Schantz, C., Minye, H., Fabritius, A.-L., et al. (2005). Mice with Ppt1Δex4 mutation replicate the INCL phenotype and show an inflammation-associated loss of interneurons. *Neurobiol. Dis.* 18, 226–241. doi:10.1016/j.nbd.2004.08.013.

Johansson, A.-C., Steen, H., Öllinger, K., and Roberg, K. (2003). Cathepsin D mediates cytochrome c release and caspase activation in human fibroblast apoptosis induced by staurosporine. *Cell Death Differ.* 10, 1253–1259. doi:10.1038/sj.cdd.4401290.

Kielar, C., Wishart, T. M., Palmer, A., Dihanich, S., Wong, A. M., Macauley, S. L., et al. (2009). Molecular correlates of axonal and synaptic pathology in mouse models of Batten disease. *Hum. Mol. Genet.* 18, 4066–4080. doi:10.1093/hmg/ddp355.

Kim, S.-J., Zhang, Z., Lee, Y.-C., and Mukherjee, A. B. (2006). Palmitoyl-protein thioesterase-1 deficiency leads to the activation of caspase-9 and contributes to rapid neurodegeneration in INCL. *Hum. Mol. Genet.* 15, 1580–6. doi:10.1093/hmg/ddl078.

Kim, S.-J., Zhang, Z., Sarkar, C., Tsai, P.-C., Lee, Y.-C., Dye, L., et al. (2008). Palmitoyl protein thioesterase-1 deficiency impairs synaptic vesicle recycling at nerve terminals, contributing to neuropathology in humans and mice. *J. Clin. Invest.* 118, 3075–86. doi:10.1172/JCI33482.

Kohan, R., Cismondi, I. A., Oller-Ramirez, A. M., Guelbert, N., Anzolini, T. V, Alonso, G., et al. (2011). Therapeutic approaches to the challenge of neuronal ceroid lipofuscinoses. *Curr. Pharm. Biotechnol.* 12, 867–83. Available at: http://www.ncbi.nlm.nih.gov/pubmed/21235444.

Koike, M., Nakanishi, H., Saftig, P., Ezaki, J., Isahara, K., Ohsawa, Y., et al. (2000). Cathepsin D deficiency induces lysosomal storage with ceroid lipofuscin in mouse CNS neurons. *J. Neurosci.* 20, 6898–906. Available at: http://www.ncbi.nlm.nih.gov/pubmed/10995834.

Kopra, O. (2004). A mouse model for Finnish variant late infantile neuronal ceroid lipofuscinosis, CLN5, reveals neuropathology associated with early aging. *Hum. Mol. Genet.* 13, 2893–2906. doi:10.1093/hmg/ddh312.

Lehtovirta, M. (2001). Palmitoyl protein thioesterase (PPT) localizes into synaptosomes and synaptic vesicles in neurons: implications for infantile neuronal ceroid lipofuscinosis

(INCL). *Hum. Mol. Genet.* 10, 69–75. doi:10.1093/hmg/10.1.69.

Levin, S. W., Baker, E. H., Zein, W. M., Zhang, Z., Quezado, Z. M. N., Miao, N., et al. (2014). Oral cysteamine bitartrate and N-acetylcysteine for patients with infantile neuronal ceroid lipofuscinosis: A pilot study. *Lancet Neurol.* 13, 777–787. doi:10.1016/S1474-4422(14)70142-5.

Lu, J.-Y., Nelvagal, H. R., Wang, L., Birnbaum, S. G., Cooper, J. D., and Hofmann, S. L. (2015). Intrathecal enzyme replacement therapy improves motor function and survival in a preclinical mouse model of infantile neuronal ceroid lipofuscinosis. *Mol. Genet. Metab.* 116, 98–105. doi:10.1016/j.ymgme.2015.05.005.

Lu, J. Y., Hu, J., and Hofmann, S. L. (2010). Human recombinant palmitoyl-protein thioesterase-1 (PPT1) for preclinical evaluation of enzyme replacement therapy for infantile neuronal ceroid lipofuscinosis. *Mol. Genet. Metab.* 99, 374–378. doi:10.1016/j.ymgme.2009.12.002.

Lyly, A., von Schantz, C., Heine, C., Schmiedt, M.-L., Sipilä, T., Jalanko, A., et al. (2009). Novel interactions of CLN5 support molecular networking between Neuronal Ceroid Lipofuscinosis proteins. *BMC Cell Biol.* 10, 83. doi:10.1186/1471-2121-10-83.

Lyly, A., von Schantz, C., Salonen, T., Kopra, O., Saarela, J., Jauhiainen, M., et al. (2007). Glycosylation, transport, and complex formation of palmitoyl protein thioesterase 1 (PPT1)--distinct characteristics in neurons. *BMC Cell Biol.* 8, 22. doi:10.1186/1471-2121-8-22.

Macauley, S. L., Wong, A. M. S., Shyng, C., Augner, D. P., Dearborn, J. T., Pearse, Y., et al. (2014). An Anti-Neuroinflammatory That Targets Dysregulated Glia Enhances the Efficacy of CNS-Directed Gene Therapy in Murine Infantile Neuronal Ceroid Lipofuscinosis. *J. Neurosci.* 34, 13077–13082. doi:10.1523/JNEUROSCI.2518-14.2014.

Mancini, C., Nassani, S., Guo, Y., Chen, Y., Giorgio, E., Brussino, A., et al. (2015). Adult-onset autosomal recessive ataxia associated with neuronal ceroid lipofuscinosis type 5 gene (CLN5) mutations. *J. Neurol.* 262, 173–178. doi:10.1007/s00415-014-7553-y.

McKenzie, M., Liolitsa, D., Akinshina, N., Campanella, M., Sisodiya, S., Hargreaves, I., et al. (2007). Mitochondrial ND5 Gene Variation Associated with Encephalomyopathy and Mitochondrial ATP Consumption. *J. Biol. Chem.* 282, 36845–36852. doi:10.1074/jbc.M704158200.

Metcalf, P., and Fusek, M. (1993). Two crystal structures for cathepsin D: the lysosomal targeting signal and active site. *EMBO J.* 12, 1293–302. Available at: http://www.ncbi.nlm.nih.gov/pubmed/8467789.

Meyer, M., Kovács, A. D., and Pearce, D. A. (2017). Decreased sensitivity of palmitoyl protein thioesterase 1-deficient neurons to chemical anoxia. *Metab. Brain Dis.* 32, 275–279. doi:10.1007/s11011-016-9919-6.

Miller, J. N., Kovács, A. D., and Pearce, D. A. (2015). The novel Cln1(R151X) mouse model of infantile neuronal ceroid lipofuscinosis (INCL) for testing nonsense suppression therapy.

Hum. Mol. Genet. 24, 185–96. doi:10.1093/hmg/ddu428.

Moharir, A., Peck, S. H., Budden, T., and Lee, S. Y. (2013). The Role of N-Glycosylation in Folding, Trafficking, and Functionality of Lysosomal Protein CLN5. *PLoS One* 8. doi:10.1371/journal.pone.0074299.

Mole SE, Williams RE, G. H. (2012). *The Neuronal Ceroid Lipofuscinoses (Batten Disease)*. , eds. S. Mole, R. Williams, and H. Goebel Oxford University Press doi:10.1093/med/9780199590018.001.0001.

Ni, H.-M., Williams, J. A., and Ding, W.-X. (2015). Mitochondrial dynamics and mitochondrial quality control. *Redox Biol.* 4, 6–13. doi:10.1016/j.redox.2014.11.006.

Ohno, K., Saito, S., Sugawara, K., Suzuki, T., Togawa, T., and Sakuraba, H. (2010). Structural basis of neuronal ceroid lipofuscinosis 1. *Brain Dev.* 32, 524–30. doi:10.1016/j.braindev.2009.08.010.

Palmer, D. N., Barry, L. A., Tyynelä, J., and Cooper, J. D. (2013). NCL disease mechanisms. *Biochim. Biophys. Acta - Mol. Basis Dis.* 1832, 1882–1893. doi:10.1016/j.bbadis.2013.05.014.

Patwardhan, G. A., Beverly, L. J., and Siskind, L. J. (2016). Sphingolipids and mitochondrial apoptosis. *J. Bioenerg. Biomembr.* 48, 153–68. doi:10.1007/s10863-015-9602-3.

Pérez-Poyato, M.-S., Milà Recansens, M., Ferrer Abizanda, I., Montero Sánchez, R., Rodríguez-Revenga, L., Cusí Sánchez, V., et al. (2011). Juvenile neuronal ceroid lipofuscinosis: clinical course and genetic studies in Spanish patients. *J. Inherit. Metab. Dis.* 34, 1083–1093. doi:10.1007/s10545-011-9323-7.

Pezzini, F., Bettinetti, L., Di Leva, F., Bianchi, M., Zoratti, E., Carrozzo, R., et al. (2017a). Transcriptomic Profiling Discloses Molecular and Cellular Events Related to Neuronal Differentiation in SH-SY5Y Neuroblastoma Cells. *Cell. Mol. Neurobiol.* 37, 665–682. doi:10.1007/s10571-016-0403-y.

Pezzini, F., Bianchi, M., Benfatto, S., Griggio, F., Doccini, S., Carrozzo, R., et al. (2017b). The Networks of Genes Encoding Palmitoylated Proteins in Axonal and Synaptic Compartments Are Affected in PPT1 Overexpressing Neuronal-Like Cells. *Front. Mol. Neurosci.* 10, 266. doi:10.3389/fnmol.2017.00266.

Pezzini, F., Gismondi, F., Tessa, A., Tonin, P., Carrozzo, R., Mole, S. E., et al. (2011). Involvement of the mitochondrial compartment in human NCL fibroblasts. *Biochem. Biophys. Res. Commun.* 416, 159–164. doi:10.1016/j.bbrc.2011.11.016.

Platt, F. M. (2014). Sphingolipid lysosomal storage disorders. *Nature* 510, 68–75. doi:10.1038/nature13476.

Radke, J., Stenzel, W., and Goebel, H. H. (2015). Human NCL Neuropathology. *Biochim. Biophys. Acta - Mol. Basis Dis.* 1852, 2262–2266. doi:10.1016/j.bbadis.2015.05.007.

Ramadan, H., Al-Din, A. S., Ismail, A., Balen, F., Varma, A., Twomey, A., et al. (2007). Adult neuronal ceroid lipofuscinosis caused by deficiency in palmitoyl protein thioesterase 1. *Neurology* 68, 387–8. doi:10.1212/01.wnl.0000252825.85947.2f.

Ran, F. A., Hsu, P. D., Wright, J., Agarwala, V., Scott, D. A., and Zhang, F. (2013). Genome engineering using the CRISPR-Cas9 system. *Nat. Protoc.* 8, 2281–2308. doi:10.1038/nprot.2013.143.

Rawlings, N. D., and Barrett, A. J. (1995). Families of aspartic peptidases, and those of unknown catalytic mechanism. *Methods Enzymol.* 248, 105–20. Available at: http://www.ncbi.nlm.nih.gov/pubmed/7674916.

Sanders, S. S., Martin, D. D. O., Butland, S. L., Lavallée-Adam, M., Calzolari, D., Kay, C., et al. (2015). Curation of the Mammalian Palmitoylome Indicates a Pivotal Role for Palmitoylation in Diseases and Disorders of the Nervous System and Cancers. *PLoS Comput. Biol.* 11, e1004405. doi:10.1371/journal.pcbi.1004405.

Sanjana, N. E., Shalem, O., and Zhang, F. (2014). Improved vectors and genome-wide libraries for CRISPR screening. *Nat. Methods* 11, 783–784. doi:10.1038/nmeth.3047.

Santorelli, F. M., Garavaglia, B., Cardona, F., Nardocci, N., Bernardina, B. D., Sartori, S., et al. (2013). Molecular epidemiology of childhood neuronal ceroid-lipofuscinosis in Italy. *Orphanet J. Rare Dis.* 8, 19. doi:10.1186/1750-1172-8-19.

Sardiello, M., Palmieri, M., di Ronza, A., Medina, D. L., Valenza, M., Gennarino, V. A., et al. (2009). A Gene Network Regulating Lysosomal Biogenesis and Function. *Science (80-.).* doi:10.1126/science.1174447.

Savchenko, E., Singh, Y., Konttinen, H., Lejavova, K., Mediavilla Santos, L., Grubman, A., et al. (2017). Loss of CLN5 causes altered neurogenesis in a childhood neurodegenerative disorder. *Dis. Model. Mech.* doi:10.1242/dmm.029165.

Schmiedt, M.-L., Blom, T., Blom, T., Kopra, O., Wong, A., von Schantz-Fant, C., et al. (2012). Cln5-deficiency in mice leads to microglial activation, defective myelination and changes in lipid metabolism. *Neurobiol. Dis.* 46, 19–29. doi:10.1016/j.nbd.2011.12.009.

Scifo, E., Szwajda, A., Debski, J., Uusi-Rauva, K., Kesti, T., Dadlez, M., et al. (2013). Drafting the CLN3 protein interactome in SH-SY5Y human neuroblastoma cells: A label-free quantitative proteomics approach. *J. Proteome Res.* 12, 2101–2115. doi:10.1021/pr301125k.

Scifo, E., Szwajda, A., Soliymani, R., Pezzini, F., Bianchi, M., Dapkunas, A., et al. (2015). Proteomic analysis of the palmitoyl protein thioesterase 1 interactome in SH-SY5Y human neuroblastoma cells. *J. Proteomics* 123, 42–53. doi:10.1016/j.jprot.2015.03.038.

Seehafer, S. S., Ramirez-Montealegre, D., Wong, A. M., Chan, C.-H., Castaneda, J., Horak, M., et al. (2011). Immunosuppression alters disease severity in juvenile Batten disease mice. *J. Neuroimmunol.* 230, 169–172. doi:10.1016/j.jneuroim.2010.08.024.

Segal-Salto, M., Sapir, T., and Reiner, O. (2016). Reversible Cysteine Acylation Regulates the Activity of Human Palmitoyl-Protein Thioesterase 1 (PPT1). *PLoS One* 11, e0146466. doi:10.1371/journal.pone.0146466.

Shacka, J. J., Klocke, B. J., Young, C., Shibata, M., Olney, J. W., Uchiyama, Y., et al. (2007). Cathepsin D Deficiency Induces Persistent Neurodegeneration in the Absence of Bax-

Dependent Apoptosis. *J. Neurosci.* 27, 2081–2090. doi:10.1523/JNEUROSCI.5577-06.2007.

Siintola, E. (2006). Cathepsin D deficiency underlies congenital human neuronal ceroid-lipofuscinosis. *Brain* 129, 1438–1445. doi:10.1093/brain/awl107.

Simonati, A., Pezzini, F., Moro, F., and Santorelli, F. M. (2014). Neuronal Ceroid Lipofuscinosis: The Increasing Spectrum of an Old Disease. *Curr. Mol. Med.* 14, 1043–1051. doi:10.2174/1566524014666141010154913.

Simonati, A., Tessa, A., Bernardina, B. D., Biancheri, R., Veneselli, E., Tozzi, G., et al. (2009). Variant late infantile neuronal ceroid lipofuscinosis because of CLN1 mutations. *Pediatr. Neurol.* 40, 271–6. doi:10.1016/j.pediatrneurol.2008.10.018.

Song, W., Wang, F., Savini, M., Ake, A., di Ronza, A., Sardiello, M., et al. (2013). TFEB regulates lysosomal proteostasis. *Hum. Mol. Genet.* 22, 1994–2009. doi:10.1093/hmg/ddt052.

Staropoli, J. F., Xin, W., Barone, R., Cotman, S. L., and Sims, K. B. (2012). An atypical case of neuronal ceroid lipofuscinosis with co-inheritance of a variably penetrant POLG1mutation. *BMC Med. Genet.* 13, 50. doi:10.1186/1471-2350-13-50.

Steinfeld, R., Reinhardt, K., Schreiber, K., Hillebrand, M., Kraetzner, R., Brück, W., et al. (2006). Cathepsin D Deficiency Is Associated with a Human Neurodegenerative Disorder. *Am. J. Hum. Genet.* 78, 988–998. doi:10.1086/504159.

Tikka, S., Monogioudi, E., Gotsopoulos, A., Soliymani, R., Pezzini, F., Scifo, E., et al. (2016). Proteomic Profiling in the Brain of CLN1 Disease Model Reveals Affected Functional Modules. *NeuroMolecular Med.* 18, 109–133. doi:10.1007/s12017-015-8382-6.

Van Diggelen, O. P., Thobois, S., Tilikete, C., Zabot, M. T., Keulemans, J. L. M., Van Bunderen, P. A., et al. (2001). Adult neuronal ceroid lipofuscinosis with palmitoyl-protein thioesterase deficiency: First adult-onset patients of a childhood disease. *Ann. Neurol.* 50, 269–272. doi:10.1002/ana.1103.

Vesa, J., Hellsten, E., Verkruyse, L. A., Camp, L. A., Rapola, J., Santavuori, P., et al. (1995). Mutations in the palmitoyl protein thioesterase gene causing infantile neuronal ceroid lipofuscinosis. *Nature* 376, 584–7. doi:10.1038/376584a0.

Vesa J, Chin MH, Oelgeschläger K, Isosomppi J, DellAngelica EC, J. A., Level:, P. L. N. ceroid lipofuscinoses are connected at molecular, and CLN3, interaction of C. protein with C. and (2002). Neuronal Ceroid Lipofuscinoses Are Connected at Molecular Level: Interaction of CLN5 Protein with CLN2 and CLN3. *Mol Biol Cell* 13, 2410–2420.

Vilaça, R., Barros, I., Matmati, N., Silva, E., Martins, T., Teixeira, V., et al. (2017). The ceramide activated protein phosphatase Sit4 impairs sphingolipid dynamics, mitochondrial function and lifespan in a yeast model of Niemann-Pick type C1. *Biochim. Biophys. Acta*. doi:10.1016/j.bbadis.2017.10.010.

Virmani, T., Gupta, P., Liu, X., Kavalali, E. T., and Hofmann, S. L. (2005). Progressively reduced synaptic vesicle pool size in cultured neurons derived from neuronal ceroid

lipofuscinosis-1 knockout mice. *Neurobiol. Dis.* 20, 314–323. doi:10.1016/j.nbd.2005.03.012.

Wei, H., Zhang, Z., Saha, A., Peng, S., Chandra, G., Quezado, Z., et al. (2011). Disruption of adaptive energy metabolism and elevated ribosomal p-S6K1 levels contribute to INCL pathogenesis: Partial rescue by resveratrol. *Hum. Mol. Genet.* 20, 1111–1121. doi:10.1093/hmg/ddq555.

Whitaker, J. N., and Rhodes, R. H. (1983). The distribution of cathepsin D in rat tissues determined by immunocytochemistry. *Am. J. Anat.* 166, 417–428. doi:10.1002/aja.1001660404.

Whiting, R. E. H., Jensen, C. A., Pearce, J. W., Gillespie, L. E., Bristow, D. E., and Katz, M. L. (2016). Intracerebroventricular gene therapy that delays neurological disease progression is associated with selective preservation of retinal ganglion cells in a canine model of CLN2 disease. *Exp. Eye Res.* 146, 276–282. doi:10.1016/j.exer.2016.03.023.

Williams, R. E. (2011). "General Principles of Medical Management," in *The Neuronal Ceroid Lipofuscinoses (Batten Disease)*, ed. G. H. Mole SE, Williams RE (Oxford University Press), 50–54. doi:10.1093/med/9780199590018.003.0005.

Wong-Riley, M. T. (1989). Cytochrome oxidase: an endogenous metabolic marker for neuronal activity. *Trends Neurosci.* 12, 94–101. Available at: http://www.ncbi.nlm.nih.gov/pubmed/2469224.

Zhang, Z., Lee, Y.-C., Kim, S.-J., Choi, M. S., Tsai, P.-C., Xu, Y., et al. (2006). Palmitoyl-protein thioesterase-1 deficiency mediates the activation of the unfolded protein response and neuronal apoptosis in INCL. *Hum. Mol. Genet.* 15, 337–46. doi:10.1093/hmg/ddi451.

SUPPLEMENTARY TABLES

Table S1 *total list of mouses sacrificed this study*

Animal ID	Background	Genotype	Sex	Age at sacrifice	Stage
KKn-387-F5	C57BL/6JRcc	Cln5	male	9	late
KKn-388-F5	C57BL/6JRcc	Cln5	male	9	late
KKn-389-F5	C57BL/6JRcc	Cln5	female	9	Late
KKn-390-F5	C57BL/6JRcc	Cln5	female	9	Late
KKn-392-F5	C57BL/6JRcc	Rcc	female	9	late
KKn-393-F5	C57BL/6JRcc	Rcc	female	9	late
KKn-394-F5	C57BL/6JRcc	Rcc	male	9	late
KKn-395-F5	C57BL/6JRcc	Rcc	male	9	late
KKn-416-F5	C57BL/6JRcc	Cln5	male	3	early
KKn-417-F5	C57BL/6JRcc	Cln5	male	3	early
KKn-418-F5	C57BL/6JRcc	Cln5	female	3	early
KKn-419-F5	C57BL/6JRcc	Cln5	female	3	early
KKn-425-F6	C57BL/6JRcc	Rcc	female	3	early
KKn-426-F6	C57BL/6JRcc	Rcc	female	3	early
KKn-427-F6	C57BL/6JRcc	Rcc	female	3	early
KKn-428-F6	C57BL/6JRcc	Rcc	female	3	early

Table S2 *Differentially expressed genes (DEGs) identified by RNA-seq analysis in SH-p.wtCLN1 cell line versus SH-pcDNA3*

Legend: Gene- Gene Symbol, Ensembl ID- ENSEMBL unique gene identifier, FPKM- fragments per kilobase per million mapped reads, Log2FC- log2 fold change, FDR- false discovery rate. Originally mapped DEGs, which are

Gene	Ensembl ID	SH-pcDNA3	SH-p.wtCLN1		
		FPKM	FPKM	Log_2FC	FDR (q-value)
AARD	ENSG00000205002	0,92	0,26	-1,828	2,17E-02
AARS	ENSG00000090861	43,41	91,04	1,069	7,79E-04
ABCA5	ENSG00000154265	2,60	5,37	1,046	5,32E-03
ABCD2	ENSG00000173208	13,86	6,65	-1,059	7,79E-04
ABCG4	ENSG00000172350	3,61	1,54	-1,233	3,77E-03
ABLIM2	ENSG00000163995	4,76	2,08	-1,194	4,30E-03
ACBD7	ENSG00000176244	2,37	1,14	-1,053	4,17E-02
ACRBP	ENSG00000111644	0,99	3,12	1,663	4,30E-03
ACTL6B	ENSG00000077080	32,96	13,75	-1,261	7,79E-04
ADAM12	ENSG00000148848	28,71	11,13	-1,367	7,79E-04
ADAMTS10	ENSG00000142303	4,85	0,96	-2,341	7,79E-04
ADAMTS14	ENSG00000138316	0,84	0,30	-1,479	7,79E-04
ADAMTS6	ENSG00000049192	0,74	1,98	1,429	4,29E-02
ADAMTS9	ENSG00000163638	147,53	61,98	-1,251	7,79E-04
ADAMTSL4	ENSG00000143382	5,42	13,61	1,328	7,79E-04
ADCYAP1R1	ENSG00000078549	4,11	1,11	-1,890	7,79E-04
ADD3	ENSG00000148700	199,84	526,01	1,396	1,91E-02
ADGRA2	ENSG00000020181	6,14	12,32	1,004	2,66E-03
ADM	ENSG00000148926	2,65	8,40	1,668	7,79E-04
ADORA1	ENSG00000163485	2,11	0,60	-1,801	1,21E-02
ADPRHL1	ENSG00000153531	1,08	0,46	-1,243	2,95E-02
ADRA2A	ENSG00000150594	0,56	0,15	-1,893	2,08E-03
AFF3	ENSG00000144218	10,60	3,93	-1,430	7,79E-04
AHNAK2	ENSG00000185567	10,15	4,94	-1,038	2,08E-03
AJAP1	ENSG00000196581	1,21	2,63	1,114	3,97E-02
ALKAL2	ENSG00000189292	1,21	0,34	-1,827	1,25E-02
ALPL	ENSG00000162551	3,17	0,57	-2,488	7,79E-04
ALS2CL	ENSG00000178038	7,11	15,07	1,084	7,79E-04
AMER3	ENSG00000178171	3,07	1,53	-1,004	1,45E-03
ANKRD33	ENSG00000167612	0,72	1,84	1,351	5,81E-03
ANKRD33B	ENSG00000164236	0,45	1,51	1,761	1,45E-03
ANO3	ENSG00000134343	1,14	0,37	-1,635	2,08E-03
ANOS1	ENSG00000011201	0,06	0,49	3,020	2,10E-02
AOC2	ENSG00000131480	0,67	1,85	1,462	7,79E-04
AOC3	ENSG00000131471	0,37	0,90	1,304	3,78E-02
AOX1	ENSG00000138356	0,68	0,17	-2,020	2,27E-02
APBA1	ENSG00000107282	0,85	2,64	1,642	1,45E-03
APLN	ENSG00000171388	0,56	4,51	3,002	7,79E-04
APOL4	ENSG00000100336	4,31	10,86	1,334	7,79E-04
AQP1	ENSG00000240583	4,79	81,70	4,091	7,79E-04
ARC	ENSG00000198576	3,86	1,79	-1,105	2,08E-03
ARFGAP1	ENSG00000101199	44,73	110,16	1,300	7,79E-04
ARHGAP20	ENSG00000137727	0,57	0,11	-2,345	7,79E-04
ARHGAP42	ENSG00000165895	4,51	1,39	-1,700	2,66E-03
ARHGEF16	ENSG00000130762	2,17	0,99	-1,133	4,30E-03
ARHGEF28	ENSG00000214944	1,99	5,29	1,414	7,79E-04
ARSD	ENSG00000006756	8,58	1,76	-2,287	3,23E-03
ART5	ENSG00000167311	2,59	0,97	-1,418	5,81E-03
ASB9	ENSG00000102048	1,56	0,22	-2,836	7,79E-04
ASCL1	ENSG00000139352	0,21	4,31	4,375	7,79E-04
ASF1B	ENSG00000105011	3,40	1,07	-1,663	7,79E-04
ASPDH	ENSG00000204653	8,50	3,06	-1,474	1,41E-02
ASTN1	ENSG00000152092	6,96	2,70	-1,368	7,79E-04
ASTN2	ENSG00000148219	46,95	18,45	-1,347	7,79E-04
ATOH7	ENSG00000179774	0,10	0,67	2,710	4,90E-02

ATP7A	ENSG00000165240	20,84	8,00	-1,381	7,79E-04
AURKC	ENSG00000105146	0,30	1,68	2,460	7,79E-04
B3GAT1	ENSG00000109956	10,42	3,70	-1,493	7,79E-04
B3GNT7	ENSG00000156966	1,17	3,78	1,687	7,79E-04
BASP1	ENSG00000176788	54,09	18,31	-1,563	7,79E-04
BCAM	ENSG00000187244	2,18	4,48	1,039	2,45E-02
BCAN	ENSG00000132692	9,03	3,43	-1,395	1,45E-02
BCHE	ENSG00000114200	0,15	5,27	5,180	7,79E-04
BCL11A	ENSG00000119866	0,25	2,36	3,226	7,79E-04
BEX5	ENSG00000184515	4,82	1,90	-1,342	2,66E-03
BHLHE40	ENSG00000134107	4,34	13,20	1,606	7,79E-04
BIRC3	ENSG00000023445	4,18	1,04	-2,002	7,79E-04
BIRC5	ENSG00000089685	15,07	7,01	-1,105	7,79E-04
BMP2	ENSG00000125845	1,50	0,49	-1,603	9,07E-03
BMP7	ENSG00000101144	14,23	1,04	-3,776	3,77E-03
BNC2	ENSG00000173068	1,03	2,47	1,264	1,76E-02
BRCA1	ENSG00000012048	3,09	1,28	-1,272	1,21E-02
BRINP1	ENSG00000078725	2,65	0,40	-2,713	7,79E-04
BRIP1	ENSG00000136492	3,15	1,11	-1,500	7,79E-04
BTBD11	ENSG00000151136	1,34	0,48	-1,481	2,08E-03
BUB1	ENSG00000169679	6,67	3,16	-1,078	7,79E-04
BUB1B	ENSG00000156970	7,25	2,51	-1,530	7,79E-04
C14orf159	ENSG00000133943	6,42	1,89	-1,767	1,45E-03
C16orf74	ENSG00000154102	1,85	0,77	-1,260	3,19E-02
C1orf132	ENSG00000203709	0,17	1,30	2,899	1,45E-03
C1QL3	ENSG00000165985	0,40	2,78	2,805	7,79E-04
C1QTNF12	ENSG00000184163	1,16	6,51	2,492	7,79E-04
C1QTNF2	ENSG00000145861	0,57	0,11	-2,406	4,81E-03
C2orf70	ENSG00000173557	3,58	1,18	-1,597	1,25E-02
C6orf226	ENSG00000221821	13,19	28,54	1,114	2,08E-03
CA10	ENSG00000154975	0,70	0,10	-2,841	7,79E-04
CA12	ENSG00000074410	0,05	6,53	7,081	7,79E-04
CACNA2D2	ENSG00000007402	132,30	61,13	-1,114	7,79E-04
CACNA2D3	ENSG00000157445	1,86	7,11	1,936	7,79E-04
CACNG2	ENSG00000166862	3,13	1,46	-1,100	3,66E-02
CALB1	ENSG00000104327	14,66	2,22	-2,720	7,79E-04
CCDC160	ENSG00000203952	0,65	0,22	-1,561	2,10E-02
CCDC68	ENSG00000166510	2,00	0,96	-1,056	1,45E-02
CCL2	ENSG00000108691	103,39	25,23	-2,035	7,79E-04
CCM2L	ENSG00000101331	3,16	1,13	-1,485	3,77E-03
CCNB1	ENSG00000134057	18,81	8,70	-1,112	7,79E-04
CCNB2	ENSG00000157456	11,36	5,18	-1,134	7,79E-04
CCND1	ENSG00000110092	137,26	41,64	-1,721	7,79E-04
CCNE1	ENSG00000105173	6,90	3,28	-1,072	3,23E-03
CD177	ENSG00000204936	0,15	1,19	3,015	4,81E-03
CD7	ENSG00000173762	0,15	0,62	2,076	8,62E-03
CD9	ENSG00000010278	37,87	78,08	1,044	7,79E-04
CDC45	ENSG00000093009	4,11	1,36	-1,593	2,66E-03
CDC6	ENSG00000094804	4,36	1,16	-1,910	7,79E-04
CDCA2	ENSG00000184661	2,10	0,80	-1,388	6,77E-03
CDCA5	ENSG00000146670	9,29	3,77	-1,300	7,79E-04
CDH11	ENSG00000140937	31,83	11,98	-1,409	2,08E-03
CDH15	ENSG00000129910	2,06	0,84	-1,296	2,08E-03
CDH2	ENSG00000170558	84,67	36,72	-1,205	7,79E-04
CDH22	ENSG00000149654	0,55	0,08	-2,786	7,79E-04
CDH23	ENSG00000107736	2,67	1,28	-1,062	3,22E-02
CDK1	ENSG00000170312	28,34	13,69	-1,050	7,79E-04
CDKAL1	ENSG00000145996	23,65	11,63	-1,024	7,72E-03
CDKN1C	ENSG00000129757	10,36	48,51	2,227	7,79E-04
CDKN3	ENSG00000100526	20,98	9,58	-1,131	7,79E-04
CDO1	ENSG00000129596	9,71	4,30	-1,177	5,81E-03
CDS1	ENSG00000163624	0,50	1,12	1,149	2,41E-02
CEBPA	ENSG00000245848	1,14	2,79	1,294	1,33E-02
CEBPD	ENSG00000221869	0,11	1,43	3,766	7,79E-04
CECR6	ENSG00000183307	4,88	2,37	-1,041	7,79E-04

CELF4	ENSG00000101489	12,82	5,90	-1,119	8,62E-03
CENPE	ENSG00000138778	2,19	0,94	-1,227	4,30E-03
CENPF	ENSG00000117724	11,09	4,75	-1,224	1,37E-02
CENPI	ENSG00000102384	3,13	1,13	-1,473	4,30E-03
CENPU	ENSG00000151725	12,19	4,56	-1,419	7,72E-03
CEP44	ENSG00000164118	42,59	125,87	1,563	7,79E-04
CEP55	ENSG00000138180	5,59	2,33	-1,260	7,79E-04
CES4A	ENSG00000172824	7,22	2,68	-1,429	3,23E-03
CFAP44	ENSG00000206530	9,53	3,78	-1,333	1,80E-02
CFAP77	ENSG00000188523	4,79	2,02	-1,247	9,50E-03
CFD	ENSG00000197766	17,93	6,52	-1,459	7,79E-04
CGA	ENSG00000135346	2,18	10,88	2,320	7,79E-04
CHD5	ENSG00000116254	4,98	1,14	-2,120	7,79E-04
CHGB	ENSG00000089199	1003,23	274,61	-1,869	7,79E-04
CHPT1	ENSG00000111666	4,65	15,10	1,700	7,79E-04
CHRDL1	ENSG00000101938	4,37	1,74	-1,331	7,79E-04
CHRM3	ENSG00000133019	55,70	18,75	-1,571	7,79E-04
CHRM4	ENSG00000180720	2,26	0,75	-1,585	7,79E-04
CHRNB2	ENSG00000160716	38,04	15,43	-1,302	7,79E-04
CHRND	ENSG00000135902	4,67	17,06	1,868	7,79E-04
CHST1	ENSG00000175264	4,84	1,61	-1,584	7,79E-04
CITED4	ENSG00000179862	2,89	1,42	-1,021	4,64E-02
CKAP2L	ENSG00000169607	3,32	1,40	-1,250	4,81E-03
CKB	ENSG00000166165	301,80	124,33	-1,279	7,79E-04
CLDN5	ENSG00000184113	0,73	0,27	-1,436	4,14E-02
CLIC3	ENSG00000169583	1,87	5,08	1,438	7,79E-04
CLMN	ENSG00000165959	1,66	8,19	2,300	7,79E-04
CLSPN	ENSG00000092853	3,50	1,23	-1,508	3,77E-03
CLSTN2	ENSG00000158258	4,12	1,38	-1,579	7,79E-04
CNKSR2	ENSG00000149970	1,10	2,36	1,096	6,29E-03
CNR1	ENSG00000118432	1,19	0,17	-2,833	7,79E-04
CNTFR	ENSG00000122756	145,98	51,63	-1,500	7,79E-04
CNTN2	ENSG00000184144	4,67	2,06	-1,180	7,79E-04
COBLL1	ENSG00000082438	2,84	6,81	1,264	7,79E-04
COL17A1	ENSG00000065618	1,60	11,72	2,873	7,79E-04
COL4A2	ENSG00000134871	20,69	7,37	-1,488	7,79E-04
COLCA2	ENSG00000214290	1,84	0,23	-3,021	7,79E-04
COMP	ENSG00000105664	0,65	0,12	-2,406	7,79E-04
COQ8A	ENSG00000163050	7,34	16,31	1,152	7,79E-04
COTL1	ENSG00000103187	7,95	1,56	-2,346	7,79E-04
COX4I2	ENSG00000131055	0,21	0,93	2,174	4,81E-02
CPA1	ENSG00000091704	0,33	0,99	1,578	1,12E-02
CPLX2	ENSG00000145920	35,28	15,40	-1,195	6,77E-03
CPNE4	ENSG00000196353	5,92	2,73	-1,118	1,45E-03
CPVL	ENSG00000106066	9,45	4,30	-1,137	2,08E-03
CRABP2	ENSG00000143320	27,23	9,57	-1,508	7,79E-04
CRACR2A	ENSG00000130038	0,45	0,16	-1,501	2,20E-02
CREB3L1	ENSG00000157613	0,95	0,41	-1,193	3,09E-02
CRISPLD2	ENSG00000103196	0,57	0,14	-1,991	3,23E-03
CRMP1	ENSG00000072832	215,03	89,04	-1,272	7,79E-04
CRYM	ENSG00000103316	9,41	4,33	-1,118	2,08E-03
CSAG1	ENSG00000198930	26,11	8,53	-1,615	7,79E-04
CSPG5	ENSG00000114646	10,05	4,79	-1,069	7,79E-04
CSRP1	ENSG00000159176	25,62	11,48	-1,159	7,79E-04
CSRP2	ENSG00000175183	214,41	88,23	-1,281	7,79E-04
CTHRC1	ENSG00000164932	9,12	4,35	-1,069	7,79E-04
CTSD	ENSG00000117984	105,20	231,49	1,138	7,79E-04
CTSV	ENSG00000136943	4,54	1,83	-1,313	7,79E-04
CTU1	ENSG00000142544	2,97	6,03	1,020	2,08E-03
CUX2	ENSG00000111249	5,37	0,36	-3,915	7,79E-04
CX3CL1	ENSG00000006210	4,65	1,71	-1,441	7,79E-04
CXCL12	ENSG00000107562	3,10	1,07	-1,539	3,23E-03
CYB5R2	ENSG00000166394	1,32	3,49	1,397	3,94E-02
CYBRD1	ENSG00000071967	3,06	8,12	1,408	7,79E-04
CYP1B1	ENSG00000138061	1,27	0,46	-1,468	3,91E-02

CYP26A1	ENSG00000095596	3,38	6,81	1,010	2,66E-03
CYP26B1	ENSG00000003137	13,17	26,34	1,000	9,50E-03
CYR61	ENSG00000142871	3,26	1,55	-1,078	6,77E-03
CYS1	ENSG00000205795	3,83	1,87	-1,033	1,45E-03
DACT1	ENSG00000165617	0,28	1,09	1,965	7,79E-04
DBX1	ENSG00000109851	1,55	0,32	-2,265	1,45E-03
DCLK1	ENSG00000133083	18,82	8,94	-1,074	7,79E-04
DCLK3	ENSG00000163673	1,88	0,50	-1,908	7,79E-04
DCT	ENSG00000080166	0,40	1,08	1,442	2,06E-02
DEPDC1	ENSG00000024526	5,60	2,53	-1,149	7,79E-04
DGAT2	ENSG00000062282	2,46	0,71	-1,787	7,79E-04
DHRS2	ENSG00000100867	4,88	0,25	-4,292	7,79E-04
DHRS3	ENSG00000162496	5,58	2,22	-1,327	1,45E-03
DIAPH3	ENSG00000139734	2,03	0,97	-1,068	2,66E-03
DISP3	ENSG00000204624	5,60	2,30	-1,284	3,77E-03
DKFZP434I071	ENSG00000268471	1,72	5,33	1,629	7,79E-04
DKK1	ENSG00000107984	250,69	90,46	-1,471	7,79E-04
DLG2	ENSG00000150672	19,22	7,94	-1,276	7,79E-04
DLGAP3	ENSG00000116544	5,65	2,80	-1,011	1,45E-03
DLGAP5	ENSG00000126787	6,83	2,38	-1,521	7,79E-04
DLK1	ENSG00000185559	756,08	2754,93	1,865	7,79E-04
DMRTA2	ENSG00000142700	1,98	0,95	-1,070	1,83E-02
DNAH9	ENSG00000007174	1,12	0,02	-5,732	7,79E-04
DNER	ENSG00000187957	15,97	5,99	-1,415	7,79E-04
DNHD1	ENSG00000179532	6,69	14,61	1,127	1,12E-02
DOCK6	ENSG00000130158	19,51	39,02	1,000	3,23E-03
DPT	ENSG00000143196	2,09	0,20	-3,396	7,79E-04
DRD2	ENSG00000149295	24,68	12,34	-1,001	2,66E-03
DTL	ENSG00000143476	5,28	1,75	-1,589	3,23E-03
DUSP5	ENSG00000138166	4,17	13,43	1,688	7,79E-04
E2F1	ENSG00000101412	8,93	3,88	-1,203	7,79E-04
E2F2	ENSG00000007968	2,60	0,78	-1,730	7,79E-04
EBF3	ENSG00000108001	0,49	3,17	2,698	7,79E-04
ECHDC2	ENSG00000121310	1,14	0,43	-1,402	7,79E-04
ECM1	ENSG00000143369	0,97	2,12	1,121	1,04E-02
EDIL3	ENSG00000164176	40,81	17,96	-1,184	7,79E-04
EDNRA	ENSG00000151617	2,99	0,79	-1,918	7,79E-04
EDNRB	ENSG00000136160	0,31	2,51	3,008	7,79E-04
EEF1D	ENSG00000104529	62,90	161,46	1,360	7,79E-04
EFCAB1	ENSG00000034239	1,78	0,65	-1,461	4,41E-02
EFNB2	ENSG00000125266	23,84	7,28	-1,712	7,79E-04
EGR1	ENSG00000120738	54,88	24,36	-1,171	7,79E-04
ELAVL4	ENSG00000162374	222,74	97,52	-1,192	7,79E-04
ELFN1	ENSG00000225968	2,18	6,61	1,598	7,79E-04
ELFN2	ENSG00000166897	1,11	0,12	-3,212	7,79E-04
ELMO3	ENSG00000102890	1,17	2,42	1,055	7,25E-03
EMILIN3	ENSG00000183798	0,67	0,29	-1,204	2,72E-02
ENC1	ENSG00000171617	62,13	18,46	-1,751	4,81E-03
ENPP2	ENSG00000136960	1,57	6,61	2,074	7,79E-04
EPAS1	ENSG00000116016	36,93	126,29	1,774	7,79E-04
EPHA10	ENSG00000183317	6,24	2,35	-1,411	7,79E-04
ERFE	ENSG00000178752	4,76	12,27	1,366	1,45E-03
ERICH5	ENSG00000177459	2,17	0,39	-2,470	7,79E-04
ESRRG	ENSG00000196482	11,95	5,38	-1,152	7,79E-04
ETS1	ENSG00000134954	10,14	4,74	-1,099	3,53E-02
ETS2	ENSG00000157557	8,86	19,57	1,144	7,79E-04
EXO1	ENSG00000174371	6,68	2,31	-1,531	7,79E-04
EXPH5	ENSG00000110723	0,71	0,31	-1,216	8,62E-03
EYA4	ENSG00000112319	1,11	4,35	1,977	7,79E-04
F3	ENSG00000117525	1,88	4,22	1,165	1,41E-02
FAAH	ENSG00000117480	7,15	3,42	-1,066	1,41E-02
FADS6	ENSG00000172782	0,91	0,24	-1,922	9,07E-03
FAM110A	ENSG00000125898	4,72	1,76	-1,423	7,72E-03
FAM111B	ENSG00000189057	1,99	0,32	-2,626	7,79E-04
FAM124A	ENSG00000150510	1,37	5,09	1,897	7,79E-04

FAM129A	ENSG00000135842	2,71	5,58	1,042	7,79E-04
FAM13A	ENSG00000138640	9,40	4,46	-1,077	7,79E-04
FAM181B	ENSG00000182103	6,59	2,96	-1,157	2,08E-03
FAM184B	ENSG00000047662	0,64	1,93	1,590	7,79E-04
FAM19A4	ENSG00000163377	0,45	1,59	1,818	8,17E-03
FAM83D	ENSG00000101447	6,68	2,76	-1,277	7,79E-04
FAM89A	ENSG00000182118	10,96	5,25	-1,061	7,79E-04
FAM92B	ENSG00000153789	1,13	0,44	-1,380	3,22E-02
FBP1	ENSG00000165140	6,85	2,97	-1,207	1,45E-03
FBXO5	ENSG00000112029	9,63	4,39	-1,133	7,79E-04
FEZ1	ENSG00000149557	47,57	19,22	-1,308	7,79E-04
FGF14	ENSG00000102466	9,41	3,42	-1,461	6,77E-03
FGF19	ENSG00000162344	0,58	0,22	-1,389	3,12E-02
FGL1	ENSG00000104760	5,61	0,90	-2,636	7,79E-04
FHAD1	ENSG00000142621	3,35	1,61	-1,054	1,49E-02
FHDC1	ENSG00000137460	1,33	0,50	-1,415	7,79E-04
FLNC	ENSG00000128591	6,39	16,33	1,353	7,79E-04
FMN1	ENSG00000248905	2,49	9,66	1,958	7,79E-04
FNIP1	ENSG00000217128	4,99	10,24	1,038	1,37E-02
FOS	ENSG00000170345	12,06	5,44	-1,148	1,45E-03
FOSL2	ENSG00000075426	1,76	7,21	2,034	7,79E-04
FOXD4	ENSG00000170122	0,94	0,37	-1,346	1,87E-02
FOXN4	ENSG00000139445	1,25	0,34	-1,862	6,77E-03
FOXO1	ENSG00000150907	0,46	1,95	2,083	7,79E-04
FRMD3	ENSG00000172159	10,79	5,19	-1,056	1,53E-02
FRMPD2	ENSG00000170324	1,12	0,21	-2,387	7,79E-04
FSTL5	ENSG00000168843	37,26	10,23	-1,865	7,79E-04
FYCO1	ENSG00000163820	1,62	3,86	1,250	7,79E-04
FZD5	ENSG00000163251	1,00	4,14	2,046	7,79E-04
FZD9	ENSG00000188763	3,46	1,56	-1,152	3,23E-03
GABRA3	ENSG00000011677	4,92	1,63	-1,597	5,81E-03
GABRB3	ENSG00000166206	27,16	10,37	-1,389	1,91E-02
GABRD	ENSG00000187730	8,39	2,72	-1,627	7,79E-04
GALNT13	ENSG00000144278	5,39	1,94	-1,469	7,79E-04
GALNT14	ENSG00000158089	11,46	4,69	-1,289	4,81E-03
GAP43	ENSG00000172020	130,76	59,61	-1,133	7,79E-04
GAREM1	ENSG00000141441	17,51	8,60	-1,026	3,02E-02
GATA5	ENSG00000130700	1,66	0,66	-1,325	1,17E-02
GBP2	ENSG00000162645	0,76	2,83	1,896	7,79E-04
GCGR	ENSG00000215644	0,18	0,73	2,030	3,77E-03
GDPD3	ENSG00000102886	4,24	10,27	1,276	7,79E-04
GFPT2	ENSG00000131459	2,64	1,29	-1,036	6,29E-03
GFRA2	ENSG00000168546	1,38	3,40	1,300	4,30E-03
GINS1	ENSG00000101003	4,13	1,51	-1,454	7,79E-04
GLB1L2	ENSG00000149328	10,87	4,34	-1,324	8,17E-03
GPD1	ENSG00000167588	1,28	0,55	-1,204	2,58E-02
GPNMB	ENSG00000136235	1,67	3,58	1,105	4,14E-02
GPR19	ENSG00000183150	8,93	3,96	-1,172	1,45E-03
GPR37L1	ENSG00000170075	0,31	0,82	1,390	8,62E-03
GPR68	ENSG00000119714	3,77	1,28	-1,553	7,79E-04
GPRIN2	ENSG00000204175	2,47	0,71	-1,805	7,79E-04
GPX8	ENSG00000164294	2,49	0,09	-4,845	7,79E-04
GRAMD1B	ENSG00000023171	9,42	3,96	-1,249	7,79E-04
GREM2	ENSG00000180875	0,71	0,32	-1,148	2,45E-02
BACH1	ENSG00000156273	4,60	9,41	1,033	7,79E-04
GRIN1	ENSG00000176884	7,17	3,33	-1,106	1,45E-03
GRM1	ENSG00000152822	1,20	0,29	-2,058	4,30E-03
GRM2	ENSG00000164082	0,86	0,13	-2,679	7,79E-04
GRM7	ENSG00000196277	7,67	1,45	-2,398	1,45E-03
GSDMB	ENSG00000073605	9,25	23,42	1,340	7,25E-03
GTSE1	ENSG00000075218	5,48	2,53	-1,115	1,21E-02
GYG2	ENSG00000056998	1,34	0,20	-2,718	7,79E-04
H2AFX	ENSG00000188486	26,49	13,02	-1,025	7,79E-04
H3F3B	ENSG00000132475	586,63	1496,95	1,352	7,79E-04
HCG27	ENSG00000206344	0,37	0,97	1,391	4,20E-02

HDAC5	ENSG00000108840	13,88	30,83	1,152	7,79E-04
HES2	ENSG00000069812	2,86	0,76	-1,912	3,97E-02
HES7	ENSG00000179111	13,69	27,42	1,003	7,79E-04
HESX1	ENSG00000163666	1,65	4,57	1,473	5,32E-03
HEY1	ENSG00000164683	14,63	36,49	1,319	7,79E-04
HIF3A	ENSG00000124440	4,35	9,92	1,190	2,82E-02
HIST1H1C	ENSG00000187837	3,80	14,35	1,917	7,79E-04
HIST1H4H	ENSG00000158406	1,65	0,24	-2,757	8,17E-03
HIST2H2BE	ENSG00000184678	6,19	14,00	1,178	7,79E-04
HIST3H2A	ENSG00000181218	10,18	34,72	1,769	7,79E-04
HJURP	ENSG00000123485	4,28	1,96	-1,129	1,45E-03
HLA-B	ENSG00000234745	4,80	0,91	-2,390	7,79E-04
HMGB3	ENSG00000029993	30,65	14,90	-1,040	1,45E-03
HMMR	ENSG00000072571	8,31	3,41	-1,284	7,79E-04
HMP19	ENSG00000170091	81,41	34,86	-1,224	7,79E-04
HMX2	ENSG00000188816	1,04	0,31	-1,743	2,10E-02
HRK	ENSG00000135116	0,40	2,06	2,359	7,79E-04
HS3ST3B1	ENSG00000153976	0,22	2,14	3,280	7,79E-04
HSPA12B	ENSG00000132622	0,75	0,27	-1,470	3,99E-02
HTR6	ENSG00000158748	3,58	1,30	-1,457	4,81E-03
HTRA3	ENSG00000170801	0,53	0,09	-2,539	3,77E-03
IBA57-AS1	ENSG00000203684	0,65	3,17	2,286	1,21E-02
ID4	ENSG00000172201	4,44	0,88	-2,335	7,79E-04
IER3	ENSG00000137331	2,47	1,22	-1,015	4,41E-02
IER5L	ENSG00000188483	1,55	4,56	1,556	7,79E-04
IFIH1	ENSG00000115267	0,15	0,66	2,145	4,81E-03
IGDCC3	ENSG00000174498	1,32	2,74	1,057	1,04E-02
IGF2	ENSG00000167244	315,05	1679,21	2,414	7,79E-04
IGLON5	ENSG00000142549	55,31	26,09	-1,084	7,79E-04
IKZF1	ENSG00000185811	0,29	4,33	3,920	7,79E-04
IL32	ENSG00000008517	23,76	5,48	-2,116	7,79E-04
INA	ENSG00000148798	77,52	33,42	-1,214	7,79E-04
INHBA	ENSG00000122641	17,44	3,02	-2,528	7,79E-04
INHBE	ENSG00000139269	0,60	2,10	1,803	7,79E-04
INPP5F	ENSG00000198825	30,66	14,82	-1,049	7,79E-04
INTU	ENSG00000164066	4,55	9,53	1,067	7,79E-04
IP6K3	ENSG00000161896	1,92	6,81	1,827	7,79E-04
IRF6	ENSG00000117595	1,93	0,45	-2,093	7,79E-04
ISG15	ENSG00000187608	0,94	3,47	1,882	7,79E-04
ISLR	ENSG00000129009	28,56	10,81	-1,401	7,79E-04
ISLR2	ENSG00000167178	64,49	24,30	-1,408	7,79E-04
ITGA11	ENSG00000137809	0,24	0,91	1,899	4,30E-03
ITIH5	ENSG00000123243	4,75	1,25	-1,928	7,79E-04
ITM2A	ENSG00000078596	24,47	9,87	-1,311	7,79E-04
ITPKB	ENSG00000143772	12,81	34,59	1,434	7,79E-04
ITPRIP	ENSG00000148841	1,94	3,92	1,018	7,79E-04
JAKMIP1	ENSG00000152969	17,85	8,06	-1,147	7,79E-04
JMY	ENSG00000152409	2,08	4,24	1,025	7,79E-04
KBTBD11	ENSG00000176595	7,73	38,22	2,306	7,79E-04
KBTBD8	ENSG00000163376	1,32	0,51	-1,361	2,65E-02
KCNA3	ENSG00000177272	1,26	0,26	-2,254	2,08E-03
KCNB1	ENSG00000158445	2,78	1,23	-1,182	7,79E-04
KCNH4	ENSG00000089558	1,50	0,67	-1,157	6,29E-03
KCNH6	ENSG00000173826	16,04	7,82	-1,036	7,79E-04
KCNIP1	ENSG00000182132	0,53	0,12	-2,162	1,91E-02
KCNJ2	ENSG00000123700	2,14	0,71	-1,589	2,66E-03
KCNK1	ENSG00000135750	19,93	7,27	-1,455	7,79E-04
KCNK3	ENSG00000171303	6,84	3,13	-1,126	7,79E-04
KCNK6	ENSG00000099337	1,82	0,86	-1,086	1,45E-02
KCNQ3	ENSG00000184156	0,93	0,17	-2,458	1,45E-03
KCNQ5	ENSG00000185760	1,95	4,46	1,195	2,89E-02
KIAA0907	ENSG00000132680	31,16	66,28	1,089	7,79E-04
KIAA1549L	ENSG00000110427	1,44	0,44	-1,704	1,04E-02
KIAA1755	ENSG00000149633	1,33	0,10	-3,684	7,79E-04
KIF11	ENSG00000138160	5,66	2,35	-1,272	7,79E-04

KIF14	ENSG00000118193	2,72	1,09	-1,324	7,79E-04
KIF1C	ENSG00000129250	3,01	8,33	1,469	7,79E-04
KIF21A	ENSG00000139116	178,98	84,92	-1,076	7,79E-04
KIF21B	ENSG00000116852	2,88	0,46	-2,644	7,79E-04
KIF23	ENSG00000137807	7,01	3,31	-1,081	2,51E-02
KIF4A	ENSG00000090889	6,28	2,00	-1,653	3,22E-02
KIFC1	ENSG00000237649	9,27	4,26	-1,123	1,33E-02
KISS1R	ENSG00000116014	12,34	5,69	-1,117	1,37E-02
KLHDC8A	ENSG00000162873	0,83	0,21	-1,968	3,23E-03
KLHL35	ENSG00000149243	2,25	0,65	-1,785	3,23E-03
KLK14	ENSG00000129437	0,48	1,40	1,549	7,25E-03
KRT80	ENSG00000167767	1,35	0,47	-1,525	7,79E-04
LAMA4	ENSG00000112769	7,07	1,30	-2,448	7,79E-04
LAMA5	ENSG00000130702	97,82	220,51	1,173	1,72E-02
LAMP3	ENSG00000078081	1,01	2,87	1,506	7,79E-04
LBH	ENSG00000213626	23,86	8,97	-1,412	7,79E-04
LCNL1	ENSG00000214402	0,46	3,90	3,085	7,79E-04
LCP1	ENSG00000136167	6,04	1,14	-2,410	7,79E-04
LDLRAP1	ENSG00000157978	3,54	1,74	-1,026	7,72E-03
LDOC1	ENSG00000182195	17,94	8,73	-1,039	7,79E-04
LEAP2	ENSG00000164406	0,89	2,03	1,194	2,99E-02
LGI3	ENSG00000168481	4,15	1,95	-1,091	2,66E-03
LHFPL4	ENSG00000156959	19,19	9,35	-1,037	7,79E-04
LHX8	ENSG00000162624	0,07	4,18	5,870	7,79E-04
LIF	ENSG00000128342	2,25	0,70	-1,685	7,79E-04
LINC00632	ENSG00000203930	11,41	27,67	1,279	7,79E-04
LINC01587	ENSG00000082929	2,58	0,92	-1,489	9,94E-03
LINGO2	ENSG00000174482	12,91	5,10	-1,339	7,79E-04
LMNTD1	ENSG00000152936	5,15	1,85	-1,481	2,31E-02
LMX1B	ENSG00000136944	0,25	1,33	2,392	7,79E-04
GLYATL1	ENSG00000166840	0,67	0,15	-2,190	7,79E-04
LOC100996455	ENSG00000181908	0,50	0,16	-1,593	1,91E-02
LPP	ENSG00000145012	0,56	0,24	-1,242	2,92E-02
LRGUK	ENSG00000155530	1,81	0,73	-1,309	3,23E-03
LRP1B	ENSG00000168702	0,51	0,18	-1,495	1,72E-02
LRRC32	ENSG00000137507	0,72	0,16	-2,195	3,23E-03
LRRC63	ENSG00000173988	1,71	0,75	-1,192	2,31E-02
LRRC66	ENSG00000188993	0,52	0,12	-2,071	9,50E-03
LST1	ENSG00000204482	0,31	0,73	1,259	2,95E-02
LTBP1	ENSG00000049323	1,38	3,43	1,315	7,79E-04
LUM	ENSG00000139329	50,13	19,58	-1,356	7,79E-04
LYNX1	ENSG00000180155	24,55	10,49	-1,228	3,23E-03
MAB21L2	ENSG00000181541	7,96	51,94	2,706	8,62E-03
MAD2L1	ENSG00000164109	24,54	11,15	-1,138	7,79E-04
MAGEA10	ENSG00000124260	12,25	3,41	-1,843	7,79E-04
MAGEA12	ENSG00000213401	27,68	9,63	-1,523	7,79E-04
MAGEA6	ENSG00000197172	21,23	7,19	-1,561	5,81E-03
MAGEC1	ENSG00000155495	1,26	0,28	-2,188	3,88E-02
MAGEC2	ENSG00000046774	0,87	0,19	-2,162	6,77E-03
MAML2	ENSG00000184384	1,42	0,31	-2,175	7,79E-04
MAN1C1	ENSG00000117643	1,43	0,46	-1,642	1,45E-03
MAOB	ENSG00000069535	6,11	2,06	-1,571	7,79E-04
MAP3K5	ENSG00000197442	1,31	4,58	1,808	7,79E-04
MARCH1	ENSG00000145416	0,62	2,46	1,995	7,79E-04
MARCH11	ENSG00000183654	102,05	25,48	-2,002	7,79E-04
MARCH4	ENSG00000144583	18,38	7,30	-1,333	7,79E-04
MCM10	ENSG00000065328	2,70	0,84	-1,678	7,79E-04
MCTP2	ENSG00000140563	1,99	0,45	-2,135	7,79E-04
MECOM	ENSG00000085276	0,88	0,13	-2,750	7,79E-04
MEGF11	ENSG00000157890	2,64	0,90	-1,562	8,17E-03
MELK	ENSG00000165304	11,72	4,75	-1,303	7,79E-04
MEST	ENSG00000106484	2,92	14,16	2,279	7,79E-04
METTL22	ENSG00000067365	18,68	48,65	1,381	3,23E-03
MFAP4	ENSG00000166482	129,72	424,33	1,710	7,79E-04
MGAT4C	ENSG00000182050	0,84	0,28	-1,585	3,53E-02

MGAT5B	ENSG00000167889	19,57	9,66	-1,019	7,79E-04
MICB	ENSG00000204516	0,88	0,10	-3,121	1,21E-02
MID1	ENSG00000101871	1,63	0,69	-1,246	2,38E-02
MIXL1	ENSG00000185155	1,56	0,43	-1,856	1,21E-02
MKI67	ENSG00000148773	6,88	2,41	-1,513	7,79E-04
MKKS	ENSG00000125863	20,98	10,23	-1,037	7,79E-04
MLXIP	ENSG00000175727	10,15	21,66	1,094	7,79E-04
MMD2	ENSG00000136297	1,20	0,38	-1,663	2,08E-03
MON2	ENSG00000061987	12,12	33,25	1,456	7,79E-04
MPZ	ENSG00000158887	1,23	3,51	1,513	7,25E-03
MRAP2	ENSG00000135324	16,12	6,62	-1,283	7,79E-04
MTMR11	ENSG00000014914	1,12	4,06	1,862	7,79E-04
MUC4	ENSG00000145113	0,65	0,26	-1,352	3,91E-02
MXRA8	ENSG00000162576	35,46	122,87	1,793	7,79E-04
MYBL2	ENSG00000101057	14,92	5,79	-1,366	7,79E-04
MYC	ENSG00000136997	2,30	0,41	-2,504	7,79E-04
MYCL	ENSG00000116990	2,13	5,30	1,316	7,79E-04
MYCN	ENSG00000134323	1,98	3,98	1,008	4,81E-03
MYLIP	ENSG00000007944	2,12	4,46	1,073	1,45E-03
MYLK	ENSG00000065534	9,57	3,40	-1,494	7,79E-04
NAA25	ENSG00000111300	5,57	12,77	1,198	7,79E-04
NAGS	ENSG00000161653	1,72	0,82	-1,057	1,83E-02
NAPB	ENSG00000125814	31,98	14,23	-1,168	7,79E-04
NCAN	ENSG00000130287	10,66	2,68	-1,990	7,79E-04
NCAPG	ENSG00000109805	5,88	2,20	-1,419	4,58E-02
NCAPH	ENSG00000121152	4,18	1,83	-1,192	5,32E-03
NDC80	ENSG00000080986	4,39	1,84	-1,254	3,77E-03
NDRG1	ENSG00000104419	10,55	28,73	1,445	7,79E-04
NEDD9	ENSG00000111859	3,85	11,98	1,638	7,79E-04
NEFH	ENSG00000100285	14,98	5,37	-1,481	7,79E-04
NEFM	ENSG00000104722	50,12	14,98	-1,742	7,79E-04
NEIL3	ENSG00000109674	2,00	0,66	-1,601	7,79E-04
NEK10	ENSG00000163491	1,05	0,45	-1,218	4,41E-02
NEK2	ENSG00000117650	8,17	3,95	-1,050	7,79E-04
NEK6	ENSG00000119408	3,00	1,35	-1,147	2,66E-03
NELL1	ENSG00000165973	16,30	7,57	-1,106	3,23E-03
NELL2	ENSG00000184613	22,44	57,54	1,359	7,79E-04
NFATC4	ENSG00000100968	6,92	17,44	1,333	2,66E-03
NGFR	ENSG00000064300	20,25	59,04	1,544	7,79E-04
NKAIN4	ENSG00000101198	1,11	0,13	-3,073	7,79E-04
NKX2-5	ENSG00000183072	0,09	1,83	4,385	7,79E-04
NME5	ENSG00000112981	6,84	2,65	-1,366	7,72E-03
NMNAT2	ENSG00000157064	48,86	21,69	-1,172	5,81E-03
NMRK2	ENSG00000077009	0,91	0,21	-2,121	1,29E-02
NMU	ENSG00000109255	13,49	5,57	-1,275	7,79E-04
NNAT	ENSG00000053438	212,18	48,86	-2,119	7,79E-04
NOB1	ENSG00000141101	7,82	17,08	1,126	7,79E-04
NOL6	ENSG00000165271	8,96	17,98	1,005	7,79E-04
NPIPA7	ENSG00000214967	0,74	2,22	1,591	3,23E-03
NPPC	ENSG00000163273	0,71	11,01	3,952	7,79E-04
NPTX2	ENSG00000106236	85,45	36,53	-1,226	7,79E-04
NPY	ENSG00000122585	1613,76	765,48	-1,076	2,08E-03
NR4A1	ENSG00000123358	13,99	37,67	1,429	7,79E-04
NRCAM	ENSG00000091129	223,14	99,20	-1,170	7,79E-04
NRGN	ENSG00000154146	17,01	4,70	-1,857	2,08E-03
NRSN1	ENSG00000152954	29,68	13,72	-1,113	7,79E-04
NRXN1	ENSG00000179915	13,85	5,43	-1,350	7,79E-04
NSG1	ENSG00000168824	50,99	22,87	-1,157	3,99E-02
NT5E	ENSG00000135318	4,77	0,86	-2,464	7,79E-04
NTM	ENSG00000182667	1,01	0,19	-2,434	7,79E-04
NTNG1	ENSG00000162631	0,87	0,27	-1,676	4,30E-03
NUDT11	ENSG00000196368	4,12	1,25	-1,721	7,79E-04
NUPR1	ENSG00000176046	0,11	1,68	3,905	5,81E-03
NUSAP1	ENSG00000137804	27,79	12,72	-1,128	7,79E-04
NXT2	ENSG00000101888	3,58	11,64	1,701	7,79E-04

NYAP2	ENSG00000144460	1,91	0,70	-1,444	2,08E-03
OLFM3	ENSG00000118733	7,52	2,21	-1,767	7,79E-04
OLFML3	ENSG00000116774	5,04	1,88	-1,423	7,79E-04
OPRM1	ENSG00000112038	16,94	5,36	-1,659	7,79E-04
ORC1	ENSG00000085840	0,96	0,42	-1,202	9,07E-03
OSBPL7	ENSG00000006025	8,44	18,31	1,118	7,79E-04
OSCAR	ENSG00000170909	0,27	1,97	2,864	7,79E-04
OTOR	ENSG00000125879	3,26	0,67	-2,284	2,08E-03
PADI2	ENSG00000117115	0,47	0,09	-2,331	7,79E-04
PAEP	ENSG00000122133	0,14	0,48	1,798	3,31E-02
PAH	ENSG00000171759	0,01	0,56	6,136	7,79E-04
PAK5	ENSG00000101349	1,65	0,76	-1,125	5,32E-03
PAPPA2	ENSG00000116183	0,51	3,20	2,635	7,79E-04
PAPSS2	ENSG00000198682	2,12	0,96	-1,140	8,17E-03
PARP11	ENSG00000111224	1,93	0,93	-1,046	2,13E-02
PATJ	ENSG00000132849	3,25	7,40	1,185	7,79E-04
PCDH17	ENSG00000118946	0,95	0,38	-1,325	7,79E-04
PCDH18	ENSG00000189184	3,55	1,70	-1,065	7,79E-04
PCDH20	ENSG00000197991	0,80	3,93	2,298	7,79E-04
PCDH9	ENSG00000184226	1,36	0,12	-3,443	7,79E-04
PCDHB2	ENSG00000112852	4,41	0,80	-2,470	7,79E-04
PCNA	ENSG00000132646	58,26	21,47	-1,441	7,79E-04
PDCD4	ENSG00000150593	49,52	109,55	1,146	7,25E-03
PDE3A	ENSG00000172572	7,92	21,51	1,442	7,79E-04
PDK4	ENSG00000004799	1,50	3,63	1,274	7,79E-04
PDZK1	ENSG00000174827	2,85	1,28	-1,151	3,57E-02
PHACTR3	ENSG00000087495	3,54	1,74	-1,024	5,81E-03
PHF21B	ENSG00000056487	42,15	20,08	-1,070	7,79E-04
PHKG1	ENSG00000164776	0,55	1,45	1,404	1,25E-02
PHLDA2	ENSG00000181649	1,94	0,54	-1,845	7,72E-03
PHYHIPL	ENSG00000165443	40,86	14,97	-1,448	7,79E-04
PIFO	ENSG00000173947	2,14	0,56	-1,938	1,12E-02
PIMREG	ENSG00000129195	5,26	2,21	-1,251	9,07E-03
PIWIL2	ENSG00000197181	0,18	1,62	3,165	7,79E-04
PKP2	ENSG00000057294	2,36	5,33	1,175	1,08E-02
PLAUR	ENSG00000011422	5,98	2,96	-1,015	1,83E-02
PLCXD3	ENSG00000182836	47,70	22,70	-1,071	7,79E-04
PLEKHA2	ENSG00000169499	8,14	17,27	1,085	7,79E-04
PLEKHB1	ENSG00000021300	12,08	5,93	-1,026	7,79E-04
PLIN5	ENSG00000214456	1,06	0,43	-1,316	4,95E-02
PLK2	ENSG00000145632	22,97	10,47	-1,133	4,44E-02
PLLP	ENSG00000102934	3,22	1,58	-1,030	3,28E-02
PLPP3	ENSG00000162407	8,24	3,08	-1,418	7,79E-04
PLPP4	ENSG00000203805	3,42	0,56	-2,621	7,79E-04
PLXDC2	ENSG00000120594	0,30	1,05	1,795	7,79E-04
PLXNA4	ENSG00000221866	4,98	1,07	-2,225	7,79E-04
PNCK	ENSG00000130822	12,68	31,59	1,317	7,25E-03
PNMA3	ENSG00000183837	3,14	1,47	-1,097	1,04E-02
POC1A	ENSG00000164087	3,20	1,47	-1,117	8,17E-03
POLQ	ENSG00000051341	1,22	0,44	-1,468	1,08E-02
POPDC2	ENSG00000121577	43,20	9,39	-2,202	7,79E-04
POU3F3	ENSG00000198914	6,32	2,82	-1,161	7,79E-04
POU5F1	ENSG00000204531	1,88	0,70	-1,414	4,81E-03
PPEF1	ENSG00000086717	1,96	0,40	-2,291	7,79E-04
PPP2R2B	ENSG00000156475	1,97	0,65	-1,597	7,79E-04
PPP2R2C	ENSG00000074211	27,99	11,08	-1,337	7,79E-04
PPT1	ENSG00000131238	49,89	7512,55	7,235	7,79E-04
PQLC2L	ENSG00000174899	1,33	0,00	-Infinity	7,79E-04
PRKCA	ENSG00000154229	7,37	2,71	-1,445	7,79E-04
PRLHR	ENSG00000119973	4,51	1,50	-1,590	7,79E-04
PRNP	ENSG00000171867	14,09	6,46	-1,124	1,45E-03
PROCA1	ENSG00000167525	3,92	7,85	1,003	1,25E-02
PRR29	ENSG00000224383	5,11	2,05	-1,316	3,06E-02
PRRX2	ENSG00000167157	3,55	0,73	-2,282	7,79E-04
PRSS35	ENSG00000146250	2,72	1,22	-1,159	3,23E-03

PRTFDC1	ENSG00000099256	1,10	0,26	-2,093	8,62E-03
PRTG	ENSG00000166450	4,34	10,79	1,315	7,79E-04
PTCHD4	ENSG00000244694	4,57	1,08	-2,075	7,79E-04
PTER	ENSG00000165983	0,38	2,83	2,905	7,79E-04
PTGDS	ENSG00000107317	2,91	21,45	2,882	7,79E-04
PTGER3	ENSG00000050628	1,61	0,72	-1,156	1,65E-02
PTGIS	ENSG00000124212	1,13	0,40	-1,511	6,77E-03
PTPN14	ENSG00000152104	1,32	2,99	1,180	2,75E-02
PTPN3	ENSG00000070159	3,19	11,68	1,874	7,79E-04
PTPRD	ENSG00000153707	0,29	2,20	2,930	7,79E-04
PTPRM	ENSG00000173482	27,35	56,52	1,047	7,79E-04
PTPRO	ENSG00000151490	9,44	3,92	-1,267	4,55E-02
PTTG1	ENSG00000164611	40,74	19,98	-1,028	7,79E-04
PXDC1	ENSG00000168994	2,10	4,24	1,014	9,07E-03
QPCT	ENSG00000115828	0,66	1,87	1,502	4,30E-03
QRICH2	ENSG00000129646	2,76	1,30	-1,086	8,17E-03
RALGAPA2	ENSG00000188559	5,69	2,78	-1,034	5,81E-03
RASGEF1A	ENSG00000198915	0,46	0,05	-3,101	4,81E-03
RASL11B	ENSG00000128045	19,69	6,81	-1,531	7,79E-04
RASSF2	ENSG00000101265	3,91	1,68	-1,219	7,79E-04
RBP7	ENSG00000162444	1,40	0,35	-1,989	1,29E-02
RBPMS	ENSG00000157110	16,42	48,41	1,560	7,79E-04
RCN3	ENSG00000142552	12,71	5,94	-1,099	3,23E-03
RDH16	ENSG00000139547	0,33	1,21	1,860	7,79E-04
RELN	ENSG00000189056	3,42	13,91	2,025	8,17E-03
REN	ENSG00000143839	0,11	0,72	2,741	6,29E-03
RGMA	ENSG00000182175	4,61	1,78	-1,376	7,79E-04
RGPD5	ENSG00000015568	1,08	2,99	1,466	6,29E-03
RGS2	ENSG00000116741	66,26	18,61	-1,832	7,79E-04
RGS3	ENSG00000138835	5,06	2,47	-1,036	2,08E-03
RGS4	ENSG00000117152	83,55	325,66	1,963	7,79E-04
RHBDF1	ENSG00000007384	11,82	24,69	1,063	7,79E-04
RHOV	ENSG00000104140	1,08	0,48	-1,156	3,88E-02
RICTOR	ENSG00000164327	3,47	7,16	1,043	2,66E-03
RIMS4	ENSG00000101098	19,27	7,98	-1,272	7,79E-04
RIT2	ENSG00000152214	5,99	2,79	-1,104	2,65E-02
RMI2	ENSG00000175643	5,10	1,72	-1,567	7,79E-04
RND1	ENSG00000172602	2,01	0,69	-1,538	1,45E-03
ROBO2	ENSG00000185008	4,31	22,44	2,380	7,79E-04
ROPN1B	ENSG00000114547	0,50	0,15	-1,710	1,17E-02
RPH3A	ENSG00000089169	11,23	3,10	-1,857	1,98E-02
RPL22L1	ENSG00000163584	18,82	38,70	1,040	1,45E-03
RRAGD	ENSG00000025039	6,41	16,19	1,336	7,79E-04
RRM2	ENSG00000171848	17,79	3,75	-2,246	7,79E-04
RSPH4A	ENSG00000111834	0,63	0,17	-1,907	3,23E-03
RUFY4	ENSG00000188282	0,14	1,23	3,139	4,81E-03
RYR1	ENSG00000196218	1,39	0,21	-2,763	7,25E-03
S100A10	ENSG00000197747	26,15	4,28	-2,611	7,79E-04
S100A4	ENSG00000196154	5,04	1,50	-1,749	8,17E-03
S100B	ENSG00000160307	12,34	3,57	-1,789	7,79E-04
S1PR3	ENSG00000213694	6,51	3,18	-1,036	1,45E-03
SAFB2	ENSG00000130254	14,92	36,36	1,285	3,94E-02
SAMD9	ENSG00000205413	0,43	1,43	1,734	7,79E-04
SBSPON	ENSG00000164764	1,14	0,54	-1,075	3,57E-02
SCARA3	ENSG00000168077	6,31	1,80	-1,807	7,79E-04
SCML4	ENSG00000146285	1,86	0,87	-1,100	4,49E-02
SCN2B	ENSG00000149575	0,56	0,07	-3,058	2,08E-03
SCN4B	ENSG00000177098	8,70	1,86	-2,225	7,79E-04
SCRG1	ENSG00000164106	2,36	6,23	1,400	7,79E-04
SCUBE3	ENSG00000146197	0,49	0,23	-1,055	2,24E-02
SEL1L3	ENSG00000091490	13,47	4,75	-1,504	5,81E-03
SEMA3C	ENSG00000075223	110,38	22,25	-2,311	7,79E-04
SEMA5B	ENSG00000082684	37,46	75,10	1,004	7,79E-04
SERPINE2	ENSG00000135919	0,80	2,81	1,807	7,79E-04
SERPING1	ENSG00000149131	22,06	10,29	-1,101	7,79E-04

SERTM1	ENSG00000180440	2,49	0,90	-1,470	2,66E-03
SEZ6L	ENSG00000100095	35,50	15,95	-1,155	2,66E-03
SFT2D1	ENSG00000198818	27,77	59,31	1,095	7,79E-04
SH2D5	ENSG00000189410	0,66	1,70	1,371	6,29E-03
SHCBP1	ENSG00000171241	2,10	0,75	-1,490	1,57E-02
SHD	ENSG00000105251	23,90	54,39	1,186	7,79E-04
SIK1	ENSG00000142178	2,25	7,73	1,778	7,79E-04
SIRPA	ENSG00000198053	0,39	1,29	1,714	7,79E-04
SIX6	ENSG00000184302	3,46	1,67	-1,052	1,80E-02
SKA3	ENSG00000165480	3,18	0,88	-1,850	7,79E-04
SKP2	ENSG00000145604	11,98	26,75	1,159	7,79E-04
SLC15A2	ENSG00000163406	0,55	1,52	1,473	4,67E-02
SLC18A2	ENSG00000165646	11,21	33,42	1,576	7,79E-04
SLC18A3	ENSG00000187714	56,36	25,97	-1,118	7,79E-04
SLC25A45	ENSG00000162241	6,66	3,25	-1,036	9,94E-03
SLC2A10	ENSG00000197496	2,44	0,97	-1,326	4,46E-02
SLC2A6	ENSG00000160326	11,84	5,56	-1,090	7,79E-04
SLC30A3	ENSG00000115194	4,45	2,19	-1,024	1,29E-02
SLC35F3	ENSG00000183780	3,32	0,74	-2,171	7,79E-04
SLC44A2	ENSG00000129353	103,84	258,21	1,314	7,79E-04
SLC46A3	ENSG00000139508	0,52	2,07	1,990	7,79E-04
SLC5A5	ENSG00000105641	2,80	0,45	-2,648	1,08E-02
SLC6A19	ENSG00000174358	0,11	1,12	3,293	7,79E-04
SLC6A2	ENSG00000103546	192,99	70,94	-1,444	2,66E-03
SLC7A10	ENSG00000130876	3,90	1,44	-1,435	2,08E-03
SLC8A3	ENSG00000100678	24,42	9,18	-1,411	7,79E-04
SLIT2	ENSG00000145147	5,93	1,34	-2,143	7,79E-04
SMPD3	ENSG00000103056	8,77	3,16	-1,475	6,29E-03
SNAP25	ENSG00000132639	141,62	63,79	-1,151	7,79E-04
SNAP91	ENSG00000065609	30,54	13,48	-1,180	7,79E-04
SNTG2	ENSG00000172554	2,96	1,06	-1,489	9,07E-03
SOSTDC1	ENSG00000171243	3,64	1,50	-1,283	2,08E-03
SOX13	ENSG00000143842	3,68	1,64	-1,163	4,30E-03
SPARC	ENSG00000113140	53,05	121,65	1,197	7,79E-04
SPC25	ENSG00000152253	7,34	2,46	-1,579	7,79E-04
SPEF1	ENSG00000101222	2,00	0,67	-1,567	5,81E-03
SPON2	ENSG00000159674	3,13	11,21	1,842	7,79E-04
SPP1	ENSG00000118785	3,11	1,20	-1,377	1,04E-02
SPTB	ENSG00000070182	3,84	8,54	1,152	1,45E-03
SPTSSB	ENSG00000196542	3,60	0,92	-1,974	7,79E-04
SRRM4	ENSG00000139767	6,24	2,55	-1,292	3,77E-03
SSFA2	ENSG00000138434	7,28	16,50	1,180	7,79E-04
SSUH2	ENSG00000125046	1,06	0,25	-2,068	1,04E-02
ST8SIA2	ENSG00000140557	7,40	2,40	-1,622	7,79E-04
ST8SIA5	ENSG00000101638	0,46	0,10	-2,202	2,95E-02
STARD13	ENSG00000133121	3,18	7,32	1,203	7,79E-04
STEAP2	ENSG00000157214	2,86	6,16	1,105	7,79E-04
STS	ENSG00000101846	1,60	0,72	-1,150	5,81E-03
SULT4A1	ENSG00000130540	13,17	5,74	-1,199	7,79E-04
SUSD2	ENSG00000099994	1,29	10,85	3,077	7,79E-04
SV2C	ENSG00000122012	17,01	5,25	-1,696	7,79E-04
SYBU	ENSG00000147642	4,36	1,52	-1,518	7,79E-04
SYNPO2	ENSG00000172403	53,59	22,26	-1,268	7,79E-04
SYPL1	ENSG00000008282	18,84	41,51	1,140	7,79E-04
SYT13	ENSG00000019505	6,10	1,05	-2,537	7,79E-04
SYT8	ENSG00000149043	1,65	5,56	1,756	7,79E-04
SYTL1	ENSG00000142765	4,66	12,52	1,426	7,79E-04
SYTL2	ENSG00000137501	2,60	0,98	-1,405	3,47E-02
T	ENSG00000164458	0,98	0,46	-1,078	4,58E-02
TAC3	ENSG00000166863	5,73	13,00	1,181	2,08E-03
TAF4B	ENSG00000141384	0,49	1,25	1,341	7,79E-04
TBC1D15	ENSG00000121749	9,92	22,93	1,209	7,79E-04
TBX18	ENSG00000112837	1,93	3,93	1,022	7,79E-04
TBX3	ENSG00000135111	11,46	4,31	-1,409	7,79E-04
TCEAL2	ENSG00000184905	3,20	1,00	-1,686	7,79E-04

TCERG1L	ENSG00000176769	0,74	0,27	-1,479	1,04E-02
TCF15	ENSG00000125878	1,05	0,18	-2,550	7,25E-03
TF	ENSG00000091513	0,23	0,64	1,461	2,13E-02
TFAP2E	ENSG00000116819	1,74	3,89	1,159	7,79E-04
TFAP4	ENSG00000090447	3,23	7,10	1,136	7,79E-04
TFPI	ENSG00000003436	0,22	2,27	3,395	1,45E-03
TGFA	ENSG00000163235	1,19	0,47	-1,343	3,60E-02
TGM2	ENSG00000198959	4,60	0,72	-2,666	4,81E-03
THSD4	ENSG00000187720	21,99	9,81	-1,165	7,79E-04
THY1	ENSG00000154096	63,97	28,55	-1,164	4,81E-03
TIMP3	ENSG00000100234	15,35	37,19	1,276	7,79E-04
TK1	ENSG00000167900	6,50	1,94	-1,747	7,79E-04
TLE1	ENSG00000196781	9,75	22,72	1,221	7,79E-04
TLE2	ENSG00000065717	13,62	53,97	1,986	7,79E-04
TLE3	ENSG00000140332	32,31	10,22	-1,660	7,79E-04
TLE4	ENSG00000106829	6,65	13,62	1,035	1,37E-02
TLE6	ENSG00000104953	3,68	10,14	1,464	4,30E-03
TLL2	ENSG00000095587	0,69	0,18	-1,956	1,45E-03
TLR2	ENSG00000137462	0,62	0,11	-2,457	7,79E-04
TLR3	ENSG00000164342	0,11	0,55	2,322	1,04E-02
TM4SF1	ENSG00000169908	0,16	1,77	3,460	7,79E-04
TMC4	ENSG00000167608	4,20	1,96	-1,099	4,55E-02
TMEM105	ENSG00000185332	0,45	1,36	1,587	4,84E-02
TMEM133	ENSG00000170647	4,96	1,48	-1,743	7,79E-04
TMEM178B	ENSG00000261115	8,36	3,20	-1,386	7,79E-04
TMEM215	ENSG00000188133	0,70	0,32	-1,138	3,66E-02
TMEM39A	ENSG00000176142	10,87	25,31	1,220	1,45E-03
TMPRSS6	ENSG00000187045	0,14	0,54	1,923	5,32E-03
TNC	ENSG00000041982	0,81	0,26	-1,615	2,08E-03
TNF	ENSG00000232810	0,94	0,10	-3,198	1,45E-03
TNFRSF14	ENSG00000157873	1,42	4,44	1,643	1,04E-02
TNFRSF1A	ENSG00000067182	1,17	12,63	3,439	7,79E-04
TNFRSF1B	ENSG00000028137	0,48	0,09	-2,337	2,85E-02
TNFRSF9	ENSG00000049249	6,45	1,18	-2,447	7,79E-04
TNFSF9	ENSG00000125657	0,69	0,16	-2,134	4,81E-02
TNN	ENSG00000120332	0,91	0,13	-2,751	7,79E-04
TNNI1	ENSG00000159173	0,16	0,68	2,044	2,45E-02
TNNI2	ENSG00000130598	1,70	5,35	1,656	7,79E-04
TNNT2	ENSG00000118194	0,25	1,21	2,292	7,79E-04
TNNT3	ENSG00000130595	0,68	6,77	3,306	7,79E-04
TNR	ENSG00000116147	3,92	1,69	-1,211	7,79E-04
TOP2A	ENSG00000131747	21,60	10,22	-1,080	7,79E-04
TOX2	ENSG00000124191	29,81	10,32	-1,530	7,79E-04
TPM1	ENSG00000140416	79,49	164,64	1,050	1,45E-03
TPM2	ENSG00000198467	18,70	38,69	1,049	7,79E-04
TRHDE	ENSG00000072657	0,29	1,35	2,210	3,81E-02
TRIM67	ENSG00000119283	6,19	2,45	-1,338	7,79E-04
TSC22D4	ENSG00000166925	17,56	37,98	1,113	7,79E-04
TTC14	ENSG00000163728	16,31	37,49	1,201	1,87E-02
TTK	ENSG00000112742	4,12	1,96	-1,068	4,30E-03
TUBB4A	ENSG00000104833	48,17	17,09	-1,495	7,79E-04
UBE2C	ENSG00000175063	31,37	15,58	-1,009	7,79E-04
UBE2QL1	ENSG00000215218	2,86	1,10	-1,377	7,79E-04
UBE2T	ENSG00000077152	53,16	23,94	-1,151	7,79E-04
UCN	ENSG00000163794	2,94	7,48	1,348	6,29E-03
UFL1	ENSG00000014123	5,69	14,84	1,383	7,79E-04
ULBP2	ENSG00000131015	1,87	0,66	-1,503	5,81E-03
UNC5D	ENSG00000156687	2,67	0,27	-3,313	7,79E-04
UVSSA	ENSG00000163945	12,26	27,73	1,178	7,79E-04
VASN	ENSG00000168140	7,03	21,62	1,621	3,63E-02
VCAN	ENSG00000038427	39,91	10,34	-1,948	7,79E-04
VEGFA	ENSG00000112715	71,80	203,88	1,506	7,79E-04
VMO1	ENSG00000182853	0,67	1,63	1,283	3,35E-02
VSTM2L	ENSG00000132821	14,28	5,39	-1,404	7,79E-04
VWDE	ENSG00000146530	2,54	5,10	1,006	1,65E-02

WASF3	ENSG00000132970	10,65	4,59	-1,213	7,79E-04
WNT10B	ENSG00000169884	1,79	0,60	-1,575	1,45E-03
WNT5A	ENSG00000114251	0,12	3,69	4,907	7,79E-04
XPNPEP2	ENSG00000122121	1,63	0,37	-2,129	4,30E-03
XRCC2	ENSG00000196584	2,31	1,09	-1,082	5,81E-03
YBX2	ENSG00000006047	42,74	16,33	-1,388	7,79E-04
ZC3H12A	ENSG00000163874	0,90	1,90	1,075	1,33E-02
ZC3H12B	ENSG00000102053	0,43	0,93	1,117	5,32E-03
ZFP3	ENSG00000180787	4,56	2,10	-1,119	7,79E-04
ZMAT4	ENSG00000165061	1,07	3,81	1,830	4,81E-03
ZNF226	ENSG00000167380	21,17	44,46	1,070	2,58E-02
ZNF283	ENSG00000167637	4,47	9,05	1,018	2,69E-02
ZNF333	ENSG00000160961	8,22	23,36	1,507	7,79E-04
ZNF334	ENSG00000198185	6,96	2,51	-1,472	7,79E-04
ZNF445	ENSG00000185219	7,11	14,43	1,021	7,79E-04
ZNF454	ENSG00000178187	0,84	0,37	-1,166	4,64E-02
ZNF467	ENSG00000181444	19,98	40,26	1,011	7,79E-04
ZNF804A	ENSG00000170396	0,16	1,03	2,714	7,79E-04
ZNF841	ENSG00000197608	6,34	13,53	1,095	3,22E-02
ZWINT	ENSG00000122952	10,11	3,20	-1,660	7,79E-04
ZYG11A	ENSG00000203995	1,52	0,62	-1,303	7,79E-04

Legend: Sequences which have changed the original Ensembl ID (in green) or have been retired (n/a, in red).

Gene	Ensembl ID	SH-pcDNA3	SH-p.wtCLN1		
		FPKM	FPKM	Log_2FC	FDR (q-value)
AC012215.1	ENSG00000233863 (n/a	1,33	0,13	-3,400	2,95E-02
AC110771.1	ENSG00000269302 (n/a	0,36	1,50	2,063	8,62E-03
AL358813.2	ENSG00000203815 (n/a	0,49	0,00	-Infinity	7,79E-04
C6ORF50	ENSG00000145965 (n/a	1,51	6,46	2,101	7,79E-04
FLJ00418	ENSG00000268927 (n/a	9,91	30,28	1,611	7,79E-04
GDF10	ENSG00000107623 (n/a) ENSG00000266524	2,77	6,68	1,268	7,79E-04
LIMS3	ENSG00000240428 (n/a	0,30	1,14	1,950	2,66E-03
PCDHB16	ENSG00000196963 (n/a	0,96	3,73	1,956	7,79E-04
TXNIP	ENSG00000117289 (n/a) ENSG00000265972*	100,05	242,22	1,276	7,79E-04
XAGE1D	ENSG00000204376 (n/a	1,51	0,33	-2,181	9,94E-03
XKR7	ENSG00000101321 (n/a	5,09	2,52	-1,016	7,72E-03

* possible successor

Table S3 *Differentially expressed genes (DEGs) identified by RNA-seq analysis in SH-p.L222P cell line versus SH-pcDNA3*

Legend: Gene- Gene Symbol, Ensembl ID- ENSEMBL unique gene identifier, FPKM- fragments per kilobase per million mapped reads, Log2FC- log2 fold change, FDR- false discovery rate. Originally mapped DEGs, which are currently no more available or show a different Ensembl ID , are reported separetely at the end of the table.

Gene	Ensembl ID	SH-pcDNA3	SH-p.L222P		
		FPKM	FPKM	Log_2FC	FDR (q-value)
ACOT2	ENSG00000119673	7,62	3,39	-1,168	7,79E-04
ADAMTS10	ENSG00000142303	4,85	0,56	-3,108	7,79E-04
ADAMTS15	ENSG00000166106	0,14	0,45	1,700	2,08E-03
ADCYAP1R1	ENSG00000078549	4,11	1,80	-1,193	7,79E-04
ALKAL2	ENSG00000189292	1,21	0,37	-1,711	3,09E-02
ANO3	ENSG00000134343	1,14	0,26	-2,138	7,79E-04
ANO9	ENSG00000185101	2,67	0,25	-3,389	7,79E-04
AQP3	ENSG00000165272	3,81	1,79	-1,088	5,32E-03
ARSD	ENSG00000006756	8,58	1,99	-2,110	7,79E-04
ASB9	ENSG00000102048	1,56	0,45	-1,794	9,94E-03
ASCL1	ENSG00000139352	0,21	0,73	1,805	7,25E-03
BEX5	ENSG00000184515	4,82	1,78	-1,436	7,79E-04
BMP7	ENSG00000101144	14,23	3,85	-1,886	7,79E-04
BRINP2	ENSG00000198797	0,64	0,26	-1,298	4,17E-02
C19ORF42	ENSG00000268790	0,83	0,00	-Infinity	2,85E-02
C8orf46	ENSG00000169085	0,49	0,07	-2,790	2,66E-03
CA10	ENSG00000154975	0,70	0,23	-1,593	2,99E-02
CADM3	ENSG00000162706	0,46	0,06	-3,039	2,92E-02
CALB1	ENSG00000104327	14,66	6,06	-1,275	7,79E-04
CCDC80	ENSG00000091986	4,75	2,03	-1,227	2,45E-02
CCL2	ENSG00000108691	103,39	5,94	-4,120	7,79E-04
CCNO	ENSG00000152669	2,25	0,13	-4,139	7,79E-04
CD44	ENSG00000026508	1,52	0,32	-2,235	7,79E-04
CD99	ENSG00000002586	93,99	30,28	-1,634	7,79E-04
CDH20	ENSG00000101542	1,01	0,29	-1,782	8,62E-03
CDH22	ENSG00000149654	0,55	0,20	-1,488	1,87E-02
CFAP53	ENSG00000172361	1,43	0,70	-1,030	2,27E-02
CHRM2	ENSG00000181072	1,83	0,60	-1,617	2,66E-03
CNR1	ENSG00000118432	1,19	0,42	-1,483	4,73E-02
CNTFR	ENSG00000122756	145,98	68,45	-1,093	7,79E-04
COL17A1	ENSG00000065618	1,60	5,93	1,890	7,79E-04
COL27A1	ENSG00000196739	0,60	0,17	-1,858	9,50E-03
COLCA2	ENSG00000214290	1,84	0,49	-1,900	2,66E-03
COLEC12	ENSG00000158270	0,40	2,12	2,388	7,79E-04
COMP	ENSG00000105664	0,65	0,24	-1,470	3,38E-02
CPS1	ENSG00000021826	1,39	0,30	-2,217	7,79E-04
CRABP2	ENSG00000143320	27,23	10,87	-1,325	7,79E-04
CRISPLD2	ENSG00000103196	0,57	0,22	-1,369	3,25E-02
CUX2	ENSG00000111249	5,37	1,20	-2,166	7,79E-04
CXCL12	ENSG00000107562	3,10	0,91	-1,766	7,79E-04
CYP27C1	ENSG00000186684	0,74	0,31	-1,279	9,07E-03
CYR61	ENSG00000142871	3,26	1,12	-1,539	7,79E-04
CYTL1	ENSG00000170891	2,65	1,08	-1,293	1,53E-02
DBX1	ENSG00000109851	1,55	0,67	-1,211	1,72E-02
DDC	ENSG00000132437	71,24	144,67	1,022	7,79E-04
DDX60	ENSG00000137628	1,20	0,51	-1,242	4,95E-02
DHRS2	ENSG00000100867	4,88	1,56	-1,647	7,79E-04
DKK2	ENSG00000155011	18,40	9,17	-1,005	2,66E-03
DLG2	ENSG00000150672	19,22	8,43	-1,190	7,79E-04
DNAH9	ENSG00000007174	1,12	0,07	-4,092	1,45E-03
DNAJB11	ENSG00000090520	82,11	184,74	1,170	7,79E-04

DPT	ENSG00000143196	2,09	0,32	-2,724	7,79E-04
EBI3	ENSG00000105246	0,86	0,13	-2,700	2,20E-02
EDNRA	ENSG00000151617	2,99	0,44	-2,757	7,79E-04
EGR1	ENSG00000120738	54,88	24,74	-1,149	7,79E-04
EGR2	ENSG00000122877	0,58	0,22	-1,407	1,91E-02
ELFN2	ENSG00000166897	1,11	0,30	-1,900	7,79E-04
ENKUR	ENSG00000151023	0,57	0,12	-2,247	1,65E-02
EPB41L2	ENSG00000079819	0,66	0,22	-1,563	1,04E-02
ERICH5	ENSG00000177459	2,17	0,76	-1,515	8,62E-03
EVC2	ENSG00000173040	0,59	0,01	-6,060	2,08E-03
FABP6	ENSG00000170231	0,77	1,77	1,198	4,44E-02
FAM129A	ENSG00000135842	2,71	6,23	1,202	7,79E-04
FAM20C	ENSG00000177706	1,85	0,52	-1,828	1,45E-03
FAM89A	ENSG00000182118	10,96	4,02	-1,448	7,79E-04
FGF19	ENSG00000162344	0,58	0,05	-3,431	1,21E-02
FGL1	ENSG00000104760	5,61	1,56	-1,850	7,79E-04
FOXC1	ENSG00000054598	11,30	3,94	-1,519	7,79E-04
GBP2	ENSG00000162645	0,76	0,26	-1,543	1,83E-02
GBX2	ENSG00000168505	0,53	1,96	1,898	4,46E-02
GDF15	ENSG00000130513	66,01	20,62	-1,679	7,79E-04
GFRA2	ENSG00000168546	1,38	3,20	1,213	1,17E-02
GLB1L3	ENSG00000166105	1,80	0,77	-1,229	9,50E-03
GRAMD2	ENSG00000175318	1,51	0,74	-1,027	4,84E-02
GRIP1	ENSG00000155974	3,47	0,94	-1,877	1,45E-03
GYG2	ENSG00000056998	1,34	0,11	-3,605	7,79E-04
HGF	ENSG00000019991	13,55	2,07	-2,711	7,79E-04
HHEX	ENSG00000152804	0,75	0,33	-1,167	3,63E-02
HIC1	ENSG00000177374	6,74	3,26	-1,048	5,32E-03
HIST1H4H	ENSG00000158406	1,65	0,41	-2,005	2,02E-02
HMGN4	ENSG00000182952	50,63	105,52	1,059	7,79E-04
HMX2	ENSG00000188816	1,04	0,17	-2,619	2,66E-03
HS3ST3B1	ENSG00000153976	0,22	0,58	1,395	4,76E-02
ID4	ENSG00000172201	4,44	0,93	-2,256	7,79E-04
IER3	ENSG00000137331	2,47	0,57	-2,118	7,79E-04
IFI44	ENSG00000137965	3,94	1,07	-1,877	7,79E-04
IGDCC4	ENSG00000103742	1,55	0,78	-1,003	3,09E-02
IKZF1	ENSG00000185811	0,29	0,79	1,467	4,14E-02
IL32	ENSG00000008517	23,76	1,79	-3,728	7,79E-04
INPP5D	ENSG00000168918	2,45	0,74	-1,718	7,79E-04
ITGA11	ENSG00000137809	0,24	0,68	1,495	3,06E-02
ITM2A	ENSG00000078596	24,47	7,43	-1,720	7,79E-04
KCNAB1	ENSG00000169282	1,15	2,31	1,007	4,30E-03
KCNJ2	ENSG00000123700	2,14	0,96	-1,154	2,66E-03
KCNJ9	ENSG00000162728	1,19	0,56	-1,076	5,81E-03
KCNQ3	ENSG00000184156	0,93	0,43	-1,112	9,94E-03
KCNQ5	ENSG00000185760	1,95	3,94	1,017	7,79E-04
KIAA1549L	ENSG00000110427	1,44	0,47	-1,618	7,79E-04
KIF21B	ENSG00000116852	2,88	1,02	-1,506	7,79E-04
KITLG	ENSG00000049130	6,59	2,75	-1,259	7,79E-04
KLHDC7B	ENSG00000130487	0,19	0,53	1,492	9,50E-03
LAMA4	ENSG00000112769	7,07	3,20	-1,146	7,79E-04
LAMP3	ENSG00000078081	1,01	3,88	1,942	7,79E-04
LCP1	ENSG00000136167	6,04	2,26	-1,420	7,79E-04
LIF	ENSG00000128342	2,25	0,79	-1,515	3,23E-03
LRRC32	ENSG00000137507	0,72	0,18	-1,991	7,79E-04
LRRC66	ENSG00000188993	0,52	0,23	-1,166	2,95E-02
LTB	ENSG00000227507	0,68	0,16	-2,124	2,34E-02
LUM	ENSG00000139329	50,13	22,16	-1,177	7,79E-04
MAML2	ENSG00000184384	1,42	0,55	-1,371	7,79E-04
MAP1LC3C	ENSG00000197769	0,79	0,24	-1,697	2,92E-02
MBP	ENSG00000197971	1,35	0,45	-1,593	7,79E-04
MCTP2	ENSG00000140563	1,99	0,78	-1,355	4,30E-03

MICB	ENSG00000204516	0,88	0,26	-1,778	3,41E-02
MIXL1	ENSG00000185155	1,56	0,39	-1,996	3,77E-03
MSN	ENSG00000147065	6,13	0,11	-5,781	7,79E-04
MUC19	ENSG00000205592	0,63	0,01	-5,642	7,79E-04
MYC	ENSG00000136997	2,30	0,89	-1,373	7,79E-04
MYOZ3	ENSG00000164591	1,40	0,46	-1,617	1,98E-02
NECAB2	ENSG00000103154	0,83	0,25	-1,727	2,13E-02
NGB	ENSG00000165553	0,49	0,00	-Infinity	7,79E-04
NKAIN4	ENSG00000101198	1,11	0,19	-2,578	3,23E-03
NOD2	ENSG00000167207	0,14	0,45	1,642	4,32E-02
NOTCH1	ENSG00000148400	3,60	1,58	-1,190	7,79E-04
NPW	ENSG00000183971	3,76	0,67	-2,500	7,79E-04
NT5E	ENSG00000135318	4,77	2,19	-1,124	3,23E-03
NTRK3	ENSG00000140538	0,54	0,16	-1,726	3,72E-02
NUDT11	ENSG00000196368	4,12	1,23	-1,739	7,79E-04
NXT2	ENSG00000101888	3,58	9,87	1,463	7,79E-04
ODAM	ENSG00000109205	4,58	1,21	-1,920	7,79E-04
OLFML1	ENSG00000183801	2,25	0,80	-1,498	1,37E-02
OSCAR	ENSG00000170909	0,27	1,45	2,419	7,79E-04
PCDH17	ENSG00000118946	0,95	0,45	-1,078	1,08E-02
PCDH18	ENSG00000189184	3,55	1,69	-1,069	7,79E-04
PCDHB2	ENSG00000112852	4,41	1,37	-1,688	7,79E-04
PCSK2	ENSG00000125851	2,97	0,74	-2,000	1,45E-03
PLPP4	ENSG00000203805	3,42	1,46	-1,231	2,45E-02
PLXNA4	ENSG00000221866	4,98	1,88	-1,409	7,79E-04
PPEF1	ENSG00000086717	1,96	0,46	-2,080	7,79E-04
PPFIA2	ENSG00000139220	0,22	0,73	1,697	1,37E-02
PPT1	ENSG00000131238	49,89	12387,80	7,956	7,79E-04
PQLC2L	ENSG00000174899	1,33	0,00	-Infinity	7,79E-04
PRKCA	ENSG00000154229	7,37	2,56	-1,526	7,79E-04
PROKR2	ENSG00000101292	6,59	2,67	-1,302	7,79E-04
PRPH	ENSG00000135406	15,17	4,01	-1,921	2,66E-03
PRSS16	ENSG00000112812	0,63	2,22	1,824	7,79E-04
PRSS35	ENSG00000146250	2,72	1,12	-1,282	2,08E-03
PTCHD4	ENSG00000244694	4,57	1,58	-1,533	7,79E-04
PTGIR	ENSG00000160013	10,32	2,85	-1,855	7,79E-04
PTPRD	ENSG00000153707	0,29	0,88	1,609	4,79E-02
PXDNL	ENSG00000147485	1,29	2,64	1,038	1,25E-02
PYCARD	ENSG00000103490	1,13	0,39	-1,516	2,10E-02
RAB38	ENSG00000123892	1,17	0,38	-1,629	4,30E-03
RAMP3	ENSG00000122679	0,41	1,08	1,380	3,12E-02
RASGEF1A	ENSG00000198915	0,46	0,08	-2,459	4,30E-03
RBFOX1	ENSG00000078328	0,13	0,57	2,113	2,66E-03
RBP7	ENSG00000162444	1,40	0,52	-1,426	4,41E-02
RCN1	ENSG00000049449	20,14	9,79	-1,041	7,79E-04
RELB	ENSG00000104856	5,28	1,95	-1,436	7,79E-04
REN	ENSG00000143839	0,11	1,22	3,501	3,77E-03
RGMA	ENSG00000182175	4,61	2,27	-1,021	7,79E-04
RGS13	ENSG00000127074	1,55	0,58	-1,413	1,80E-02
RGS2	ENSG00000116741	66,26	30,21	-1,133	7,79E-04
RND1	ENSG00000172602	2,01	0,86	-1,228	1,17E-02
RRAD	ENSG00000166592	1,05	0,43	-1,292	3,06E-02
RSPO4	ENSG00000101282	2,82	0,54	-2,386	7,79E-04
SALL1	ENSG00000103449	1,11	6,18	2,481	7,79E-04
SAMD9	ENSG00000205413	0,43	1,01	1,232	7,79E-04
SCML4	ENSG00000146285	1,86	0,71	-1,395	1,08E-02
SCN2B	ENSG00000149575	0,56	0,21	-1,424	2,08E-03
SCN4B	ENSG00000177098	8,70	4,17	-1,059	7,79E-04
SEMA3C	ENSG00000075223	110,38	44,55	-1,309	7,79E-04
SERPINE1	ENSG00000106366	1,65	0,81	-1,022	1,49E-02
SIRPA	ENSG00000198053	0,39	1,22	1,635	7,79E-04
SLC18A1	ENSG00000036565	152,76	305,58	1,000	7,79E-04

SLC18A2	ENSG00000165646	11,21	26,87	1,262	7,79E-04
SLC24A2	ENSG00000155886	0,97	3,24	1,743	7,79E-04
SLC32A1	ENSG00000101438	0,79	1,63	1,048	2,17E-02
SLC46A3	ENSG00000139508	0,52	1,25	1,266	8,17E-03
SLC52A1	ENSG00000132517	0,88	0,36	-1,302	1,61E-02
SLC5A5	ENSG00000105641	2,80	1,00	-1,490	9,50E-03
SLC6A19	ENSG00000174358	0,11	2,87	4,647	7,79E-04
SLC7A5	ENSG00000103257	30,96	62,39	1,011	7,79E-04
SLC7A8	ENSG00000092068	0,82	0,06	-3,674	7,79E-04
SLC8A1	ENSG00000183023	0,86	0,26	-1,745	7,79E-04
SLIT2	ENSG00000145147	5,93	1,32	-2,161	7,79E-04
SLITRK6	ENSG00000184564	1,28	0,35	-1,875	7,79E-04
SNTG2	ENSG00000172554	2,96	1,12	-1,408	4,81E-03
SOX9	ENSG00000125398	5,79	2,02	-1,517	7,79E-04
ST6GAL2	ENSG00000144057	2,81	1,32	-1,093	7,79E-04
SYT13	ENSG00000019505	6,10	2,68	-1,190	7,79E-04
TCEAL2	ENSG00000184905	3,20	1,28	-1,324	7,79E-04
TLE2	ENSG00000065717	13,62	36,20	1,410	7,79E-04
TM4SF1	ENSG00000169908	0,16	0,74	2,195	2,27E-02
TNFAIP6	ENSG00000123610	1,96	0,59	-1,738	2,66E-03
TNFRSF9	ENSG00000049249	6,45	0,84	-2,932	7,79E-04
TPRN	ENSG00000176058	26,82	5,29	-2,343	7,79E-04
UNC5D	ENSG00000156687	2,67	0,14	-4,224	7,79E-04
VAMP5	ENSG00000168899	1,16	5,19	2,166	7,79E-04
VCAN	ENSG00000038427	39,91	12,58	-1,665	2,08E-03
VSTM2A	ENSG00000170419	5,82	14,69	1,336	7,79E-04
WNT16	ENSG00000002745	0,61	0,25	-1,321	2,95E-02
XPNPEP2	ENSG00000122121	1,63	0,62	-1,408	3,41E-02
ZC3H12B	ENSG00000102053	0,43	0,93	1,118	5,32E-03
ZDHHC15	ENSG00000102383	0,16	4,74	4,846	7,79E-04
ZFR2	ENSG00000105278	1,91	6,03	1,658	1,72E-02
ZNF454	ENSG00000178187	0,84	0,40	-1,072	4,35E-02
ZNF560	ENSG00000198028	0,79	0,20	-1,975	6,29E-03
ZNF804A	ENSG00000170396	0,16	1,31	3,064	7,79E-04

Legend: Sequences which have changed the original Ensembl ID (in green) or have been retired (n/a, in red).

Gene	Ensembl ID	SH-pcDNA3	SH-p.L222P		
		FPKM	FPKM	Log_2FC	FDR (q-value)
GDF10	ENSG00000107623 (n/a) ENSG00000266524	2,77	10,71	1,948	7,79E-04
PCDHB16	ENSG00000196963 (n/a)	0,96	4,17	2,118	7,79E-04
RBP3	ENSG00000107618 (n/a)	0,15	0,76	2,344	7,79E-04

Table S4 *Differentially expressed genes (DEGs) identified by RNA-seq analysis in SH-p.M57Nfs*45cell line versus SH-pcDNA3*

Legend: Gene- Gene Symbol, Ensembl ID- ENSEMBL unique gene identifier, FPKM- fragments per kilobase per million mapped reads, Log2FC- log2 fold change, FDR- false discovery rate. Originally mapped DEGs, which are currently no more available or show a different Ensembl ID , are reported separetely at the end of the table.

Gene	Ensembl ID	SH-pcDNA3	SH-p.M57Nfs*45		
		FPKM	FPKM	Log_2FC	FDR (q-value)
ADRB2	ENSG00000169252	1,06	0,49	-1,115	4,87E-02
ANKRD33	ENSG00000167612	0,72	1,64	1,180	2,41E-02
ANO9	ENSG00000185101	2,67	0,45	-2,560	5,81E-03
APCDD1L	ENSG00000198768	0,92	0,38	-1,285	1,49E-02
APOE	ENSG00000130203	3,15	1,57	-1,004	3,81E-02
ARSD	ENSG00000006756	8,58	0,73	-3,553	7,79E-04
ASB9	ENSG00000102048	1,56	0,30	-2,368	7,79E-04
ASF1B	ENSG00000105011	3,40	1,62	-1,068	1,21E-02
ATP1B1	ENSG00000143153	240,14	579,29	1,270	7,79E-04
BCHE	ENSG00000114200	0,15	6,07	5,385	7,79E-04
BIRC3	ENSG00000023445	4,18	0,59	-2,828	7,79E-04
BNIPL	ENSG00000163141	0,36	1,27	1,834	2,92E-02
C11orf53	ENSG00000150750	0,61	1,78	1,557	1,17E-02
C21orf90	ENSG00000182912	19,20	9,59	-1,002	1,53E-02
CA10	ENSG00000154975	0,70	0,21	-1,701	3,81E-02
CACNA2D3	ENSG00000157445	1,86	0,60	-1,633	4,76E-02
CACNG1	ENSG00000108878	0,76	1,97	1,380	9,07E-03
CALCA	ENSG00000110680	3,89	0,38	-3,359	3,09E-02
CARTPT	ENSG00000164326	31,89	12,89	-1,306	7,79E-04
CCDC144A	ENSG00000170160	0,32	1,30	2,035	7,79E-04
CCDC160	ENSG00000203952	0,65	0,21	-1,634	3,15E-02
CCL2	ENSG00000108691	103,39	6,93	-3,899	7,79E-04
CCNO	ENSG00000152669	2,25	0,14	-4,006	2,08E-03
CD36	ENSG00000135218	0,20	0,50	1,351	3,78E-02
CD74	ENSG00000019582	0,85	0,32	-1,419	2,06E-02
CD99	ENSG00000002586	93,99	39,29	-1,259	7,79E-04
CDC45	ENSG00000093009	4,11	1,85	-1,154	2,48E-02
CDC6	ENSG00000094804	4,36	1,95	-1,157	7,79E-04
CDH20	ENSG00000101542	1,01	0,31	-1,705	3,77E-03
CDH4	ENSG00000179242	0,53	0,23	-1,225	2,17E-02
CDKAL1	ENSG00000145996	23,65	7,69	-1,621	7,79E-04
CGA	ENSG00000135346	2,18	0,64	-1,768	2,55E-02
CGNL1	ENSG00000128849	1,13	0,41	-1,470	7,79E-04
CHGA	ENSG00000100604	316,63	156,93	-1,013	7,79E-04
CHST1	ENSG00000175264	4,84	2,18	-1,152	7,79E-04
CILP	ENSG00000138615	1,38	0,52	-1,401	7,79E-04
CNTN2	ENSG00000184144	4,67	1,28	-1,872	7,79E-04
CNTN6	ENSG00000134115	1,27	0,57	-1,158	4,41E-02
CNTNAP2	ENSG00000174469	1,71	0,31	-2,468	7,79E-04
COBL	ENSG00000106078	1,43	0,68	-1,069	1,12E-02
COL17A1	ENSG00000065618	1,60	0,50	-1,682	1,17E-02
COLCA2	ENSG00000214290	1,84	4,03	1,134	2,69E-02
COTL1	ENSG00000103187	7,95	2,90	-1,452	7,79E-04
CRISPLD2	ENSG00000103196	0,57	0,23	-1,282	3,66E-02
CXCL12	ENSG00000107562	3,10	0,23	-3,780	7,79E-04
CYB5R2	ENSG00000166394	1,32	0,46	-1,512	2,45E-02
CYR61	ENSG00000142871	3,26	6,56	1,008	3,23E-03
DDC	ENSG00000132437	71,24	35,60	-1,001	7,79E-04
DHRS2	ENSG00000100867	4,88	2,10	-1,212	5,32E-03

DNER	ENSG00000187957	15,97	6,62	-1,271	7,79E-04
DOK4	ENSG00000125170	100,78	43,05	-1,227	7,79E-04
DPP6	ENSG00000130226	8,14	3,02	-1,432	7,79E-04
DPT	ENSG00000143196	2,09	23,28	3,475	7,79E-04
DTL	ENSG00000143476	5,28	2,36	-1,159	4,93E-02
E2F1	ENSG00000101412	8,93	3,96	-1,173	7,79E-04
E2F2	ENSG00000007968	2,60	1,29	-1,008	5,32E-03
EBI3	ENSG00000105246	0,86	0,10	-3,082	2,38E-02
EDIL3	ENSG00000164176	40,81	15,80	-1,369	7,79E-04
EDNRA	ENSG00000151617	2,99	11,13	1,895	7,79E-04
EGFLAM	ENSG00000164318	0,98	0,17	-2,518	7,79E-04
EGR1	ENSG00000120738	54,88	8,39	-2,709	7,79E-04
EGR2	ENSG00000122877	0,58	0,21	-1,511	1,21E-02
ELFN1	ENSG00000225968	2,18	5,01	1,197	7,79E-04
EPB41L4B	ENSG00000095203	2,60	1,27	-1,036	6,77E-03
EVC2	ENSG00000173040	0,59	0,29	-1,021	2,31E-02
FAM111B	ENSG00000189057	1,99	0,74	-1,428	2,08E-03
FAM30A	ENSG00000226777	11,52	2,75	-2,066	7,79E-04
FAM92B	ENSG00000153789	1,13	0,34	-1,741	3,77E-03
FBP1	ENSG00000165140	6,85	2,70	-1,345	7,79E-04
FGF19	ENSG00000162344	0,58	1,65	1,519	7,79E-04
FOS	ENSG00000170345	12,06	3,85	-1,646	7,79E-04
GBX2	ENSG00000168505	0,53	2,09	1,987	3,47E-02
GFRA2	ENSG00000168546	1,38	0,41	-1,764	7,79E-04
GPR1	ENSG00000183671	1,37	3,93	1,519	1,41E-02
GPX8	ENSG00000164294	2,49	0,06	-5,424	7,79E-04
GREM2	ENSG00000180875	0,71	0,19	-1,908	7,79E-04
GRIK4	ENSG00000149403	0,35	1,33	1,946	7,79E-04
GYG2	ENSG00000056998	1,34	0,13	-3,369	7,79E-04
HES2	ENSG00000069812	2,86	0,65	-2,144	2,08E-03
HGF	ENSG00000019991	13,55	2,69	-2,332	7,79E-04
HIST1H4H	ENSG00000158406	1,65	0,18	-3,160	1,25E-02
HRK	ENSG00000135116	0,40	0,96	1,259	1,95E-02
HS6ST3	ENSG00000185352	0,48	1,29	1,438	3,23E-03
HTRA3	ENSG00000170801	0,53	0,11	-2,298	7,25E-03
IER3	ENSG00000137331	2,47	0,92	-1,430	4,81E-03
IFI44	ENSG00000137965	3,94	1,56	-1,335	1,65E-02
IGDCC3	ENSG00000174498	1,32	0,27	-2,281	7,79E-04
IGF2	ENSG00000167244	315,05	151,59	-1,055	7,79E-04
IGFBP5	ENSG00000115461	5,53	11,54	1,062	7,79E-04
IL13RA2	ENSG00000123496	17,90	6,82	-1,391	7,79E-04
IL32	ENSG00000008517	23,76	2,69	-3,145	7,79E-04
IL34	ENSG00000157368	1,27	0,43	-1,559	1,83E-02
INSC	ENSG00000188487	1,20	0,44	-1,450	1,21E-02
KCNJ2	ENSG00000123700	2,14	0,72	-1,562	7,79E-04
KCNJ9	ENSG00000162728	1,19	0,57	-1,047	1,08E-02
KLHDC8A	ENSG00000162873	0,83	0,35	-1,247	3,81E-02
KRT18	ENSG00000111057	0,98	0,33	-1,562	4,81E-03
KRT80	ENSG00000167767	1,35	0,66	-1,037	1,65E-02
LINGO4	ENSG00000213171	0,61	0,12	-2,304	1,87E-02
LRRC10B	ENSG00000204950	5,24	2,36	-1,149	7,79E-04
LRRN2	ENSG00000170382	3,43	0,84	-2,028	7,79E-04
LRRN3	ENSG00000173114	6,46	1,95	-1,725	3,25E-02
MAB21L2	ENSG00000181541	7,96	1,03	-2,945	4,30E-03
MAGEA10	ENSG00000124260	12,25	4,88	-1,329	7,79E-04
MAGEC2	ENSG00000046774	0,87	2,54	1,546	7,79E-04
MAP1LC3C	ENSG00000197769	0,79	1,85	1,231	3,78E-02
MB	ENSG00000198125	0,89	0,29	-1,618	9,94E-03
MBNL2	ENSG00000139793	14,93	31,44	1,074	4,30E-03
MBP	ENSG00000197971	1,35	0,10	-3,798	7,79E-04
MCM10	ENSG00000065328	2,70	1,13	-1,262	7,79E-04

MCTP2	ENSG00000140563	1,99	0,84	-1,236	1,17E-02
MDGA1	ENSG00000112139	0,55	1,52	1,465	2,41E-02
MGST1	ENSG00000008394	1,53	0,17	-3,153	7,79E-04
MICAL2	ENSG00000133816	1,92	0,90	-1,095	1,37E-02
MKRN3	ENSG00000179455	2,27	4,88	1,104	1,72E-02
MSN	ENSG00000147065	6,13	0,58	-3,413	7,79E-04
MT1F	ENSG00000198417	3,04	0,96	-1,667	1,29E-02
NDN	ENSG00000182636	0,17	2,40	3,782	7,79E-04
NEDD9	ENSG00000111859	3,85	0,90	-2,100	7,79E-04
NELL2	ENSG00000184613	22,44	9,79	-1,197	7,79E-04
NFASC	ENSG00000163531	30,40	11,56	-1,395	7,79E-04
NRXN3	ENSG00000021645	2,53	0,72	-1,818	2,08E-03
NTNG2	ENSG00000196358	2,26	5,25	1,213	3,85E-02
NXPH4	ENSG00000182379	2,35	1,02	-1,208	1,45E-02
NXT2	ENSG00000101888	3,58	11,71	1,710	7,79E-04
OAF	ENSG00000184232	1,17	2,70	1,202	2,95E-02
OAS1	ENSG00000089127	4,75	2,26	-1,073	1,72E-02
ODAM	ENSG00000109205	4,58	0,52	-3,148	7,79E-04
OLFML1	ENSG00000183801	2,25	0,37	-2,604	1,04E-02
ORC1	ENSG00000085840	0,96	0,44	-1,113	2,13E-02
OSCAR	ENSG00000170909	0,27	1,52	2,486	7,79E-04
OTOR	ENSG00000125879	3,26	1,59	-1,042	3,85E-02
P2RY6	ENSG00000171631	0,99	0,28	-1,796	2,41E-02
PCDH17	ENSG00000118946	0,95	0,41	-1,213	2,08E-03
PCDHB2	ENSG00000112852	4,41	1,39	-1,668	7,79E-04
PHLDA1	ENSG00000139289	9,05	3,85	-1,234	7,79E-04
POLQ	ENSG00000051341	1,22	0,48	-1,339	2,10E-02
PPP4R4	ENSG00000119698	1,19	0,28	-2,070	2,08E-03
PPT1	ENSG00000131238	49,89	4312,73	6,434	7,79E-04
PQLC2L	ENSG00000174899	1,33	0,00	-Infinity	7,79E-04
PROKR2	ENSG00000101292	6,59	13,98	1,084	7,79E-04
PRPH	ENSG00000135406	15,17	2,46	-2,626	7,79E-04
PRR16	ENSG00000184838	8,37	3,82	-1,133	8,62E-03
PRSS8	ENSG00000052344	1,27	0,35	-1,850	2,66E-03
PTGER3	ENSG00000050628	1,61	0,59	-1,439	7,79E-04
QPCT	ENSG00000115828	0,66	1,57	1,257	2,62E-02
RASGEF1A	ENSG00000198915	0,46	0,14	-1,710	4,61E-02
RASL10A	ENSG00000100276	2,78	1,09	-1,356	6,29E-03
RDH16	ENSG00000139547	0,33	0,82	1,297	1,33E-02
RELB	ENSG00000104856	5,28	2,53	-1,061	5,81E-03
RERG	ENSG00000134533	0,68	0,09	-2,894	4,20E-02
RETREG1	ENSG00000154153	5,02	2,35	-1,097	1,45E-03
RGS13	ENSG00000127074	1,55	0,48	-1,687	1,69E-02
RINL	ENSG00000187994	2,75	1,10	-1,314	8,62E-03
RND1	ENSG00000172602	2,01	0,93	-1,119	2,10E-02
RRM2	ENSG00000171848	17,79	7,03	-1,339	2,08E-03
RSPH4A	ENSG00000111834	0,63	0,20	-1,677	6,77E-03
RSPO4	ENSG00000101282	2,82	1,19	-1,239	1,25E-02
S100A10	ENSG00000197747	26,15	10,70	-1,290	7,79E-04
SALL1	ENSG00000103449	1,11	0,20	-2,460	1,04E-02
SAMD9L	ENSG00000177409	0,94	0,42	-1,169	3,19E-02
SCML4	ENSG00000146285	1,86	0,53	-1,799	1,45E-03
SEPT7L	ENSG00000120555	1,03	2,55	1,308	2,75E-02
SERPINA5	ENSG00000188488	21,33	7,89	-1,436	7,79E-04
SERPINE2	ENSG00000135919	0,80	0,17	-2,198	9,07E-03
SH3TC2	ENSG00000169247	0,64	0,08	-3,022	7,79E-04
SHCBP1	ENSG00000171241	2,10	0,97	-1,113	4,23E-02
SLC12A8	ENSG00000221955	0,97	0,22	-2,156	2,85E-02
SLC18A1	ENSG00000036565	152,76	70,67	-1,112	7,79E-04
SLC24A2	ENSG00000155886	0,97	0,40	-1,278	1,53E-02
SLC35F3	ENSG00000183780	3,32	1,48	-1,165	2,66E-03

SLC7A8	ENSG00000092068	0,82	0,15	-2,429	1,45E-03
SLIT2	ENSG00000145147	5,93	14,74	1,315	7,79E-04
SMOC1	ENSG00000198732	0,44	2,49	2,514	6,77E-03
SNCAIP	ENSG00000064692	0,32	1,25	1,988	7,79E-04
SOX6	ENSG00000110693	1,53	0,35	-2,108	3,97E-02
SOX9	ENSG00000125398	5,79	2,78	-1,058	7,79E-04
SPAG6	ENSG00000077327	2,09	5,81	1,472	7,79E-04
SPP1	ENSG00000118785	3,11	0,99	-1,657	2,08E-03
ST6GAL1	ENSG00000073849	8,29	3,97	-1,062	7,79E-04
ST8SIA2	ENSG00000140557	7,40	3,01	-1,295	7,79E-04
STAT4	ENSG00000138378	1,36	2,81	1,046	2,34E-02
STUM	ENSG00000203685	2,95	1,18	-1,321	7,79E-04
SV2B	ENSG00000185518	0,51	0,15	-1,722	1,04E-02
SYT13	ENSG00000019505	6,10	2,84	-1,103	7,79E-04
T	ENSG00000164458	0,98	0,47	-1,070	4,67E-02
TACC2	ENSG00000138162	5,53	2,13	-1,374	7,72E-03
TBX18	ENSG00000112837	1,93	0,69	-1,490	7,79E-04
TIMP1	ENSG00000102265	37,25	5,92	-2,654	1,72E-02
TK1	ENSG00000167900	6,50	2,68	-1,278	2,08E-03
TMEM105	ENSG00000185332	0,45	1,37	1,601	4,73E-02
TMEM255A	ENSG00000125355	3,88	1,88	-1,047	5,32E-03
TNF	ENSG00000232810	0,94	0,05	-4,132	2,41E-02
TNFAIP6	ENSG00000123610	1,96	4,68	1,253	3,77E-03
TNFRSF9	ENSG00000049249	6,45	0,50	-3,701	7,79E-04
TNR	ENSG00000116147	3,92	8,54	1,123	7,79E-04
TRAF1	ENSG00000056558	0,50	0,13	-1,969	7,79E-04
UNC5D	ENSG00000156687	2,67	6,38	1,258	7,79E-04
VAMP5	ENSG00000168899	1,16	6,07	2,393	7,79E-04
VPS13D	ENSG00000048707	9,53	19,86	1,059	7,79E-04
WFDC3	ENSG00000124116	0,16	0,55	1,759	3,19E-02
ZC3H12B	ENSG00000102053	0,43	0,86	1,000	1,80E-02
ZDHHC15	ENSG00000102383	0,16	4,23	4,682	7,79E-04
ZNF385D	ENSG00000151789	1,47	0,44	-1,727	5,32E-03
ZNF662	ENSG00000182983	0,05	4,03	6,384	1,12E-02
ZNF676	ENSG00000196109	0,07	0,72	3,292	4,30E-03

Legend: Sequences which have changed the original Ensembl ID (in green) or have been retired (n/a, in red).

Gene	Ensembl ID	SH-pcDNA3	SH-p.M57Nfs*45		
		FPKM	FPKM	Log_2FC	FDR (q-value)
RPS17	ENSG00000184779 (n/a)	0,16	0,65	2,066	2,02E-02
PCDHB16	ENSG00000196963 (n/a)	0,96	3,07	1,675	7,79E-04
AC012215.1	ENSG00000233863 (n/a)	1,33	4,08	1,615	3,47E-02
GABRQ	ENSG00000147402 (n/a)	1,48	0,53	-1,476	7,79E-04
ZNF229	ENSG00000167383 (n/a)	2,85	0,41	-2,783	1,53E-02

Table S5 *Palmitoylation survey of DEGs identified in SH-p.wtCLN1 transcriptomic profile.*

Legend: Gene- Gene Symbol, Ensembl ID- ENSEMBL unique gene identifier, Uniprot ID- Uniprot unique protein identifier, Description- Gene Description, Log2FC- log2 fold change, red- upregulated, green- downregulated, n.c.- expression not changed (considering both |log2FC|>1 and q-value<0.05 thresholds), l- enclosed in the database.

						Palmitoylated Proteins Databases		
			Log2FC (versus SH-pcDNA3)			Curated Sanders' database	SwissPalm	SwissPalm (Predicted)
Gene	Ensembl ID	Uniprot ID	SH-p.wtCLN1	SH-p.L222P	SH-p.M57Nfs*45			
AARS	ENSG00000090861	SYAC_HUMAN	1,07	n.c.	n.c.	●	●	
ABLIM2	ENSG00000163995	ABLM2_HUMAN	-1,19	n.c.	n.c.	●		●
ADORA1	ENSG00000163485	AA1R_HUMAN	-1,80	n.c.	n.c.		●	
AHNAK2	ENSG00000185567	AHNK2_HUMAN	-1,04	n.c.	n.c.	●	●	●
ALPL	ENSG00000162551	PPBT_HUMAN	-2,49	n.c.	n.c.	●		●
ARFGAP1	ENSG00000101199	ARFG1_HUMAN	1,30	n.c.	n.c.	●		●
ASTN1	ENSG00000152092	ASTN1_HUMAN	-1,37	n.c.	n.c.	●		●
BASP1	ENSG00000176788	BASP1_HUMAN	-1,56	n.c.	n.c.		●	
BCAM	ENSG00000187244	BCAM_HUMAN	1,04	n.c.	n.c.	●	●	●
CD7	ENSG00000173762	CD7_HUMAN	2,08	n.c.	n.c.		●	
CD9	ENSG00000010278	HUMAN; G8JLH6_H	1,04	n.c.	n.c.	●	●	●
CDK1	ENSG00000170312	CDK1_HUMAN	-1,05	n.c.	n.c.	●	●	
CDKAL1	ENSG00000145996	CDKAL_HUMAN	-1,02	n.c.	-1,62	●	●	●
CKB	ENSG00000166165	KCRB_HUMAN	-1,28	n.c.	n.c.	●		
CLDN5	ENSG00000184113	CLD5_HUMAN	-1,44	n.c.	n.c.	●	●	●
CNR1	ENSG00000118432	CNR1_HUMAN	-2,83	-1,48	n.c.	●	●	●
CNTFR	ENSG00000122756	CNTFR_HUMAN	-1,50	-1,09	n.c.	●		●
COL17A1	ENSG00000065618	COHA1_HUMAN	2,87	1,89	-1,68		●	●
COL4A2	ENSG00000134871	CO4A2_HUMAN	-1,49	n.c.	n.c.	●	●	●
COTL1	ENSG00000103187	COTL1_HUMAN	-2,35	n.c.	-1,45	●	●	
CRMP1	ENSG00000072832	DPYL1_HUMAN	-1,27	n.c.	n.c.	●		
CSRP1	ENSG00000159176	CSRP1_HUMAN	-1,16	n.c.	n.c.		●	●
CTSD	ENSG00000117984	CATD_HUMAN	1,14	n.c.	n.c.	●	●	●
CYBRD1	ENSG00000071967	CYBR1_HUMAN	1,41	n.c.	n.c.		●	●
DCLK1	ENSG00000133083	DCLK1_HUMAN	-1,07	n.c.	n.c.		●	●
DLG2	ENSG00000150672	DLG2_HUMAN	-1,28	-1,19	n.c.	●		●
DLGAP3	ENSG00000116544	DLGP3_HUMAN	-1,01	n.c.	n.c.		●	●
DRD2	ENSG00000149295	DRD2_HUMAN	-1,00	n.c.	n.c.		●	
EDNRA	ENSG00000151617	EDNRA_HUMAN	-1,92	-2,76	1,89		●	●
EDNRB	ENSG00000136160	EDNRB_HUMAN	3,01	n.c.	n.c.		●	●
EEF1D	ENSG00000104529	EF1D_HUMAN	1,36	n.c.	n.c.	●	●	●

F3	ENSG00000117525	TF_HUMAN	**1,16**	n.c.	n.c.	●	●	
FLNC	ENSG00000128591	FLNC_HUMAN	**1,35**	n.c.	n.c.		●	
GAP43	ENSG00000172020	NEUM_HUMAN	**-1,13**	n.c.	n.c.	●	●	●
GPR68	ENSG00000119714	OGR1_HUMAN	**-1,55**	n.c.	n.c.		●	●
GPX8	ENSG00000164294	GPX8_HUMAN	**-4,84**	n.c.	**-5,42**	●	●	●
H2AFX	ENSG00000188486	H2AX_HUMAN	**-1,02**	n.c.	n.c.	●	●	
H3F3B	ENSG00000132475	H33_HUMAN	**1,35**	n.c.	n.c.	●	●	
HIST1H1C	ENSG00000187837	H12_HUMAN	**1,92**	n.c.	n.c.		●	
HIST1H4H	ENSG00000158406	H4_HUMAN	**-2,76**	**-2,00**	**-3,16**		●	
HIST2H2BE	ENSG00000184678	H2B2E_HUMAN	**1,18**	n.c.	n.c.		●	
HIST3H2A	ENSG00000181218	H2A3_HUMAN	**1,77**	n.c.	n.c.		●	
HLA-B	ENSG00000234745	]; 1B47_HUMAN; 1[	**-2,39**	n.c.	n.c.		●	●
IL32	ENSG00000008517	IL32_HUMAN	**-2,12**	**-3,73**	**-3,15**		●	●
INA	ENSG00000148798	AINX_HUMAN	**-1,21**	n.c.	n.c.	●	●	●
INPP5F	ENSG00000198825	SAC2_HUMAN	**-1,05**	n.c.	n.c.	●	●	●
ITM2A	ENSG00000078596	ITM2A_HUMAN	**-1,31**	**-1,72**	n.c.		●	
KBTBD11	ENSG00000176595	KBTBB_HUMAN	**2,31**	n.c.	n.c.		●	●
KIF11	ENSG00000138160	KIF11_HUMAN	**-1,27**	n.c.	n.c.		●	●
LAMA4	ENSG00000112769	LAMA4_HUMAN	**-2,45**	**-1,15**	n.c.	●	●	●
LCP1	ENSG00000136167	PLSL_HUMAN	**-2,41**	**-1,42**	n.c.	●	●	
LGI3	ENSG00000168481	LGI3_HUMAN	**-1,09**	n.c.	n.c.	●		●
LRRC32	ENSG00000137507	LRC32_HUMAN	**-2,19**	**-1,99**	n.c.	●	●	●
MAD2L1	ENSG00000164109	MD2L1_HUMAN	**-1,14**	n.c.	n.c.		●	
MAOB	ENSG00000069535	AOFB_HUMAN	**-1,57**	n.c.	n.c.	●		●
MICB	ENSG00000204516	MICB_HUMAN	**-3,12**	**-1,78**	n.c.		●	●
MKI67	ENSG00000148773	KI67_HUMAN	**-1,51**	n.c.	n.c.	●	●	
NDRG1	ENSG00000104419	NDRG1_HUMAN	**1,45**	n.c.	n.c.		●	●
NEFH	ENSG00000100285	NFH_HUMAN	**-1,48**	n.c.	n.c.		●	
NEFM	ENSG00000104722	NFM_HUMAN	**-1,74**	n.c.	n.c.	●	●	
NELL1	ENSG00000165973	NELL1_HUMAN	**-1,11**	n.c.	n.c.		●	●
NOL6	ENSG00000165271	NOL6_HUMAN	**1,00**	n.c.	n.c.		●	
NRCAM	ENSG00000091129	NRCAM_HUMAN	**-1,17**	n.c.	n.c.	●	●	●
NRXN1	ENSG00000179915	NRX1A_HUMAN	**-1,35**	n.c.	n.c.		●	●
NT5E	ENSG00000135318	5NTD_HUMAN	**-2,46**	**-1,12**	n.c.		●	●
NTM	ENSG00000182667	NTRI_HUMAN	**-2,43**	n.c.	n.c.	●		●
OPRM1	ENSG00000112038	OPRM_HUMAN	**-1,66**	n.c.	n.c.		●	●
PAPSS2	ENSG00000198682	PAPS2_HUMAN	**-1,14**	n.c.	n.c.		●	
PCDH17	ENSG00000118946	PCD17_HUMAN	**-1,33**	**-1,08**	**-1,21**	●	●	●
PCDH9	ENSG00000184226	PCDH9_HUMAN	**-3,44**	n.c.	n.c.	●		●
PCNA	ENSG00000132646	PCNA_HUMAN	**-1,44**	n.c.	n.c.	●	●	
PDCD4	ENSG00000150593	PDCD4_HUMAN	**1,15**	n.c.	n.c.		●	
PHYHIPL	ENSG00000165443	PHIPL_HUMAN	**-1,45**	n.c.	n.c.	●		●
PKP2	ENSG00000057294	PKP2_HUMAN	**1,17**	n.c.	n.c.		●	
PLAUR	ENSG00000011422	UPAR_HUMAN	**-1,02**	n.c.	n.c.		●	●

PPT1	ENSG00000131238	PPT1_HUMAN	**7,23**	**7,96**	**6,43**		●	●
PRKCA	ENSG00000154229	KPCA_HUMAN	**-1,45**	**-1,53**	n.c.	●	●	●
PRNP	ENSG00000171867	)_HUMAN; PRIO_H	**-1,12**	n.c.	n.c.		●	●
RALGAPA2	ENSG00000188559	RGPA2_HUMAN	**-1,03**	n.c.	n.c.	●	●	●
RGMA	ENSG00000182175	RGMA_HUMAN	**-1,38**	**-1,02**	n.c.	●		●
RGS2	ENSG00000116741	RGS2_HUMAN	**-1,83**	**-1,13**	n.c.		●	●
RGS3	ENSG00000138835	RGS3_HUMAN	**-1,04**	n.c.	n.c.		●	●
RGS4	ENSG00000117152	RGS4_HUMAN	**1,96**	n.c.	n.c.		●	●
RHBDF1	ENSG00000007384	RHDF1_HUMAN	**1,06**	n.c.	n.c.		●	●
RPH3A	ENSG00000089169	RP3A_HUMAN	**-1,86**	n.c.	n.c.		●	
S100A10	ENSG00000197747	S10AA_HUMAN	**-2,61**	n.c.	**-1,29**		●	
SAFB2	ENSG00000130254	SAFB2_HUMAN	**1,29**	n.c.	n.c.		●	
SCML4	ENSG00000146285	SCML4_HUMAN	**-1,10**	**-1,40**	**-1,80**		●	●
SEZ6L	ENSG00000100095	SE6L1_HUMAN	**-1,15**	n.c.	n.c.	●		●
SFT2D1	ENSG00000198818	SFT2A_HUMAN	**1,09**	n.c.	n.c.	●	●	●
SLC2A6	ENSG00000160326	GTR6_HUMAN	**-1,09**	n.c.	n.c.	●	●	●
SLC44A2	ENSG00000129353	CTL2_HUMAN	**1,31**	n.c.	n.c.	●	●	●
SMPD3	ENSG00000103056	NSMA2_HUMAN	**-1,48**	n.c.	n.c.	●	●	●
SNAP25	ENSG00000132639	SNP25_HUMAN	**-1,15**	n.c.	n.c.	●	●	●
SNAP91	ENSG00000065609	AP180_HUMAN	**-1,18**	n.c.	n.c.	●	●	
STS	ENSG00000101846	STS_HUMAN	**-1,15**	n.c.	n.c.		●	●
SYPL1	ENSG00000008282	SYPL1_HUMAN	**1,14**	n.c.	n.c.		●	
SYT13	ENSG00000019505	SYT13_HUMAN	**-2,54**	**-1,19**	**-1,10**	●		
TF	ENSG00000091513	TRFE_HUMAN	**1,46**	n.c.	n.c.		●	●
TGFA	ENSG00000163235	TGFA_HUMAN	**-1,34**	n.c.	n.c.		●	●
TGM2	ENSG00000198959	TGM2_HUMAN	**-2,67**	n.c.	n.c.		●	●
THY1	ENSG00000154096	THY1_HUMAN	**-1,16**	n.c.	n.c.	●	●	
TLR2	ENSG00000137462	TLR2_HUMAN	**-2,46**	n.c.	n.c.		●	●
TM4SF1	ENSG00000169908	T4S1_HUMAN	**3,46**	**2,20**	n.c.	●	●	●
TNF	ENSG00000232810	TNFA_HUMAN	**-3,20**	n.c.	**-4,13**		●	
TNR	ENSG00000116147	TENR_HUMAN	**-1,21**	n.c.	**1,12**	●	●	●
TOP2A	ENSG00000131747	TOP2A_HUMAN	**-1,08**	n.c.	n.c.		●	
TPM1	ENSG00000140416	TPM1_HUMAN	**1,05**	n.c.	n.c.		●	●
TUBB4A	ENSG00000104833	TBB4A_HUMAN	**-1,50**	n.c.	n.c.		●	●
UBE2T	ENSG00000077152	UBE2T_HUMAN	**-1,15**	n.c.	n.c.	●	●	●
UFL1	ENSG00000014123	UFL1_HUMAN	**1,38**	n.c.	n.c.		●	
VASN	ENSG00000168140	VASN_HUMAN	**1,62**	n.c.	n.c.		●	●
VCAN	ENSG00000038427	CSPG2_HUMAN	**-1,95**	**-1,67**	n.c.	●	●	●

Table S6 *Palmitoylation survey of DEGs identified in SH-p.L222P transcriptomic profile.*

Legend: Gene- Gene Symbol, Ensembl ID- ENSEMBL unique gene identifier, Uniprot ID- Uniprot unique protein identifier, Description- Gene Description, Log2FC- log2 fold change, red- upregulated, green- downregulated, n.c.- expression not changed (considering both |log2FC|>1 and q-value<0.05 thresholds), l- enclosed in the database.

						Palmitoylated Proteins Databases		
			Log2FC (versus SH-pcDNA3)			Curated Sanders' database	SwissPalm	SwissPalm (Predicted)
Gene	Ensembl ID	Uniprot ID	SH-p.wtCLN1	SH-p.L222P	SH-p.M57Nfs*45			
ACOT2	ENSG00000119673	ACOT2_HUMAN	n.c.	-1,17	n.c.		●	●
CD44	ENSG00000026508	CD44_HUMAN	n.c.	-2,23	n.c.	●	●	
CD99	ENSG00000002586	CD99_HUMAN	n.c.	-1,63	-1,26	●	●	
CHRM2	ENSG00000181072	ACM2_HUMAN	n.c.	-1,62	n.c.		●	●
CNR1	ENSG00000118432	CNR1_HUMAN	-2,83	-1,48	n.c.	●	●	●
CNTFR	ENSG00000122756	CNTFR_HUMAN	-1,50	-1,09	n.c.	●		●
COL17A1	ENSG00000065618	COHA1_HUMAN	2,87	1,89	-1,68		●	●
CPS1	ENSG00000021826	CPSM_HUMAN	n.c.	-2,22	n.c.	●	●	
DLG2	ENSG00000150672	DLG2_HUMAN	-1,28	-1,19	n.c.	●		●
EDNRA	ENSG00000151617	EDNRA_HUMAN	-1,92	-2,76	1,89		●	●
HIST1H4H	ENSG00000158406	H4_HUMAN	-2,76	-2,00	-3,16		●	
IL32	ENSG00000008517	IL32_HUMAN	-2,12	-3,73	-3,15		●	●
ITM2A	ENSG00000078596	ITM2A_HUMAN	-1,31	-1,72	n.c.		●	
LAMA4	ENSG00000112769	LAMA4_HUMAN	-2,45	-1,15	n.c.	●	●	●
LCP1	ENSG00000136167	PLSL_HUMAN	-2,41	-1,42	n.c.	●	●	
LRRC32	ENSG00000137507	LRC32_HUMAN	-2,19	-1,99	n.c.	●	●	●
MBP	ENSG00000197971	MBP_HUMAN	n.c.	-1,59	-3,80	●	●	
MICB	ENSG00000204516	MICB_HUMAN	-3,12	-1,78	n.c.		●	●
MSN	ENSG00000147065	MOES_HUMAN	n.c.	-5,78	-3,41	●	●	
NT5E	ENSG00000135318	5NTD_HUMAN	-2,46	-1,12	n.c.		●	●
PCDH17	ENSG00000118946	PCD17_HUMAN	-1,33	-1,08	-1,21	●	●	●
PPT1	ENSG00000131238	PPT1_HUMAN	7,23	7,96	6,43		●	●
PRKCA	ENSG00000154229	KPCA_HUMAN	-1,45	-1,53	n.c.	●	●	●
PRPH	ENSG00000135406	PERI_HUMAN	n.c.	-1,92	-2,63	●	●	
PTGIR	ENSG00000160013	PI2R_HUMAN	n.c.	-1,86	n.c.	●	●	●
RAB38	ENSG00000123892	RAB38_HUMAN	n.c.	-1,63	n.c.	●	●	●
RGMA	ENSG00000182175	RGMA_HUMAN	-1,38	-1,02	n.c.	●		●
RGS2	ENSG00000116741	RGS2_HUMAN	-1,83	-1,13	n.c.		●	●

SCML4	ENSG00000146285	SCML4_HUMAN	**-1,10**	**-1,40**	**-1,80**		●	●
SLC18A1	ENSG00000036565	VMAT1_HUMAN	n.c.	**1,00**	**-1,11**	●		●
SLC32A1	ENSG00000101438	VIAAT_HUMAN	n.c.	**1,05**	n.c.	●		●
SLC7A5	ENSG00000103257	LAT1_HUMAN	n.c.	**1,01**	n.c.		●	●
SLC7A8	ENSG00000092068	LAT2_HUMAN	n.c.	**-3,67**	**-2,43**		●	●
SLC8A1	ENSG00000183023	NAC1_HUMAN	n.c.	**-1,74**	n.c.	●		●
SYT13	ENSG00000019505	SYT13_HUMAN	**-2,54**	**-1,19**	**-1,10**	●		
TM4SF1	ENSG00000169908	T4S1_HUMAN	**3,46**	**2,20**	n.c.	●	●	●
VAMP5	ENSG00000168899	VAMP5_HUMAN	n.c.	**2,17**	**2,39**	●	●	●
VCAN	ENSG00000038427	CSPG2_HUMAN	**-1,95**	**-1,67**	n.c.	●	●	●

Table S7 *Palmitoylation survey of DEGs identified in SH-p.M57Nfs*45 transcriptomic profile.*

Legend: Gene- Gene Symbol, Ensembl ID- ENSEMBL unique gene identifier, Uniprot ID- Uniprot unique protein identifier, Description- Gene Description, Log2FC- log2 fold change, red- upregulated, green- downregulated, n.c.- expression not changed (considering both |log2FC|>1 and q-value<0.05 thresholds), l- enclosed in the database.

						Palmitoylated Proteins Databases		
			Log2FC (versus SH-pcDNA3)			Curated Sanders' database	SwissPalm	SwissPalm (Predicted)
Gene	Ensembl ID	Uniprot ID	SH-p.wtCLN1	SH-p.L222P	SH-p.M57Nfs*45			
ADRB2	ENSG00000169252	ADRB2_HUMAN	n.c.	n.c.	-1,11		●	●
APOE	ENSG00000130203	APOE_HUMAN	n.c.	n.c.	-1,00		●	●
ATP1B1	ENSG00000143153	AT1B1_HUMAN	n.c.	n.c.	1,27	●	●	
CD36	ENSG00000135218	CD36_HUMAN	n.c.	n.c.	1,35	●	●	●
CD99	ENSG00000002586	CD99_HUMAN	n.c.	-1,63	-1,26	●	●	
CDKAL1	ENSG00000145996	CDKAL_HUMAN	-1,02	n.c.	-1,62	●	●	●
CNTNAP2	ENSG00000174469	CNTP2_HUMAN	n.c.	n.c.	-2,47		●	●
COL17A1	ENSG00000065618	COHA1_HUMAN	2,87	1,89	-1,68		●	●
COTL1	ENSG00000103187	COTL1_HUMAN	-2,35	n.c.	-1,45	●	●	
DPP6	ENSG00000130226	DPP6_HUMAN	n.c.	n.c.	-1,43	●	●	
EDNRA	ENSG00000151617	EDNRA_HUMAN	-1,92	-2,76	1,89		●	●
GPX8	ENSG00000164294	GPX8_HUMAN	-4,84	n.c.	-5,42	●	●	●
HIST1H4H	ENSG00000158406	H4_HUMAN	-2,76	-2,00	-3,16		●	
CD74	ENSG00000019582	HG2A_HUMAN	n.c.	n.c.	-1,42	●	●	
IL32	ENSG00000008517	IL32_HUMAN	-2,12	-3,73	-3,15		●	●
KRT18	ENSG00000111057	K1C18_HUMAN	n.c.	n.c.	-1,56		●	
SLC7A8	ENSG00000092068	LAT2_HUMAN	n.c.	-3,67	-2,43		●	●
MBP	ENSG00000197971	MBP_HUMAN	n.c.	-1,59	-3,80	●	●	
MDGA1	ENSG00000112139	MDGA1_HUMAN	n.c.	n.c.	1,47	●		●
MGST1	ENSG00000008394	MGST1_HUMAN	n.c.	n.c.	-3,15		●	
MSN	ENSG00000147065	MOES_HUMAN	n.c.	-5,78	-3,41	●	●	
NFASC	ENSG00000163531	NFASC_HUMAN	n.c.	n.c.	-1,39	●	●	
PCDH17	ENSG00000118946	PCD17_HUMAN	-1,33	-1,08	-1,21	●	●	●
PRPH	ENSG00000135406	PERI_HUMAN	n.c.	-1,92	-2,63	●	●	
PPT1	ENSG00000131238	PPT1_HUMAN	7,23	7,96	6,43		●	●
PRSS8	ENSG00000052344	PRSS8_HUMAN	n.c.	n.c.	-1,85	●		
S100A10	ENSG00000197747	S10AA_HUMAN	-2,61	n.c.	-1,29		●	
SCML4	ENSG00000146285	SCML4_HUMAN	-1,10	-1,40	-1,80		●	●
STAT4	ENSG00000138378	STAT4_HUMAN	n.c.	n.c.	1,05	●		
STUM	ENSG00000203685	l_HUMAN; CA095_H	n.c.	n.c.	-1,32	●	●	●
SYT13	ENSG00000019505	SYT13_HUMAN	-2,54	-1,19	-1,10	●		
TNR	ENSG00000116147	TENR_HUMAN	-1,21	n.c.	1,12	●	●	●
TIMP1	ENSG00000102265	TIMP1_HUMAN	n.c.	n.c.	-2,65	●	●	
TNF	ENSG00000232810	TNFA_HUMAN	-3,20	n.c.	-4,13		●	
VAMP5	ENSG00000168899	VAMP5_HUMAN	n.c.	2,17	2,39	●	●	●
SLC18A1	ENSG00000036565	VMAT1_HUMAN	n.c.	1,00	-1,11	●		●

Table S8 *Bioinformatic categorization of DEGs identified in SH-p.wtCLN1 and encoding palmitoyated gene products.*

Legend: Gene- Gene Symbol, Description- Gene Description, Log2FC- log2 fold change, n.c.- expression not changed considering both |log2FC|>1 and q-value<0.05 thresholds, l- enclosed in the related bioinformatic category, grey outlines- DEGs specifically assigned to SH-p.wtCLN1 which were utilized to model the network of Figure 4B.

					Bioinformatic Categorization (Ingenuity Pathway Analisys)											Bioinformatic Categorization (Cellular Component GO Term)							
		Log2FC (versus SH-pcDNA3)			Cellular Development	Cellular Growth and Proliferation	Cell Morphology	Cell-To-Cell Signaling and Interaction	Cellular Assembly and Organization	Nervous System Development and Function		neuritogenesis	branching of neurites	branching of neurons	growth of neurites	Neuronal Part	Neuronal projection	Axon	Synapse	Synapse Part	Cell Projection	Neurofilament	Growth Cone
Gene	**Gene Description**	**SH-p.wtCLN1**	**SH-p.L222P**	**SH-p.M57Nfs*45**																			
AARS	alanyl-tRNA synthetase	1,07	n.c.	n.c.		●																	
ABLIM2	actin binding LIM protein family member 2	-1,19	n.c.	n.c.																			
ADORA1	adenosine A1 receptor	-1,80	n.c.	n.c.												●	●	●	●	●	●		
AHNAK2	AHNAK nucleoprotein 2	-1,04	n.c.	n.c.																			
ALPL	alkaline phosphatase, liver/bone/kidney	-2,49	n.c.	n.c.	●		●			●													
ARFGAP1	ADP ribosylation factor GTPase activating protein 1	1,30	n.c.	n.c.															●	●			
ASTN1	astrotactin 1	-1,37	n.c.	n.c.			●			●						●							
BASP1	brain abundant membrane attached signal protein 1	-1,56	n.c.	n.c.	●	●	●		●	●		●		●	●	●	●				●		●
BCAM	basal cell adhesion molecule (Lutheran blood group)	1,04	n.c.	n.c.																			
CD7	CD7 molecule	2,08	n.c.	n.c.				●															
CD9	CD9 molecule	1,04	n.c.	n.c.	●	●	●	●	●	●					●								
CDK1	cyclin dependent kinase 1	-1,05	n.c.	n.c.	●	●	●		●	●					●								
CDKAL1	CDK5 regulatory subunit associated protein 1 like 1	-1,02	n.c.	-1,62																			
CKB	creatine kinase B	-1,28	n.c.	n.c.	●	●	●		●	●		●				●	●				●		
CLDN5	claudin 5	-1,44	n.c.	n.c.												●	●	●			●		
CNR1	cannabinoid receptor 1	-2,83	-1,48	n.c.	●	●	●	●	●	●		●	●	●	●	●	●	●	●	●	●		●
CNTFR	ciliary neurotrophic factor receptor	-1,50	-1,09	n.c.	●	●	●	●		●													
COL17A1	collagen type XVII alpha 1 chain	2,87	1,89	-1,68			●																
COL4A2	collagen type IV alpha 2 chain	-1,49	n.c.	n.c.	●	●																	
COTL1	coactosin like F-actin binding protein 1	-2,35	n.c.	-1,45																			
CRMP1	collapsin response mediator protein 1	-1,27	n.c.	n.c.	●	●	●	●	●	●		●	●	●									
CSRP1	cysteine and glycine rich protein 1	-1,16	n.c.	n.c.	●	●	●		●	●		●	●	●	●								
CTSD	cathepsin D	1,14	n.c.	n.c.	●	●	●		●	●													
CYBRD1	cytochrome b reductase 1	1,41	n.c.	n.c.																	●		
DCLK1	doublecortin like kinase 1	-1,07	n.c.	n.c.	●	●	●	●	●	●		●			●				●	●			
DLG2	discs large MAGUK scaffold protein 2	-1,28	-1,19	n.c.				●		●						●	●	●	●	●	●		
DLGAP3	DLG associated protein 3	-1,01	n.c.	n.c.	●	●		●	●	●									●	●			
DRD2	dopamine receptor D2	-1,00	n.c.	n.c.	●	●	●	●	●	●		●	●	●		●	●	●	●	●	●		
EDNRA	endothelin receptor type A	-1,92	-2,76	1,89	●	●	●		●	●		●											
EDNRB	endothelin receptor type B	3,01	n.c.	n.c.	●	●	●			●													
EEF1D	eukaryotic translation elongation factor 1 delta	1,36	n.c.	n.c.	●	●																	
F3	coagulation factor III, tissue factor	1,16	n.c.	n.c.																			
FLNC	filamin C	1,35	n.c.	n.c.	●	●	●		●														
GAP43	growth associated protein 43	-1,13	n.c.	n.c.	●	●	●	●	●	●		●	●	●	●	●	●	●	●	●	●		●
GPR68	G protein-coupled receptor 68	-1,55	n.c.	n.c.	●																		
GPX8	glutathione peroxidase 8 (putative)	-4,84	n.c.	-5,42																			
H2AFX	H2A histone family member X	-1,02	n.c.	n.c.		●																	
H3F3B	H3 histone family member 3B	1,35	n.c.	n.c.	●	●	●																
HIST1H1C	histone cluster 1 H1 family member c	1,92	n.c.	n.c.																			
HIST1H4H	histone cluster 1 H4 family member h	-2,76	-2,00	-3,16	●																		
HIST2H2BE	histone cluster 2 H2B family member e	1,18	n.c.	n.c.																			
HIST3H2A	histone cluster 3 H2A	1,77	n.c.	n.c.																			
HLA-B	major histocompatibility complex, class I, B	-2,39	n.c.	n.c.																			
IL32	interleukin 32	-2,12	-3,73	-3,15	●	●	●	●															
INA	internexin neuronal intermediate filament protein alpha	-1,21	n.c.	n.c.					●													●	
INPP5F	inositol polyphosphate-5-phosphatase F	-1,05	n.c.	n.c.	●	●			●	●					●	●	●	●			●		
ITM2A	integral membrane protein 2A	-1,31	-1,72	n.c.																			
KBTBD11	kelch repeat and BTB domain containing 11	2,31	n.c.	n.c.																			
KIF11	kinesin family member 11	-1,27	n.c.	n.c.		●	●		●														
LAMA4	laminin subunit alpha 4	-2,45	-1,15	n.c.	●	●	●	●		●													
LCP1	lymphocyte cytosolic protein 1	-2,41	-1,42	n.c.	●	●	●		●												●		
LGI3	leucine rich repeat LGI family member 3	-1,09	n.c.	n.c.												●	●		●	●	●		
LRRC32	leucine rich repeat containing 32	-2,19	-1,99	n.c.		●																	
MAD2L1	mitotic arrest deficient 2 like 1	-1,14	n.c.	n.c.		●		●	●														
MAOB	monoamine oxidase B	-1,57	n.c.	n.c.				●		●													
MICB	MHC class I polypeptide-related sequence B	-3,12	-1,78	n.c.																			
MKI67	marker of proliferation Ki-67	-1,51	n.c.	n.c.	●	●																	
NDRG1	N-myc downstream regulated 1	1,45	n.c.	n.c.	●	●		●	●														
NEFH	neurofilament heavy	-1,48	n.c.	n.c.	●	●	●	●	●	●		●	●	●	●	●	●	●	●	●	●	●	
NEFM	neurofilament medium	-1,74	n.c.	n.c.	●	●	●		●	●		●	●	●		●	●	●			●	●	
NELL1	neural EGFL like 1	-1,11	n.c.	n.c.	●	●		●															
NOL6	nucleolar protein 6	1,00	n.c.	n.c.																			
NRCAM	neuronal cell adhesion molecule	-1,17	n.c.	n.c.	●	●	●	●	●	●		●	●	●	●	●	●	●	●		●		
NRXN1	neurexin 1	-1,35	n.c.	n.c.	●	●	●	●	●	●					●	●	●	●	●	●	●		●
NT5E	5'-nucleotidase ecto	-2,46	-1,12	n.c.		●		●		●													

NTM	neurotrimin	-2,43	n.c.	n.c.																			
OPRM1	opioid receptor mu 1	-1,66	n.c.	n.c.	●	●	●	●	●	●		●	●	●		●	●	●	●	●	●		
PAPSS2	3'-phosphoadenosine 5'-phosphosulfate synthase 2	-1,14	n.c.	n.c.		●																	
PCDH17	protocadherin 17	-1,33	-1,08	-1,21				●		●													
PCDH9	protocadherin 9	-3,44	n.c.	n.c.												●	●				●		●
PCNA	proliferating cell nuclear antigen	-1,44	n.c.	n.c.	●	●																	
PDCD4	programmed cell death 4	1,15	n.c.	n.c.	●	●			●														
PHYHIPL	phytanoyl-CoA 2-hydroxylase interacting protein like	-1,45	n.c.	n.c.																			
PKP2	plakophilin 2	1,17	n.c.	n.c.																			
PLAUR	plasminogen activator, urokinase receptor	-1,02	n.c.	n.c.																	●		
PPT1	palmitoyl-protein thioesterase 1	7,23	7,96	6,43	●	●	●	●	●	●						●	●	●	●	●	●		
PRKCA	protein kinase C alpha	-1,45	-1,53	n.c.	●	●	●	●	●	●		●											
PRNP	prion protein	-1,12	n.c.	n.c.	●	●	●	●	●	●		●	●	●	●								
RALGAPA2	Ral GTPase activating protein catalytic alpha subunit 2	-1,03	n.c.	n.c.																			
RGMA	repulsive guidance molecule family member a	-1,38	-1,02	n.c.				●		●						●	●				●		
RGS2	regulator of G-protein signaling 2	-1,83	-1,13	n.c.	●	●	●	●	●	●						●	●				●		
RGS3	regulator of G-protein signaling 3	-1,04	n.c.	n.c.	●			●															
RGS4	regulator of G-protein signaling 4	1,96	n.c.	n.c.	●	●	●	●		●													
RHBDF1	rhomboid 5 homolog 1	1,06	n.c.	n.c.		●	●			●													
RPH3A	rabphilin 3A	-1,86	n.c.	n.c.												●	●			●	●	●	
S100A10	S100 calcium binding protein A10	-2,61	n.c.	-1,29	●	●		●	●														
SAFB2	scaffold attachment factor B2	1,29	n.c.	n.c.																			
SCML4	sex comb on midleg like 4 (Drosophila)	-1,10	-1,40	-1,80																			
SEZ6L	seizure related 6 homolog like	-1,15	n.c.	n.c.	●	●		●	●	●						●							
SFT2D1	SFT2 domain containing 1	1,09	n.c.	n.c.																			
SLC2A6	solute carrier family 2 member 6	-1,09	n.c.	n.c.																			
SLC44A2	solute carrier family 44 member 2	1,31	n.c.	n.c.																			
SMPD3	sphingomyelin phosphodiesterase 3	-1,48	n.c.	n.c.	●	●				●													
SNAP25	synaptosome associated protein 25	-1,15	n.c.	n.c.				●		●						●	●	●	●	●	●		●
SNAP91	synaptosome associated protein 91	-1,18	n.c.	n.c.	●	●	●	●	●	●		●											
STS	steroid sulfatase	-1,15	n.c.	n.c.		●																	
SYPL1	synaptophysin like 1	1,14	n.c.	n.c.				●		●						●				●	●		
SYT13	synaptotagmin 13	-2,54	-1,19	-1,10												●				●	●		
TF	transferrin	1,46	n.c.	n.c.																			
TGFA	transforming growth factor alpha	-1,34	n.c.	n.c.																			
TGM2	transglutaminase 2	-2,67	n.c.	n.c.	●	●	●	●	●	●					●								
THY1	Thy-1 cell surface antigen	-1,16	n.c.	n.c.	●	●	●	●	●	●		●				●	●				●		●
TLR2	toll like receptor 2	-2,46	n.c.	n.c.	●	●	●	●		●											●		
TM4SF1	transmembrane 4 L six family member 1	3,46	2,20	n.c.			●		●														
TNF	tumor necrosis factor	-3,20	n.c.	-4,13	●	●	●	●	●	●		●	●	●	●								
TNR	tenascin R	-1,21	n.c.	1,12	●	●	●	●	●	●		●	●	●									
TOP2A	topoisomerase (DNA) II alpha	-1,08	n.c.	n.c.	●	●			●														
TPM1	tropomyosin 1 (alpha)	1,05	n.c.	n.c.	●	●	●		●												●		
TUBB4A	tubulin beta 4A class IVa	-1,50	n.c.	n.c.					●							●	●	●			●		
UBE2T	ubiquitin conjugating enzyme E2 T	-1,15	n.c.	n.c.																			
UFL1	UFM1 specific ligase 1	1,38	n.c.	n.c.	●	●										●	●				●		
VASN	vasorin	1,62	n.c.	n.c.																			
VCAN	versican	-1,95	-1,67	n.c.	●	●	●	●	●	●					●								

Table S9 *Differentially expressed proteins specifically dysregulated in CLN5 KO mitochondria*

Accession	IDs	Unique peptides	Anova (p)	Fold Change	Log_2FC	Mito total score/7
P06744	**GPI**	*3*	*2,17E-02*	*9,64*	*3,27*	3
P00558	**PGK1**	*16*	*1,42E-05*	*3,33*	*1,74*	4
P53396	**ACLY**	*6*	*2,86E-07*	*2,36*	*1,24*	6
P10599	**TXN**	*10*	*9,44E-06*	*2,14*	*1,10*	5
O43615	**TIMM44**	*4*	*1,20E-03*	*1,97*	*0,98*	7
P12277	**CKB**	*8*	*1,92E-06*	*1,96*	*0,97*	4
P01116	**KRAS**	*2*	*3,49E-02*	*1,93*	*0,95*	4
O75874	**IDH1**	*2*	*1,53E-03*	*1,91*	*0,93*	5
P63104	**YWHAZ**	*10*	*1,42E-03*	*1,87*	*0,90*	5
P63096	**GNAI1**	*2*	*6,23E-06*	*1,71*	*0,77*	3
Q9NP58	**ABCB6**	*3*	*8,89E-08*	*1,70*	*0,77*	5
P36542	**ATP5C1**	*14*	*4,01E-04*	*0,67*	*-0,58*	6
O75439	**PMPCB**	*4*	*4,24E-12*	*0,67*	*-0,58*	7
P49411	**TUFM**	*19*	*2,03E-05*	*0,66*	*-0,59*	7
P49448	**GLUD2**	*10*	*5,62E-06*	*0,66*	*-0,59*	6
P11310	**ACADM**	*4*	*9,11E-04*	*0,66*	*-0,59*	7
Q7L0Y3	**TRMT10C**	*4*	*6,22E-06*	*0,66*	*-0,60*	8
Q00325	**SLC25A3**	*17*	*8,42E-06*	*0,66*	*-0,60*	7
P36957	**DLST**	*6*	*1,47E-03*	*0,65*	*-0,63*	7
Q5JRX3	**PITRM1**	*3*	*8,22E-09*	*0,65*	*-0,63*	7
P13804	**ETFA**	*16*	*6,36E-06*	*0,65*	*-0,63*	7
P54886	**ALDH18A1**	*7*	*1,66E-05*	*0,64*	*-0,64*	7
P99999	**CYCS**	*10*	*3,14E-06*	*0,64*	*-0,64*	7
P60709	**ACTB**	*90*	*2,62E-07*	*0,64*	*-0,65*	4
Q12849	**GRSF1**	*5*	*3,09E-09*	*0,63*	*-0,68*	7
O94925	**GLS**	*2*	*3,72E-08*	*0,62*	*-0,69*	7
Q15031	**LARS2**	*3*	*1,51E-05*	*0,62*	*-0,69*	7
Q99714	**HSD17B10**	*9*	*9,70E-07*	*0,62*	*-0,69*	6
P82930	**MRPS34**	*2*	*4,68E-05*	*0,62*	*-0,70*	7
P82673	**MRPS35**	*2*	*4,52E-07*	*0,61*	*-0,70*	7
P54819	**AK2**	*11*	*5,61E-09*	*0,61*	*-0,71*	6
P11279	**LAMP1**	*17*	*1,53E-03*	*0,60*	*-0,73*	3
P07237	**P4HB**	*31*	*2,88E-14*	*0,60*	*-0,74*	5
Q9Y3B7	**MRPL11**	*5*	*1,58E-12*	*0,60*	*-0,75*	6
P09669	**COX6C**	*7*	*8,40E-04*	*0,60*	*-0,75*	7
Q9NPJ3	**ACOT13**	*2*	*7,46E-07*	*0,59*	*-0,77*	6
Q96C01	**FAM136A**	*4*	*1,62E-05*	*0,58*	*-0,78*	7
Q96I63	**YME1L1**	*3*	*1,25E-02*	*0,58*	*-0,79*	7
Q16740	**CLPP**	*5*	*5,64E-05*	*0,57*	*-0,80*	7
Q9Y696	**CLIC4**	*3*	*6,46E-03*	*0,56*	*-0,83*	5
Q96RP9	**GFM1**	*3*	*8,46E-04*	*0,56*	*-0,85*	7
O75964	**ATP5L**	*6*	*1,20E-04*	*0,54*	*-0,88*	7
P08559	**PDHA1**	*5*	*3,09E-02*	*0,54*	*-0,89*	6
P41219	**PRPH**	*2*	*5,50E-06*	*0,53*	*-0,90*	3
Q99798	**ACO2**	*20*	*6,58E-09*	*0,53*	*-0,91*	7
O00483	**NDUFA4**	*4*	*1,18E-06*	*0,53*	*-0,92*	7

Q9H9B4	**SFXN1**	*8*	*4,62E-04*	*0,51*	*-0,96*	7
Q15286	**RAB35**	*6*	*1,32E-10*	*0,51*	*-0,97*	5
P30101	**PDIA3**	*9*	*3,56E-04*	*0,51*	*-0,99*	4
Q9NYK5	**MRPL39**	*2*	*6,16E-03*	*0,50*	*-1,00*	6
Q9NVH1	**DNAJC11**	*3*	*2,29E-13*	*0,49*	*-1,04*	7
P50213	**IDH3A**	*4*	*1,45E-05*	*0,49*	*-1,04*	7
Q9BWH2	**FUNDC2**	*5*	*2,41E-08*	*0,47*	*-1,08*	6
Q07021	**C1QBP**	*6*	*3,05E-02*	*0,46*	*-1,11*	7
Q04837	**SSBP1**	*15*	*1,01E-11*	*0,46*	*-1,12*	7
P28838	**LAP3**	*3*	*1,10E-07*	*0,44*	*-1,19*	6
P27797	**CALR**	*13*	*6,06E-09*	*0,44*	*-1,19*	4
P22314	**UBA1**	*4*	*2,79E-02*	*0,41*	*-1,27*	3
Q9NX14	**NDUFB11**	*2*	*2,49E-06*	*0,41*	*-1,29*	7
Q9H2V7	**SPNS1**	*5*	*3,68E-03*	*0,40*	*-1,33*	4
P84095	**RHOG**	*3*	*1,03E-02*	*0,28*	*-1,82*	3
O00217	**NDUFS8**	*2*	*1,09E-03*	*0,08*	*-3,71*	7

Table S10 *Differentially expressed proteins specifically dysregulated in CLN5 KO lysosomes*

Accession	IDs	Unique peptides	Anova (p)	Fold Change	Log_2FC
P06280	**AGAL**	17	*0,00E+00*	*2,86*	*1,52*
P16278	**BGAL**	2	*9,16E-04*	*2,57*	*1,36*
P08962	**CD63**	12	*2,00E-06*	*2,41*	*1,27*
Q9NUM4	**T106B**	7	*3,38E-04*	*1,98*	*0,99*
P63096	**GNAI1**	2	*1,49E-04*	*1,89*	*0,92*
P15586	**GNS**	4	*0,00E+00*	*1,88*	*0,91*
P07686	**HEXB**	9	*2,00E-06*	*1,86*	*0,90*
P10619	**PPGB**	2	*1,68E-03*	*1,79*	*0,84*
Q9BV40	**VAMP8**	2	*9,18E-08*	*1,70*	*0,77*
P60520	**GBRL2**	2	*5,31E-09*	*1,67*	*0,74*
P07858	**CATB**	6	*1,00E-06*	*1,66*	*0,73*
Q8WTV0	**SCRB1**	7	*2,00E-06*	*1,64*	*0,71*
Q92820	**GGH**	11	*6,72E-04*	*1,64*	*0,71*
Q8TCT9	**HM13**	8	*1,00E-06*	*1,62*	*0,70*
P51148	**RAB5C**	4	*0,00E+00*	*1,60*	*0,68*
Q9UIQ6	**LCAP**	13	*1,06E-04*	*1,54*	*0,62*
O95782	**AP2A1**	5	*4,10E-05*	*0,58*	*-0,79*
Q9UNK0	**STX8**	2	*5,08E-03*	*0,50*	*-1,01*
O75503	**CLN5**	2	*0,00E+00*	*0,38*	*-1,41*

Table S11 *Differentially expressed proteins specifically dysregulated dysregulated in mitochondrial fraction from presymptomatic Cln5 -/- mice*

Accession	IDs	Unique peptides	Anova (p)	Fold Change	Log_2FC	Mito total score score/7
Q9Z1P6	**Ndufa7**	4	2,07E-02	2,54	-0,41	7
Q91VM9	**Ppa2**	2	1,94E-03	1,59	-0,20	7
Q8BL66	**Eea1**	2	1,26E-02	1,56	-0,19	3
P11798	**Camk2a**	23	2,99E-02	1,55	-0,19	4
Q61879	**Myh10**	11	1,08E-02	1,53	-0,18	4
Q9D2G2	**Dlst**	14	3,59E-02	1,47	-0,17	7
P99028	**Uqcrh**	2	4,50E-02	1,46	-0,17	7
O35143	**Atpif1**	3	1,30E-03	1,41	0,15	7
P70349	**Hint1**	2	1,28E-02	1,36	-0,13	5
Q06185	**Atp5i**	2	3,03E-03	1,32	-0,12	7
P09103	**P4hb**	2	4,76E-04	1,29	0,11	5
P03930	**Mtatp8**	3	1,54E-02	1,29	-0,11	5
P56382	**Atp5e**	4	3,69E-06	1,28	0,11	7
P50544	**Acadvl**	2	7,58E-06	1,24	-0,09	7
Q9CZU6	**Cs**	16	4,85E-02	1,24	-0,09	7
P35564	**Canx**	6	9,69E-03	1,22	0,09	3
O09111	**Ndufb11**	2	3,79E-04	1,21	-0,08	7
P10639	**Txn**	3	1,36E-02	1,20	0,08	5

Table S12 *Differentially expressed proteins specifically dysregulated dysregulated in mitochondrial fraction from symptomatic Cln5 -/- mice*

Accession	IDs	Unique peptides	Anova (p)	Max fold change	LOG FC	Mito total score score/7
P62806	**Hist1h4a**	7	2,52E-02	1,59	0,67	3
Q9CZW5	**Tomm70**	22	9,65E-03	1,51	0,60	7
P84096	**Rhog**	2	1,07E-02	1,50	0,58	3
P56391	**Cox6b1**	2	3,87E-02	1,43	0,52	7
P45952	**Acadm**	4	2,76E-02	1,42	0,50	7
Q9CZU6	**Cs**	16	9,78E-04	1,38	0,46	7
Q791T5	**Mtch1**	2	1,46E-04	1,36	0,44	7
Q9Z2I0	**Letm1**	6	4,19E-04	1,32	0,40	7
Q3V3R1	**Mthfd1l**	2	1,28E-03	1,31	0,39	7
Q62465	**Vat1**	2	9,91E-04	1,31	0,39	4
P70296	**Pebp1**	4	1,18E-02	1,30	0,38	4
Q60605	**Myl6**	3	1,65E-03	1,30	0,38	3
Q925I1	**Atad3**	6	2,35E-03	1,29	0,37	7
P54071	**Idh2**	2	1,17E-04	1,26	0,33	7
P29758	**Oat**	2	4,50E-03	1,25	0,33	7
Q925N0	**Sfxn5**	5	8,00E-04	1,22	0,29	7
P30275	**Ckmt1**	18	2,77E-04	1,22	0,28	7
Q921G7	**Etfdh**	5	1,01E-02	0,81	-0,31	7
P35564	**Canx**	6	2,78E-03	0,80	-0,32	3
Q9DC69	**Ndufa9**	4	2,65E-02	0,80	-0,33	7
Q9Z2Q6	**Sept5**	6	3,00E-04	0,80	-0,33	3
P48771	**Cox7a2**	3	1,38E-03	0,80	-0,33	7
P16330	**Cnp**	32	1,00E-04	0,79	-0,34	3
Q6PHN9	**Rab35**	3	1,81E-04	0,73	-0,46	7
P70349	**Hint1**	2	2,50E-02	0,65	-0,61	5
P62823	**Rab3c**	3	3,17E-02	0,64	-0,64	3
Q9D6J6	**Ndufv2**	4	2,28E-03	0,57	-0,81	7
P16627	**Hspa1l**	6	2,04E-02	0,57	-0,82	3

APPENDIX

List of primary antibodies used in this study

Primary antibodies used for immunofluorescence (IF) assay were as follows:
rabbit polyclonal anti-PPT1 (1:50, Cat# HPA021546, Sigma Aldrich), which recognized a C-terminal region (aa 223-306), mouse monoclonal anti-LAMP2 (1:400, H4B4 clone, Cat# ab25631, Abcam), mouse monoclonal SMI31R (specific for phosphorylated heavy chain neurofilament; 1:200, Cat# SMI31R, Covance), rabbit monoclonal anti-βIII tubulin (1:200, clone EP1569Y, Cat# 04-1049, Merck Millipore), mouse monoclonal anti Porin (1:500, clone 89-173/033, Cat# MSA05, MitoScience)

Primary antibodies used for western blotting analysis were as follows:
rabbit monoclonal anti CLN5 (1:1000, clone EPR12197B, Cat# ab170899, abcam), mouse monoclonal anti Cathepsin D (1:3000, clone CTD-19, Cat# C0715, Sigma Aldrich), mouse monoclonal anti complex III subunit Core2 (1:1000, clone 13G12AF12BB11, Cat# MS304, MitoSciences), rabbit polyclonal anti β-tubulin (1:1000, Cat# 2146, Cell Signaling), mouse monoclonal anti P62 (1:1000, clone 3/P62, Cat# 610832, BD biosciences), rabbit monoclonal anti LC3B (1:1000, Cat# L7543, Sigma Aldrich), mouse monoclonal anti SDHA (1:5000, clone 2E2GC12FBAE2, Cat# MS204, MitoSciences), mouse monoclonal anti LAMP2 (1:100, clone H4B4, Cat# ab25631, abcam), mouse monoclonal anti GAPDH (1:8000, clone 6C5, Cat# ab8245, abcam), mouse monoclonal anti Porin (1:8000, clone 89-173/033, Cat# MSA05, MitoScience), mouse monoclonal anti-neurofilament 160/200 (1:500, Clone RMdO20, Cat# N2912, Sigma Aldrich), rabbit polyclonal anti-CRMP1 (1:2000, Cat# C2868, Sigma-Aldrich), rabbit polyclonal anti-GAP43 (1:2000, Cat# AB5220, Chemicon, Merck Millipore), rabbit polyclonal anti-SNAP25 (1:10,000, Cat# S9684, Sigma-Aldrich), rabbit polyclonal β-III tubulin (1:1000, Cat# CSB-PA03874A0Rb, Cusabio), rabbit polyclonal anti ACO2 (1:1000, Cat# A305-302A-M, Bethyl laboratories), rabbit polyclonal anti ATP5L 1:500, Cat# A305-486A-M, Bethyl laboratories), mouse monoclonal anti FUNDC2 (1:500, clone 2G12, Cat# sc-517152, Santa Cruz Biotechnology), mouse monoclonal anti GLA (1:500, Cat# EMS 20817, Elabscience), rabbit polyclonal anti HEXB (1:500, Cat# EPP13904, Elabscience)

CTSD patient

The diagnostic studies described were approved by the ethics committee of IRCCS-Stella Maris, Pisa, Italy. All the procedures were performed in compliance with the Helsinki Declaration of 1975.

This 4-year-old girl, the second child of healthy, non-consanguineous parents, was born by normal delivery at 41 weeks of gestation; her birth weight was 3400 gr (50th centile), length 50 cm (50th centile), and head circumference 35 cm (50th centile). An 8-year-old sister is healthy. A dramatic deceleration of the head growth rate was noted in the second month of life. The patient's psychomotor development was normal until the age of five months, when she showed neuro-developmental regression. She abruptly stopped smiling, grasping objects and rolling. At that age, her head circumference was 38 cm, markedly below the 3rd centile. Since then, she has never achieved the sitting position, or reached any other neuro-developmental milestones. At 8 months, brain MRI showed marked atrophy of the supra-tentorial structures. Other investigations (serum and metabolic blood screening, echocardiogram, EEG and gene testing for MECP2) were normal. At the age of 18 months, the patient presented upper limb jerks; a diagnosis of epilepsy was made and treatment with valproic acid (25 mg/kg/day) was started with little effect. At the age of 2 years, she started to present axial and upper limb spasms. A combination of vigabatrin (80 mg/kg/day) and nitrazepam (0.25 mg/kg/day) was tried, but failed to reduce spasm frequency and duration. The child's neurological conditions worsened progressively: she developed swallowing and respiratory difficulties, and percutaneous endoscopic gastrostomy was necessary due to feeding difficulties. The girl was referred to us (SS, SR, IT) at the age of 3 years. On admission she was alert, but barely responsive and displayed profound global delay; speech and utterances were absent. Her head circumference was 40 cm. Neurological evaluation revealed axial hypotonia, tetraparetic, hypotonic limbs with extensor toe responses, upper limb dystonia and oral dyskinetic movements. The child's responses to sounds and voices were poor. Her vision seemed to be severely impaired: she could neither track nor fixate objects; she showed erratic eye movements as well as downward conjugate gaze; her pupils were dilated and responded smoothly to light. An electrocardiogram, performed following a supra-ventricular tachycardia episode, revealed a prolonged QT interval. The echocardiogram was consistent with severe, asymptomatic hypertrophic cardiomyopathy. Beta-blocker treatment (metoprolol; 4.2 mg/day) was started after a third episode of supra-ventricular tachycardia. Awake and sleep video-EEG polygraphy showed marked low-voltage, non-responsive electrical activity; erratic, massive myoclonic jerks were not related to abnormal cortical activity. Brain MRI at the age of 4 years showed worsening global cerebral atrophy, with extensive gray and white matter loss, also extending to the cerebellar structures (Figure 1B). Flash visual evoked responses were abolished and the electroretinogram showed a markedly abnormal photoreceptor response. Electromyography, neurography and cerebrospinal fluid analysis were

all normal. Ultrastructural examination of a skin punch biopsy specimen revealed the presence of GROD-like structures, scattered in the cytoplasm of fibrocytic processes (Figure 19). These findings prompted us to test the enzyme activity of palmitoyl protein thioesterase (PPT1) in cultured skin fibroblasts and to analyze the coding exons (using Sanger sequencing) and the mRNA expression of CLN1/PPT1 (by means of qPCR analysis). PPT1 activity and gene testing were normal. We then applied a novel, highly sensitive multiplex enzyme assay developed on dried blood spots (DBSs) in order to analyze, in a single test, the activities of PPT1, tripeptidyl peptidase, and cathepsin D (CTSD). Fluorimetric and mass spectrometric determination of CTSD disclosed significantly reduced levels of activity in the patient. The enzyme activities of the mother and sister were mildly reduced compared to healthy controls, whereas the father had values only slightly below those of healthy controls. Thereafter, using capillary Sanger sequencing, we analysed the coding region of CTSD and detected a novel homozygous mutation (c.205G>A, p.Glu69Lys) in the patient. The mutation was heterozygous in her parents and elder sister and not detected in 200 healthy control chromosomes. It was also absent in polymorphic human variation databases and scored as a predictably deleterious variant in silico. Western blotting in cultured skin fibroblasts using a monoclonal anti-cathepsin D antibody (clone C0715, Sigma-Aldrich, St. Louis, MO) showed a significant reduction of the 34 kDa band representing the mature protein.